

THE DEVELOPMENT OF EXCITATORY SYNAPSES AND COMPLEX BEHAVIOR

by

JENNIFER LYN HOY

A DISSERTATION

Presented to the Department of Biology
and the Graduate School of the University of Oregon
in partial fulfillment of the requirements
for the degree of
Doctor of Philosophy

September 2011

DISSERTATION APPROVAL PAGE

Student: Jennifer L Hoy

Title: The Development of Excitatory Synapses and Complex Behavior

This dissertation has been accepted and approved in partial fulfillment of the requirements for the Doctor of Philosophy degree in the Department of Biology by:

William Roberts	Chairperson
Philip Washbourne	Advisor
Victoria Herman	Member
Michael Wehr	Member
Judith Eisen	Member
Clifford Kentros	Outside Member

and

Kimberly Andrews Espy	Vice President for Research & Innovation/Dean of the Graduate School
-----------------------	--

Original approval signatures are on file with the University of Oregon Graduate School.

Degree awarded September 2011

© 2011 Jennifer Lyn Hoy

DISSERTATION ABSTRACT

Jennifer Lyn Hoy

Doctor of Philosophy

Department of Biology

September 2011

Title: The Development of Excitatory Synapses and Complex Behavior

Approved: _____
Philip Washbourne

Excitatory glutamatergic synapses facilitate important aspects of communication between the neurons that govern complex forms of behavior. Accordingly, small differences in the molecular composition of glutamatergic synapses have been suggested to underlie neurodevelopment disorders, drive evolutionary changes in brain function and behavior, and enhance specific aspects of cognition in mammals. The appropriate development and later function of these structures in the adult involves the well-coordinated activities of hundreds of molecules. Therefore, an important goal in neuroscience is to identify and characterize how specific molecules contribute to the development of excitatory synapses as well as how manipulations of their function impact neural systems and behavior throughout life. This dissertation describes two important contributions toward this effort, 1) that the newly discovered molecule, Synaptic Cell Adhesion Molecule 1 (SynCAM1) specifically contributes to the early stages of glutamatergic synapse formation and 2) that Neuroligin1 (NL1) contributes to the mature function of glutamatergic synapses and mature forms of behavior *in vivo*.

In the first set of experiments, I developed an *in vitro* cell based assay in order to determine the minimal molecular components necessary to recruit developmentally

relevant glutamate receptor subtypes to sites of adhesion mediated by SynCAM1. In these experiments we discovered that protein 4.1B interacted with SynCAM1 in order to cause the specific recruitment of the NMDA type glutamate receptor containing the NR2B subunit. In the second set of experiments, we show that expression of NL1 missing the terminal 55 amino acids enhanced short term learning and flexibility in behaving mice while increasing the number of immature excitatory postsynaptic structures. Interestingly, this behavioral profile had components more consistent with 1 month old juvenile controls than age matched control littermates. In contrast, full length NL1 overexpression impaired learning and enhanced perseverance while yielding an increase in the proportion of synapses with mature characteristics. These results suggest that NL1's C-terminus drives the synaptic maturation process that shapes the development of complex behavior. Both studies bolster our understanding of how specific molecules impact the development of excitatory synapses and complex behavior.

This dissertation includes both my previously published and unpublished co-authored material.

CURRICULUM VITAE

NAME OF AUTHOR: Jennifer Lyn Hoy

GRADUATE AND UNDERGRADUATE SCHOOLS ATTENDED:

University of Oregon, Eugene
University of Arizona, Tucson

DEGREES AWARDED:

Doctor of Philosophy, Biology 2011, University of Oregon
Bachelor of Science, Molecular and Cellular Biology, 2003, University of
Arizona

AREAS OF SPECIAL INTEREST:

Neuroscience
Genetics and Behavior

GRANTS, AWARDS, AND HONORS:

Oregon Center for the Optics (OCO) Integrative science proposal award,
Novel Strategies for Enhanced Quantitative Characterization of Mouse Behavior
in Standard Learning and Memory Tests, University of Oregon, 2010

Women in Graduate Science (WGS) travel award Society for Neuroscience,
University of Oregon, 2009

NIH/APA DPN pre-doctoral fellowship: 5 T32 MH18882, Development of
Excitatory Synapses and Learning and Memory, University of Oregon, 2006

PUBLICATIONS:

Hoy J.L., Constable, J.R.L., Arias R.J., Chebac R., Kyweriga M., Schnell E., Davis L., Wehr M., Washbourne P.E. (2011) The intracellular region of NL1 regulates behavioral and synaptic maturation (Submitted to Neuron).

Hoy J.L., Constable, J., Vicini S., Fu Z., Washbourne P.E. (2009) SynCAM1 recruits NMDA receptors via Protein 4.1B. *Mol Cell Neurosci* 42:466-483

ACKNOWLEDGMENTS

I wish to express sincere appreciation to my advisor Philip Washbourne for his support and guidance in conducting this research, generously providing outside training where necessary and help in preparing the manuscripts. It has been an invaluable training experience to watch him establish his lab. I greatly value the contributions of all of my committee members, Bill Roberts, Judith Eisen, Tory Herman, Mike Wehr and Cliff Kentros. Their thoughts and criticisms were important to this work and my progress. I also appreciate that Peg Morrow, Ellen McCumsey, Mike McHorse, Don Pate, Mikel Rhodes and Donna Overall being so good at what they do ensured that I stayed physically healthy and paid on time. The support and early “training” that came from many family members, principally my mother and stepfather, my aunt and uncle, and grandparents, was also critical in allowing me to accomplish this task. This work was funded in part by Autism speaks, the NINDS (RO1 NS065795), and the NIH and the APA (5 T32 MH18882).

Dedicated to my mother, who taught me to observe the beauty in all of life and how to persevere, and to my husband who harbors the same wonder in the way of the world.

TABLE OF CONTENTS

Chapter	Page
I. INTRODUCTION	1
II. THE NOVEL CELL ADHESION MOLECULE SYNCAM1 CONTRIBUTES TOWARDS THE EARLY DEVELOPMENTAL STAGES OF GLUTAMATERGIC SYNAPSE FORMATION: SYNCAM1 RECRUITS NMDA RECEPTORS VIA PROTEIN 4.1B	4
1. Introduction	4
2. Results	6
3. Discussion	30
4. Methods	34
III. THE INTRACELLULAR REGION OF NL1 REGULATES BEHAVIORAL AND SYNAPTIC MATURATION	44
1. Introduction.....	44
2. Results.....	46
3. Discussion.....	72
4. Methods.....	79
IV. CONCLUSIONS	86
APPENDICES	89
A. SUPPLEMENTAL MATERIAL FOR CHAPTER II	89
B. SUPPLEMENTAL MATERIAL FOR CHAPTER III	92
REFERENCES CITED	100

LIST OF FIGURES

Figure	Page
CHAPTER II	
1. The Cell Adhesion Molecule / Receptor Recruitment Assay (CAMRA).....	7
2. Protein 4.1B is a potent SynCAM1 effector molecule, recruiting NMDARs to sites of adhesion with microsphere.	11
3. Direct interactions between SynCAM1 and protein 4.1B are mediated via key protein-protein interaction domains.	13
4. Protein 4.1B specifically enhances measures of NMDA-EPSCs and presynaptic differentiation in the HEK293 cell/neuronal co-culture assay.	18
5. Specificity of 4.1 effector proteins to glutamate receptor recruitment.	21
6. Localization of endogenous protein 4.1B in cultured hippocampal neurons.....	23
7. Protein 4.1B enhances NMDAR localization at synapses.	25
8. Protein 4.1B enhances NMDAR mediated synaptic events in cultured hippocampal neurons	29
CHAPTER III	
1. Expression of HA-NL1FL and HA-NL1ΔC in transgenic mice.....	49
2. Manipulations of NL1 intracellular signaling distinctly alters behavioral performance in learning and memory behaviors.	55
3. NL1 intracellular signaling regulates the morphological characteristics of spines and synapses in SLM	59
4. Distinct changes in synaptic protein composition in HA-NL1FL versus HA-NL1ΔC mice	63
5. Correlation between levels of NMDAR subunit NR2B in the SLM and flexibility behavior.....	66
6. Manipulations of NL1 intracellular signaling affect social behavior	69
7. Manipulations of NL1 affect sensory evoked responses in cortex	71
8. Model for NL1's role in late phases of synaptic maturation	73

CHAPTER I

INTRODUCTION

AN OVERVIEW

An important goal in neuroscience is to create a mechanistic account of the biological basis for behavior. Such an explanation may be applied ambitiously towards identifying the origin of disease states and their respective cures; or, less practically, may satisfy our deep curiosity regarding the origins of our own thoughts and actions. An important step towards generating this knowledge was the discovery that the brain most directly generates behavior through spatio-temporally regulated communication across distinct neural substrates, or neural systems. Such communication is facilitated via chemical synapses, and it is known that the function of these microscopic structures are shaped by a complex interplay between genetics and the environment in which we develop. Thus, one reasonable starting place with which to begin to understand the origins of behavior is to investigate the processes that govern synapse formation and function throughout life. The goal of the work in this dissertation was to contribute towards a significant enhancement in our understanding of the mechanisms that support the early development of one of the most prevalent forms of synapses, the excitatory glutamatergic type. An important advance also supported by this work more directly links the development of glutamatergic synapses to the progression of complex forms of behavior such as learning, memory and social interaction.

THE LINK BETWEEN SYNAPTOGENIC MOLECULES AND THE DEVELOPMENT OF SPECIFIC BEHAVIORS

Human infants are not born with the innate ability to play the violin or compose a sonata. Not much in our evolutionary history would require that such skills would be necessary at birth. Rather, infants have far greater priorities such as ensuring that they are well. Accordingly, they are born with the perceptual capabilities and motor skills necessary to perform this task minutes after birth (Cantrill et al., 2004; Creedy et al., 2008). However, with time, and the acquisition of basic skills such as learning to move

the hand with coordination, a young child could begin to rapidly acquire the ability to play a violin, or even an instrument invented yesterday. Moreover, many older adults are often faced with the unpleasant observation that young adults acquire new information and motor skills more rapidly than themselves. Luckily, those same older adults can take comfort in the fact that they are at least one up on most 5 year olds in that they have a better idea of the what, where and when that happened to them last week. All of these observations taken together, and backed up by a multitude of cognitive studies, imply that: 1) some behaviors and brain functions are largely hardwired prenatally (innate ability to suckle), 2) that the development and acquisition of specific behaviors follows a prescribed trajectory (you learn to walk before you talk) and 3) that the brain, and the neural circuits that support its function, occupy distinct states of modifiability throughout life (Lister and Barnes, 2009)

As glutamatergic synapses facilitate the proper function of individual neural systems as well as the communication between them during behavior, it is a fair assumption that the complement of molecules present at the synapse at any one stage of development shapes the characteristics of the behavior as described above. This predicts that changes in molecules that impact the process of synaptogenesis perinatally and throughout life should broadly impact those behaviors and perceptual abilities that exist at birth as well as the acquisition of later behaviors throughout life. Conversely, the acquisition of complex behaviors such as learning to speak will be specifically affected when manipulations are made to the molecules whose expression ramps up just when experience may most influence that behavior. Being able to test such predictions will be key to establishing firm links between synaptic molecules and the aspects of behavioral performance they may underlie.

To test these predictions, one must first characterize the spatio-temporal expression pattern of synaptic molecules. In parallel, studies must also define the developmental trajectories of important behaviors as well as the neural substrates that support them. The so called synaptogenic cell adhesion molecules form one class of powerful regulators of glutamatergic synapse formation and function. The expression patterns of a subset of these molecules such as synaptic cell adhesion molecule 1 (SynCAM1) and Neuroligin1 (NL1) suggest that they are in the right place at the right

times to mediate important, yet distinct, aspects of the development of the brain and behavior (Biederer, 2005; Sara et al., 2005; Washbourne et al., 2004a). Importantly, both SynCAM1 and NL1 have been found to be required for the execution of normal learning, memory and social behaviors in the adult and both have been linked to human neurological disorders such as mental retardation and autism (Wang et al., 2009; Zhiling et al., 2008). However, these molecules have both overlapping and non-overlapping expression patterns which may imply distinct contributions to neural circuit formation and function. Neurological disorders such as autism are thought to relate to malfunctions in synapse formation and function at distinct developmental periods within distinct neural substrates (Penzes et al., 2011; Zoghbi, 2003) Therefore, further work describing the molecular activities of synCAM1 and NL1, and defining how they contribute towards the function and formation of synapses at specific developmental stages, has the potential to advance our understanding of the biological basis of important complex behaviors. First, this dissertation describes the contributions of SynCAM1 towards a potentially ubiquitous role in initial glutamatergic synapse formation that may impact many stages of brain development and function. Second, I describe work that establishes how NL1 appears to play a distinct and necessary role in the maturation of excitatory synapses, a process that underlies the progression of learning, memory and social behavior in mice. As more than 1,000 different molecules are found at the glutamatergic synapse at any given developmental stage, studies such as these begin to clarify how and when they may all come together to support age typical aspects of brain function. This seems a necessary first step towards generating a satisfying understanding of how the brain produces behavior.

This dissertation includes both my previously published and unpublished co-authored material.

CHAPTER II
THE NOVEL CELL ADHESION MOLECULE SYNCAM1 CONTRIBUTES
TOWARDS THE EARLY DEVELOPMENTAL STAGES OF
GLUTAMATERGIC SYNAPSE FORMATION: SYNCAM1 RECRUITS NMDA
RECEPTORS VIA PROTEIN 4.1B

The work described in this chapter was previously published in *Molecular and Cellular Neuroscience*, Vol. 42, 2009. I am first author as I primarily developed the cell clustering based assays, gathered and analyzed the related data from neuronal and non-neuronal cultures, and wrote the manuscript with advising and editing performed by P. Washbourne and J. Constable. J. Constable also performed the biochemistry that was critical to the interpretation of the other data sets, while Z. Fu with the support of S. Vicini, performed critical functional assays to verify how protein manipulations impacted functional synaptic transmission in a developmentally relevant way.

1. INTRODUCTION

Unraveling the mechanisms by which synapses form during development of the central nervous system is essential to understanding the origin of neurodevelopmental disorders and cognitive impairment (Zoghbi, 2003). Synaptogenesis is a multi-step process that is initiated by contact between two neurons. As this contact becomes adhesive prior to becoming a synapse (Chow and Poo, 1985), it has long been hypothesized that cell adhesion molecules (CAMs) are key to the early events of synaptogenesis (Bloch, 1989). One huge stride forward in our understanding of synapse formation was the realization that CAMs not only mediate the adhesion at synapses, but also initiate the recruitment of crucial synaptic components such as synaptic vesicles in the axon and neurotransmitter receptors in the dendrite (Barrow et al., 2009; Biederer et

al., 2002; Nam and Chen, 2005; Scheiffele et al., 2000; Sytnyk et al., 2002). For review see (Washbourne et al., 2004a).

Recently, a family of immunoglobulin-domain containing CAMs, called SynCAMs, were identified as potent inducers of presynaptic terminals, when expressed in non-neuronal cells and cocultured with neurons (Biederer et al., 2002). This synaptogenic potential is shared with a handful of other CAMs, including the neuroligins (NLgns) and their presynaptic partners the neurexins (Dean et al., 2003; Scheiffele et al., 2000), netrin-G ligands (NGLs) (Kim et al., 2006) and synaptic cell adhesion-like molecules (SALMs) (Ko et al., 2006; Wang et al., 2006). While it appears that all of these molecules are able to induce the formation of the presynaptic terminal, their ability to recruit postsynaptic components has been less well studied. To date, the most heavily investigated interactions lie within the intracellular domain of NL1. NL1 can interact with the postsynaptic density protein PSD-95 through a type I PDZ binding motif (Irie et al., 1997), and can recruit NMDA-type glutamate receptors through both the PDZ binding motif and the WW domain (Barrow et al., 2009; Iida et al., 2004).

Similarly, SynCAMs also possess intracellular interaction domains including a type II PDZ binding motif and a FERM (4.1, ezrin, radixin, moesin) binding motif (Biederer, 2005; Biederer et al., 2002). Potential interacting molecules, or effectors, have been identified, however, none of these interactions have been explored for their role in postsynaptic differentiation. *In vitro* and in yeast-two-hybrid studies, SynCAM1 was shown to bind calcium/calmodulin-dependent serine protein kinase (CASK) (Biederer et al., 2002), Syntenin1 (Biederer et al., 2002; Meyer et al., 2004) and glutamate receptor interacting protein (GRIP) 1 (Meyer et al., 2004) via the C-terminal PDZ-binding domain. All three proteins are thought to play a scaffolding role in recruiting or organizing proteins at a variety of cellular junctions (Funke et al., 2005). In addition, SynCAM1 can bind to erythrocyte protein band 4.1-like 3 (protein 4.1B) via the juxtamembranous FERM binding domain (Yageta et al., 2002), an interaction which is thought to promote cell adhesion. All four molecules (CASK, Syntenin1, GRIP1 and 4.1B) are expressed in the CNS, have multiple protein-protein interaction domains and all could potentially play a role in the development of the postsynaptic specialization.

We investigated these potential effectors of SynCAM1 in terms of their ability to recruit NMDARs to sites of synaptic adhesion. We focused on NMDARs as they appear to be the first glutamate receptors recruited to synapses during synaptogenesis (Barrow et al., 2009; McAllister, 2007; Petralia et al., 1999; Washbourne et al., 2002) We identified protein 4.1B as a potent and specific SynCAM1 effector molecule for the recruitment of NMDARs. Surprisingly, we also identified protein 4.1N as a specific SynCAM1 effector for AMPAR recruitment. These results were confirmed by electrophysiological studies in an HEK293 cell/neuronal co-culture assay (Biederer and Scheiffele, 2007; Fu et al., 2003). Imaging and electrophysiological studies of hippocampal neurons in culture demonstrate an important role for protein 4.1B during synapse formation and the recruitment of NMDARs to synapses. Thus, our experiments establish 4.1 proteins as SynCAM1 effector molecules that impact necessary aspects of postsynaptic development. This molecular activity may underlie the development of glutamatergic synapses throughout the nervous system as SynCAM family members are expressed throughout the nervous system and are present at birth.

2. RESULTS

The Cell Adhesion Molecule / Receptor Recruitment Assay (CAMRA)

The initial goal of this work was to identify and characterize potential postsynaptic effector molecules for SynCAM1. We therefore characterized an assay that could be used to identify molecules sufficient to recruit glutamate receptors upon clustering of SynCAM1, or any CAM, in a postsynaptic configuration. The approach employed was an adhesion-based recruitment assay that measures microsphere mediated clustering of recombinant molecules expressed in non-neuronal COS7 cells that we call the Cell Adhesion Molecule / Receptor Recruitment Assay (CAMRA). In the CAMRA, microspheres coated with antibodies against the protein of interest bound and aggregated many copies of a specific CAM that were expressed in COS7 cells (Fig.1A). Subsequently, we visualized co-transfected molecules and determined whether they were also accumulated at the site of microsphere binding (Fig.1B).

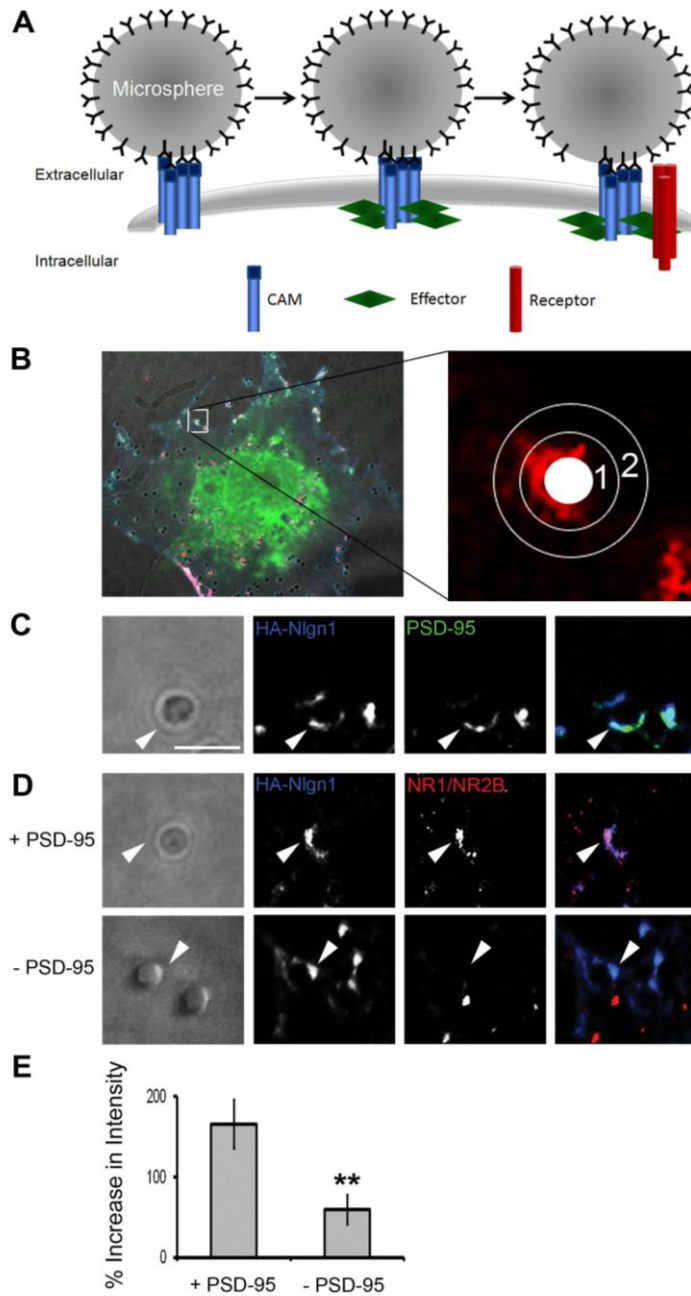


Figure 1. The Cell Adhesion Molecule / Receptor Recruitment Assay (CAMRA). (A) Model of clustering events in transfected COS7 cells after microsphere application when it is directed against tagged cell adhesion molecules (CAMs) on the surface of cells also expressing an intracellular effector molecule (Effector) and surface neurotransmitter

receptors (Receptor). **(B)** Quantification of surface receptor immunofluorescence intensity around a single microsphere. Enlarged image depicts defined areas in a single channel that are used to determine intensity increases at microsphere. An average of the intensity within the area of annulus1 equals intensity of fluorescence at microsphere, the area of annulus 2 equals intensity of fluorescence in background, while the white circle is area taken by the microsphere. The left panel depicts the microsphere in the context of the whole cell, with all three fluorescence channels, CAM (blue), effector (green) and receptor (red). **(C)** PSD-95 was recruited to areas with HA-Nlgn1 accumulation in contact with microspheres (arrow head). Scale bar equals 2 μ m. **(D)** NMDARs were recruited to sites of contact with microspheres and accumulations of Nlgn1 only when PSD-95 was co-transfected into COS7 cells. **(E)** Quantification of intensity increases of surface NMDARs at sites of contact in presence and absence of PSD-95 ($165.9 \pm 29.6\%$ vs. $59.3 \pm 18.1\%$, $p < 0.01$, $n = 14$, error bars represent s.e.m.).

We first tested the CAMRA utilizing a well characterized protein complex known to interact at the synapse: Nlgn1, PSD-95 and the NMDAR composed of NR1 and NR2B subunits. Nlgn1 interacts with PSD-95 (Irie et al., 1997) and this interaction appears to regulate NMDAR recruitment to Nlgn1 clusters in cultured hippocampal neurons (Nam and Chen, 2005). Specifically, we asked whether microsphere-directed aggregation of an HA-tagged Nlgn1 (HA-Nlgn1) would promote GFP-tagged PSD-95 (PSD-95-GFP) co-accumulation. Cells transfected with these molecules were incubated with anti-HA antibody-coated microspheres for 1 hour at 37°C. We chose this time as we have previously determined that aggregation of PSD-95 to Nlgn1 clusters takes on the order of one hour in neurons (Barrow et al., 2009). After fixation and immunolabeling, the fluorescence intensities of extracellular HA and internal GFP were measured at microspheres (Fig.1B, annulus 1) and compared to background intensity levels (Fig.1B, annulus 2). We observed a $123.9 \pm 10.9\%$ ($n = 15$) increase in fluorescence intensity of PSD-95-GFP at microspheres relative to background (Fig.1C, arrowheads). Therefore, we conclude that PSD-95-GFP was recruited to sites of HA-Nlgn1 clustering at microspheres, thus reflecting a relationship previously described (Irie et al., 1997). Further, this effect on the recruitment of PSD-95 is specific to the interaction with Nlgn1 as PSD-95-GFP did not accumulate at HA-SynCAM1 mediated sites of contact with microspheres relative to background ($11.9 \pm 4.5\%$, $n = 15$; Fig.2C and Supplemental Fig.1).

Next, we analyzed whether surface-expressed NMDARs (NR1 and GFP-NR2B) localized to sites of HA-Nlgn1 aggregation at microspheres. We chose the NR2B subunits as these receptor subunits are most relevant to the early development of the glutamatergic postsynaptic density (Durand and Konnerth, 1996; Isaac et al., 1997; Washbourne et al., 2002; Wu et al., 1996). We compared conditions in which PSD-95 was either present or absent in the transfected cells (Fig.1D). As predicted, the surface level of NMDARs (as determined by labeling of the extracellular GFP tag) was significantly higher at microspheres when PSD-95 was co-transfected ($165.9 \pm 29.6\%$ vs. $59.3 \pm 18.1\%$, $p < 0.01$, $n = 14$; Fig.1E). Thus, we conclude that the CAMRA allows us to reliably measure the accumulation of an effector molecule (PSD-95) at sites of microsphere-mediated CAM (Nlgn1) clustering, and quantify the concomitant recruitment of NMDARs in the presence of the effector.

Potential SynCAM1 effector molecules

To determine if SynCAM1 could fulfill a similar role in glutamate receptor recruitment via one of its potential effector proteins, we employed the CAMRA to identify effector molecules that were sufficient to increase the accumulation of NMDARs to sites of SynCAM1 clustering. We tested four SynCAM1 binding proteins that had been identified *in vitro*: protein 4.1B, CASK, Syntenin1 and GRIP1.

COS7 cells were transfected with HA-SynCAM1, NR1, GFP-NR2B and one of the candidate effectors and then we applied microspheres directed to HA-SynCAM1 (Fig.2A,B). In the absence of an effector, there was a small increase in the accumulation of surface NMDARs (surface GFP-NR2B; $35.4 \pm 16.33\%$) at microspheres that had clear accumulations of HA-SynCAM1 ($110.56 \pm 13.53\%$, $n = 15$; Fig.2A,B). This result was analogous to the Nlgn1-NMDAR-only co-transfected condition, and there was no significant difference between those two conditions ($p = 0.2136$; Fig.1D). Thus, we conclude that in the absence of effectors, the CAMs themselves may only promote small increases in NMDAR recruitment. PSD-95 is not predicted to interact with the intracellular domain of SynCAM1 (Biederer, 2005; Meyer et al., 2004), therefore, we measured surface NMDAR recruitment to sites of HA-SynCAM1 mediated adhesion in the presence of PSD-95-GFP as a negative control (Fig.2A). Surface NMDAR

recruitment under these conditions was not significantly different than HA-SynCAM1 alone ($33.5 \pm 7.6\%$ vs. $35.4 \pm 16.3\%$, $p = 0.5897$, $n = 15$; Fig.2B).

Of the candidate effectors examined, only the addition of protein 4.1B produced a dramatic increase in NR1/NR2B accumulation at microsphere-mediated sites of HA-SynCAM1 aggregation relative to control ($148.7 \pm 13.3\%$ vs. $35.4 \pm 16.3\%$, $p < 0.005$, $n = 15$; Fig.2A,B). Surface NMDAR intensities at microspheres applied in the presence of CASK ($71.6 \pm 16.9\%$, $p = 0.0421$, $n = 15$), Syntenin1 ($68.9 \pm 20.5\%$, $p = 0.2134$, $n = 15$), or GRIP1 ($35.2 \pm 9.1\%$, $p = 0.9669$, $n = 15$), were not significantly different from the PSD-95 condition nor each other after correction for multiple comparisons (Fig.2B). However, CASK and Syntenin1 trend towards significance suggesting that there may be a basal level of NMDAR recruitment by these effector proteins, but not by GRIP1 and PSD-95. In conclusion, the screen revealed that protein 4.1B is a potent effector molecule of SynCAM1 in recruiting NMDARs to microsphere-mediated sites of adhesion.

SynCAM1 interacts with protein 4.1B to specifically recruit NMDARs

Given the weak effect of three of the four potential effector proteins in recruiting NMDARs to SynCAM1 adhesion sites, we explored the nature and specificity of their interactions with SynCAM1 (Fig.2C and Supplemental Fig.1). We compared effector recruitment measures to our negative control: PSD-95-GFP accumulation at microsphere mediated sites of HA-SynCAM1 clustering. As measured by the percent increase of GFP-tagged effector at microspheres relative to background, HA-SynCAM1 only drives the accumulation of 4.1B ($114.1 \pm 11\%$, $p < 0.005$, $n = 15$), CASK ($123 \pm 16.9\%$, $p < 0.005$, $n = 15$) and Syntenin1 ($91.8 \pm 12.2\%$, $p < 0.005$, $n = 15$) compared to PSD-95 (Fig.2C). HA-SynCAM1 is unable to efficiently recruit GRIP1 in this assay despite previous reports of a direct interaction ($26.4 \pm 13.3\%$, $p = 0.4068$, $n = 15$). Thus, protein 4.1B, CASK and Syntenin1 are all recruited to sites of microsphere-induced SynCAM1 clustering in COS7 cells to a similar extent, yet protein 4.1B is significantly different in its ability to cause NMDAR accumulation at microspheres. Taken together, this suggests that protein 4.1B possesses the most potent recruitment activity on NMDARs compared to all effectors examined.

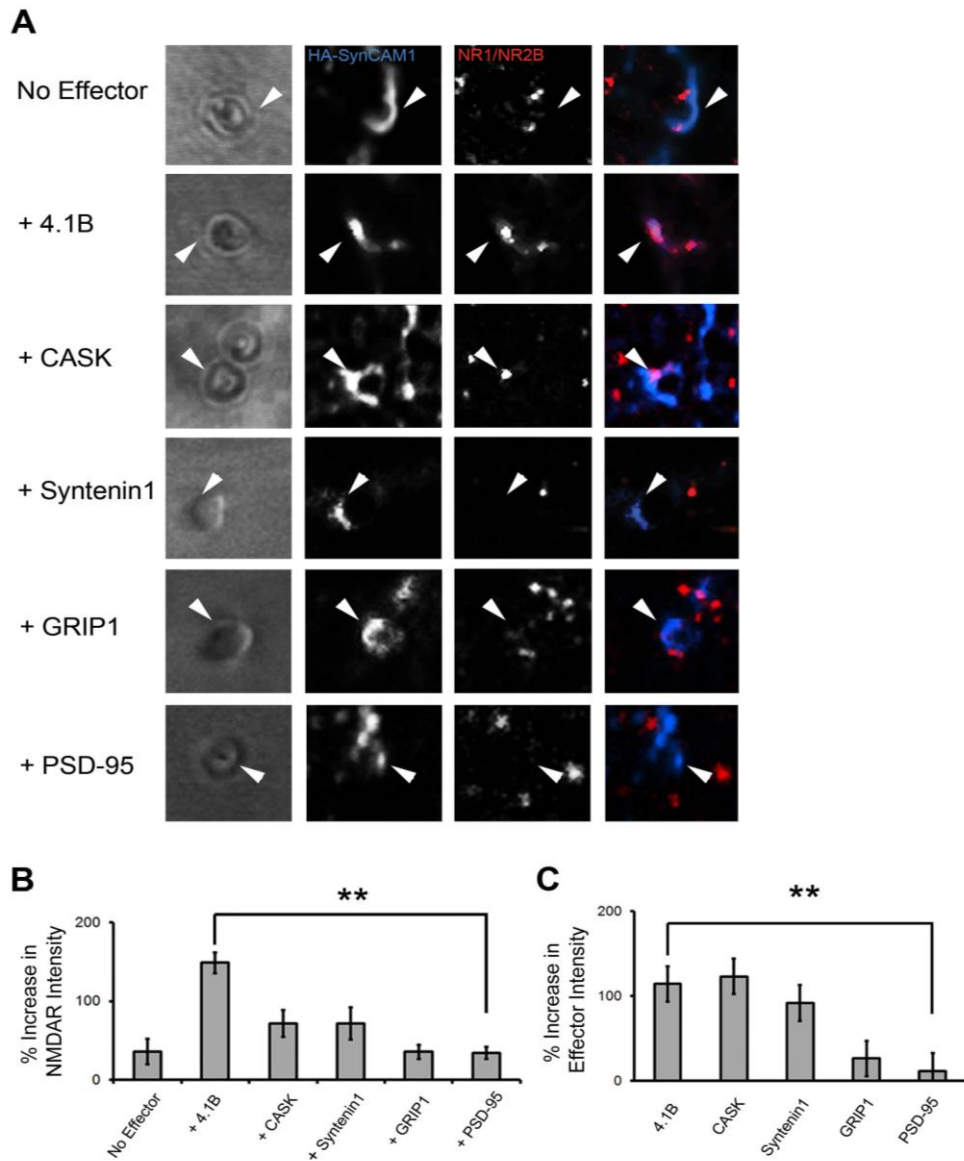


Figure 2. Protein 4.1B is a potent SynCAM1 effector molecule, recruiting NMDARs to sites of adhesion with microsphere. **(A)** Close up images of individual microspheres applied to cells transfected with SynCAM1 (blue), NMDARs (red) and one of the candidate effectors indicated on the left (not fluorescently labeled in these experiments). Arrowheads indicate examples of contact sites at microsphere where HA-SynCAM1 was aggregated. **(B)** Quantification of NMDAR recruitment via the candidate effector molecules. Protein 4.1B significantly increased intensity of receptor staining at microspheres relative to control ($148.7 \pm 13.3\%$ vs. $33.5 \pm 7.6\%$, $p < 0.005^*$, $n = 15$). **(C)** Quantification of effector recruitment via SynCAM1 to sites of adhesion at microspheres ($p < 0.005^*$, $n = 15$, error bars represent s.e.m.; * with correction for multiple comparisons).

To further explore the specificity of the interaction between SynCAM1 and protein 4.1B, we examined aggregation of 4.1B-GFP at microspheres directed towards a mutant HA-SynCAM1 lacking the FERM binding domain (HA-SynCAM1 Δ FERMb; Fig.3A). Full length 4.1B-GFP did not co-accumulate at microsphere-induced HA-SynCAM1 Δ FERMb aggregation ($29.4 \pm 9.1\%$, $n = 15$; Fig.3C,D). Similarly, 4.1B lacking its FERM domain (4.1B Δ FERM) did not accumulate at sites of HA-SynCAM1 aggregation (Fig.3B,C). To confirm that protein 4.1B was recruited specifically to clustered HA-SynCAM1 and not just to densely packed adhesion sites, we measured 4.1B-GFP accumulation using HA-NLG1 as the targeted CAM. In this case, 4.1B-GFP did not significantly co-localize to microspheres where large amounts of HA-NLG1 were localized ($16.7 \pm 6.4\%$, $n = 15$; Fig.3D). As an additional test of specificity of our CAMRA, we determined whether NMDARs would aggregate at microspheres directed against HA-SynCAM1 in the presence of 4.1B Δ FERM. As compared to the negative control, we observed no significant difference in NMDAR accumulation at microspheres under this condition ($33.9 \pm 7.6\%$ vs. $33.5 \pm 7.6\%$, $p = 0.4429$, $n = 15$).

As our assays show co-localization and not strictly a biochemical interaction, we performed immunoprecipitation experiments. Immobilization of HA-SynCAM1 on protein-A-sepharose beads led to the recovery of 4.1B-GFP from transfected COS7 cells (Fig.3E, lane 4, Bound). In contrast, HA-SynCAM1 Δ FERMb failed to co-immunoprecipitate 4.1B-GFP (Fig.3E, lane 7, Bound), while deletion of the PDZ binding domain (HA-SynCAM1 Δ PDZIIb) left the interaction with 4.1B intact (Fig.3, lane 8, Bound). Similarly, deletion of the FERM domain of 4.1B blocked recovery of 4.1B (Fig.3, lane 6, Bound), whereas deletion of the similar sized C-terminal domain (CTD; Fig.3B) did not affect interaction with HA-SynCAM1 (Fig.3E, lane 5, Bound). In conclusion, we have demonstrated that the interactions between SynCAM1 and protein 4.1B require the FERM binding domain of SynCAM1. Similarly, protein 4.1B's localization to SynCAM1 at the membrane and its effect on NMDAR recruitment is dependent upon its FERM domain.

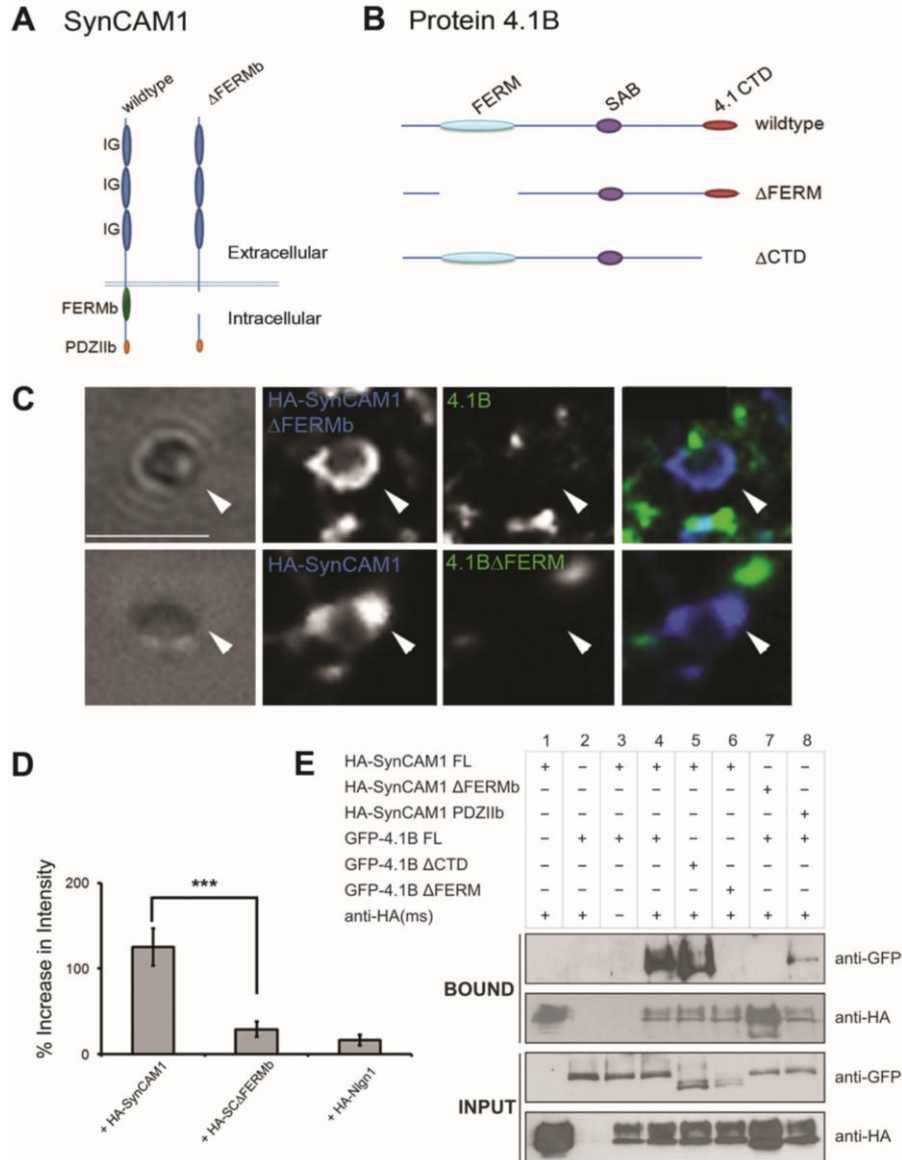


Figure 3. Direct interactions between SynCAM1 and protein 4.1B are mediated via key protein-protein interaction domains. **(A)** Model depicting known protein-protein interaction domains for SynCAM1 and the deletion mutant HA-SynCAM1ΔFERMb. **(B)** Model depicting known protein-protein interaction domains for protein 4.1B and the deletion mutants 4.1BΔFERM and 4.1BΔCTD. **(C)** Images showing the lack of recruitment of protein 4.1B to sites of contact with microspheres when mutant proteins were transfected. **(D)** Quantification of localization of protein 4.1B to microspheres in the presence of either HA-SynCAM1 full length, HA-SynCAM1ΔFERMb, or Nlg1. Protein 4.1B can only be recruited to adhesion sites with microspheres via full length SynCAM1 ($p < 0.001$, $n = 15$). Error bars represent s.e.m. **(E)** Immunoprecipitation experiments confirm the specificity of the direct interaction between SynCAM1 and protein 4.1B. Recombinant and tagged versions of SynCAM1 (HA-SynCAM1) and 4.1B (GFP-4.1B) were immunoprecipitated using an antibody to the HA tag. Bound proteins and input

proteins were visualized in Western blots using antibodies to the tags (anti-GFP and anti-HA). Deletion of the PDZ binding domain of SynCAM1 (HA-SynCAM1 Δ PDZIIb) and the C-terminal domain of 4.1B (GFP-4.1B Δ CTD) did not affect the interaction of these two partners. In contrast, deletion of the FERM binding domain of SynCAM1 (HA-SynCAM1 Δ FERMb) and the FERM domain of protein 4.1B (GFP-4.1B Δ FERM) completely abolished the interaction of SynCAM1 and protein 4.1B.

Protein 4.1B enhances synaptogenic properties of SynCAM1

Given the strong effect of protein 4.1B on the localization of NMDARs to sites of adhesion in the CAMRA, we decided to determine whether incorporation of protein 4.1B enhanced the development of a functional postsynaptic apparatus by using an HEK293 cell/neuronal co-culture assay (Fu et al., 2003). It was previously demonstrated that neurons co-cultured with non-neuronal cells expressing SynCAM1 formed functional presynaptic contacts onto those heterologous cells (Biederer et al., 2002; Sara et al., 2005). It is thought that SynCAM1 expressed in this fashion stabilizes contact with axon terminals through binding of its transsynaptic partner located in those terminals. Activity from these stabilized axons can then be sensed at the HEK cell via co-transfected glutamate receptors. If a molecule such as 4.1B should have the ability to enhance the localization of functional glutamate receptors to the sites of contact with the neurons, then we reasoned that this effect would be reflected in the properties of the mEPSC's measured in this assay.

First, we transfected HEK293 cells with SynCAM1 and NMDAR subunits (NR1 and NR2B) and co-cultured these cells with cerebellar granule neurons. Electrophysiological analysis verified the existence of synaptic currents resembling endogenous neuron-neuron synaptic responses (Fig.4A). Nearly 53% ($52.6 \pm 2.8\%$) of HEK293 cells transfected with NMDAR subunits and SynCAM1 showed miniature excitatory postsynaptic currents (mEPSCs) in the presence of TTX (Fig.4B), while mEPSCs could only be detected in 9% ($8.4 \pm 1.2\%$) of HEK293 cells transfected with only the NMDARs and GFP. This suggests that functional presynaptic terminals are forming onto HEK293 cells expressing NMDARs. Due to the high affinity of NMDARs for glutamate (Hollmann and Heinemann, 1994), it is impossible to determine whether NMDARs are localized to the 'synaptic' sites.

The addition of protein 4.1B to SynCAM1 and NMDAR transfected HEK293 cells resulted in a significant, 30% increase in the number of cells with recordable NMDAR-mEPSCs over SynCAM1 alone ($82.2 \pm 11.8\%$, $p < 0.05$, $n = 20$; Fig.4A and B). The increase in the percentage of cells with detectable mEPSCs was abolished by either removing the FERM binding domain in SynCAM1 (SynCAM1 Δ FERMb) or the FERM domain from protein 4.1B (4.1B Δ FERM; Fig. 4B). Similarly, addition of CASK, an effector molecule that interacts with SynCAM1 (Fig.2C and Supplemental Fig.1), but that did not significantly recruit NMDARs in the CAMRA (Fig.2B), did not increase the number of cells with detectable NMDAR mEPSCs above SynCAM1 alone (Fig.4B). These results suggest that 4.1B may either be increasing the localization of NMDARs to synaptic sites, as suggested by the CAMRA, or that protein 4.1B may act to increase the adhesive nature of SynCAM1 and thereby improve the formation of presynaptic terminals onto HEK293 cells.

Detailed analysis of the NMDAR-mediated mEPSC events revealed that the addition of 4.1B significantly enhanced mEPSC frequency onto HEK293 cells (300% vs. SynCAM1 alone, $p < 0.05$; $n = 10$; Fig.4A and C), when compared to cells transfected with just SynCAM1 alone. This effect was abrogated by deletion of the SynCAM-binding FERM domain (Fig.4C) and was not elicited by CASK (data not shown). Despite these strong effects on mEPSC frequency, it was surprising that we did not observe a significant increase in the peak amplitude of NMDA-mEPSCs as we expected given the CAMRA results (Fig.4D). However, we noticed that in about 35% of HEK293 cells co-expressing SynCAM1 and protein 4.1B a proportion of NMDAR-mEPSC events were larger than any observed in other experimental groups (vs. SynCAM1 only, $p = 0.085$, $n = 10$; Fig.4A, lower panel, and D). One possibility for why this effect did not strongly bear out in a significant deviation of the group mean is that we lack strict control over the expression levels of NMDARs in transfected HEK293 cells, and this particular effect may strongly depend on the levels of NMDARs present.

As already mentioned, NMDARs have a very high affinity for glutamate and may well be detecting presynaptically-released glutamate at non-synaptic sites in addition to those closely juxtaposed to axon terminals. The results of the CAMRA (Fig.2) strongly support that 4.1B facilitates an increase in the concentration of NMDARs at sites of

contact, however, it does not exclude the possibility that 4.1B may also enhance the stabilization of functional presynaptic terminals transsynaptically via SynCAM1. To test whether 4.1B's effects on the frequency of mEPSCs in the HEK293 co-culture study was at least partially due to a change in the number of stabilized presynaptic terminals, we labeled the co-cultured HEK293 cells with antibodies to SynapsinI, PSD95 and Gephyrin. We then quantified the area of SynapsinI positive regions located on transfected HEK293 cells that did not colocalize with the postsynaptic markers PSD95 or Gephyrin. We found that SynCAM1 expressed in HEK293 cells significantly increased the proportion of SynapsinI positive surface area as compared to GFP transfected only ($8.9 \pm 1.5\%$ vs. $4.9 \pm 0.9\%$, $p < 0.02$, $n=17$; Fig.4F) confirming previous studies of SynCAM1's ability to induce presynaptic differentiation on its own (Biederer et al., 2002; Sara et al., 2005). Surprisingly, the addition of 4.1B to SynCAM1 transfected HEK293 cells caused a significant increase in Synapsin I labeling relative to SynCAM1 only cells ($8.9 \pm 1.5\%$ vs. $13.9 \pm 1.7\%$, $p < .02$, $n = 17$; Fig.4E&F). Experiments using either of the deletion mutants, SynCAM1 Δ FERMb or 4.1B Δ FERM, showed that the FERM binding interaction was necessary for the increase in presynaptic stabilization that addition of protein 4.1B yielded above that of SynCAM1 alone (SynCAM1 vs. SynCAM1 Δ FERMb + 4.1B: $p = 0.26$, $n = 14$; SynCAM1 vs. SynCAM1 + 4.1B Δ FERM: $p = .49$ $n = 13$; Fig.4F). This result suggests that cytosolic protein 4.1B acts to enhance the formation of presynaptic terminals onto SynCAM1-expressing HEK293 cells.

If the enhancement of mEPSC frequency that 4.1B elicits can be wholly accounted for by the enrichment of presynaptic terminals that we measured with SynapsinI labeling, then co-transfected glutamate receptors of the AMPA type could register similar changes in mEPSC frequency when 4.1B is present in conjunction with SynCAM1. To test this, the co-culture analysis was also performed by transfecting GluR1 in place of NR1/NR2B. In this case, SynCAM1 alone was again sufficient to cause a significant increase in the percentage of cells with recordable AMPAR currents over control transfection conditions ($p < 0.05$, $n = 8$). However, the co-expression of protein 4.1B with SynCAM1 did not further increase the proportion of HEK293 cells with recordable AMPAR-mEPSCs (data not shown). This suggests that the observed morphological increase in presynaptic contact due to the addition of protein 4.1B (Fig.4F)

was not enough to significantly enhance mEPSC detection via AMPA type receptors. Taken together, the HEK/neuron co-culture studies, in conjunction with the CAMRA experiments, suggest that SynCAM1 interacts with 4.1B to facilitate enhanced localization of functional NMDARs to sites of contact and to enhance presynaptic stabilization.

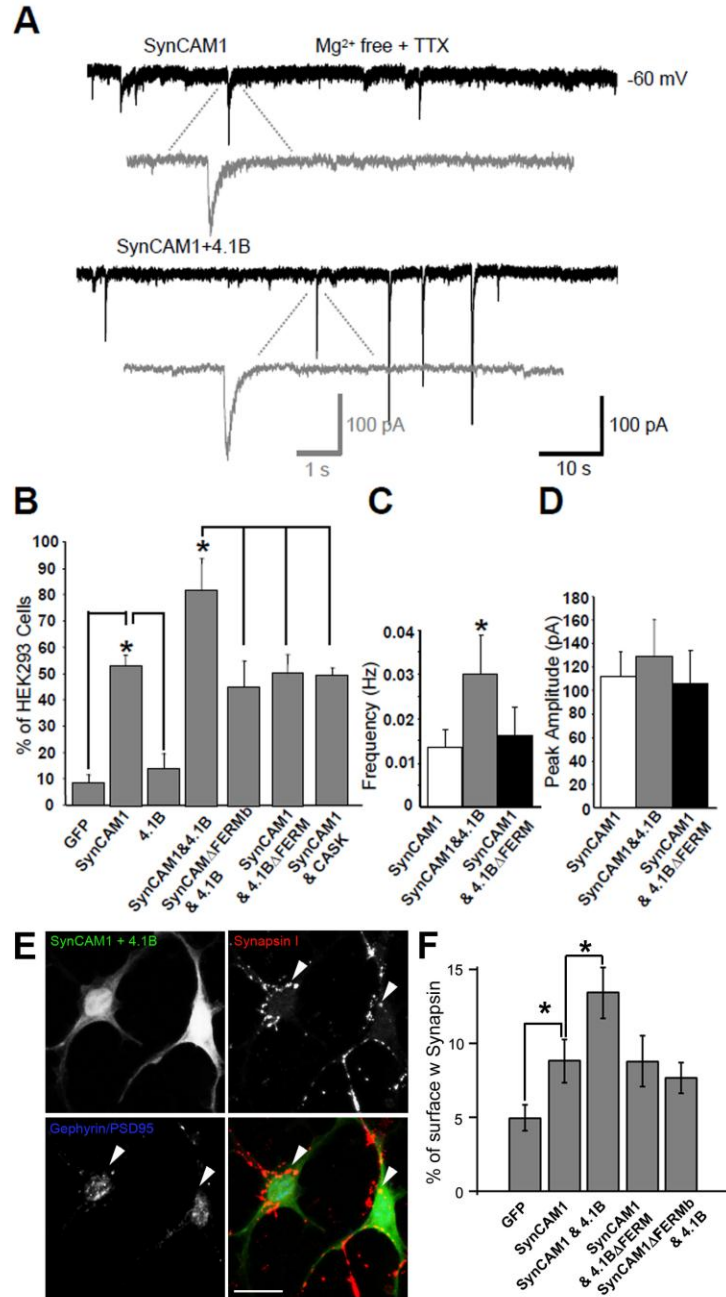


Figure 4. Protein 4.1B specifically enhances measures of NMDA-EPSCs and presynaptic differentiation in the HEK293 cell/neuronal co-culture assay. **(A)** Representative recordings of NMDA-mEPSCs from HEK293 cells transfected with either SynCAM1 and the NMDAR subunits (NR1/NR2B, top), or SynCAM1, 4.1B and the NMDAR subunits (bottom). The synaptic currents were measured in Mg²⁺-free extracellular solution with TTX. Gray traces are magnified individual NMDAR-mEPSCs. **(B)** Percentage of transfected HEK293 cells with recordable NMDA-mEPSCs in each experimental condition. SynCAM1 significantly enhanced recorded NMDA-mEPSCs over control conditions ($p < 0.05$, $n > 20$). Protein 4.1B together with SynCAM1 significantly increased the number of cells with recordable currents over SynCAM1 alone

conditions ($p < 0.05$, $n > 20$), while perturbing interactions mediated via the FERM domain canceled this increased activity. **(C)** Protein 4.1B significantly increased the frequency of NMDA-mEPSCs when compared to SynCAM1 alone conditions or the 4.1B Δ FERM mutant ($p < 0.05$, $n = 10$). **(D)** Cotransfection of protein 4.1B did not significantly increase the amplitude of NMDA-mEPSCs ($p = 0.09$, $n = 10$). Error bars represent s.e.m. **(E)** Cotransfection of protein 4.1B significantly enhanced presynaptic stabilization. Immunolabeling of HEK293 cells transfected with SynCAM1 and 4.1B (upper left), co-cultured with neurons and labeled for Synapsin I (upper right), PSD-95 and Gephyrin (lower left). Arrows indicate regions of induced presynaptic contact where markers of postsynaptic structures are missing. Scale bar equals 20 μ m. **(F)** Quantification of the percent surface area of transfected HEK293 cells covered with Synapsin I, and not PSD95 or Gephyrin, labeling under different transfection conditions. SynCAM1 significantly enhances percent surface area covered with Synapsin I over GFP conditions ($* = p < 0.02$, $n = 17$) and SynCAM1 plus 4.1B significantly increases percent surface area covered by synapsin I over SynCAM1 alone conditions ($* = p < 0.02$, $n = 17$). Error bars represent s.e.m.

Specific effect of protein 4.1 family members on glutamate receptor recruitment

We decided to confirm the specificity of the SynCAM1-4.1B effect on NMDARs and not AMPARs using our CAMRA. When we co-expressed HA-SynCAM1, 4.1B and the GluR1 subunit in COS7 cells and applied microspheres directed to HA-SynCAM1, we found that there was significantly less clustering of GluR1 relative to the induced recruitment of NR1/NR2B described earlier ($34.9 \pm 16.8\%$ vs. $148.7 \pm 13.3\%$, $p < 0.001$, $n = 15$; Fig.5A & D). This suggests there are specific mechanisms by which protein 4.1B recruits only NMDARs (NR1/NR2B).

To determine whether lack of recruitment of GluR1 is not a deficit of the CAMRA, we considered generating an alternative adhesion complex in COS7 cells that might recruit GluR1. Protein 4.1B belongs to a family of proteins that were first identified in erythrocytes (An et al., 1996) and later found to have a significant role in stabilizing the cytoskeleton by promoting the association of F-actin with tetrameric spectrin (Correas et al., 1986). The family members, coded for by distinct genes, are differentially expressed in distinct cell populations (Hoover and Bryant, 2000; Parra et al., 2000; Peters et al., 1998), but all may potentially interact with SynCAM1 via their conserved FERM domains. In particular, 4.1N is an additional family member highly expressed in neurons that localizes to postsynaptic specializations (Scott et al., 2001). Protein 4.1N interacts directly with GluR1 and promotes its recruitment to postsynaptic

densities and to the plasma membrane (Shen et al., 2000). Therefore, we determined whether SynCAM1/4.1N could form an adhesion complex at microspheres and whether this would promote GluR1 clustering (Fig.5B, C and E). As predicted, protein 4.1N is recruited to HA-SynCAM1 clusters at microspheres ($100 \pm 12.7\%$, $n = 15$; Fig.5B). Additionally, GluR1 specific clustering was induced by this complex, while NR1/NR2B could not be recruited to HA-SynCAM1/4.1N adhesion sites ($139.8 \pm 24.4\%$ vs. $33.4 \pm 7\%$, $p < 0.001$, $n = 15$; Fig.5C & E). Thus, our experiments identify an additional SynCAM1 effector molecule, protein 4.1N. Our results further suggest that NMDAR and AMPAR recruitment specificity may be mediated by differential CAM / effector adhesion complexes.

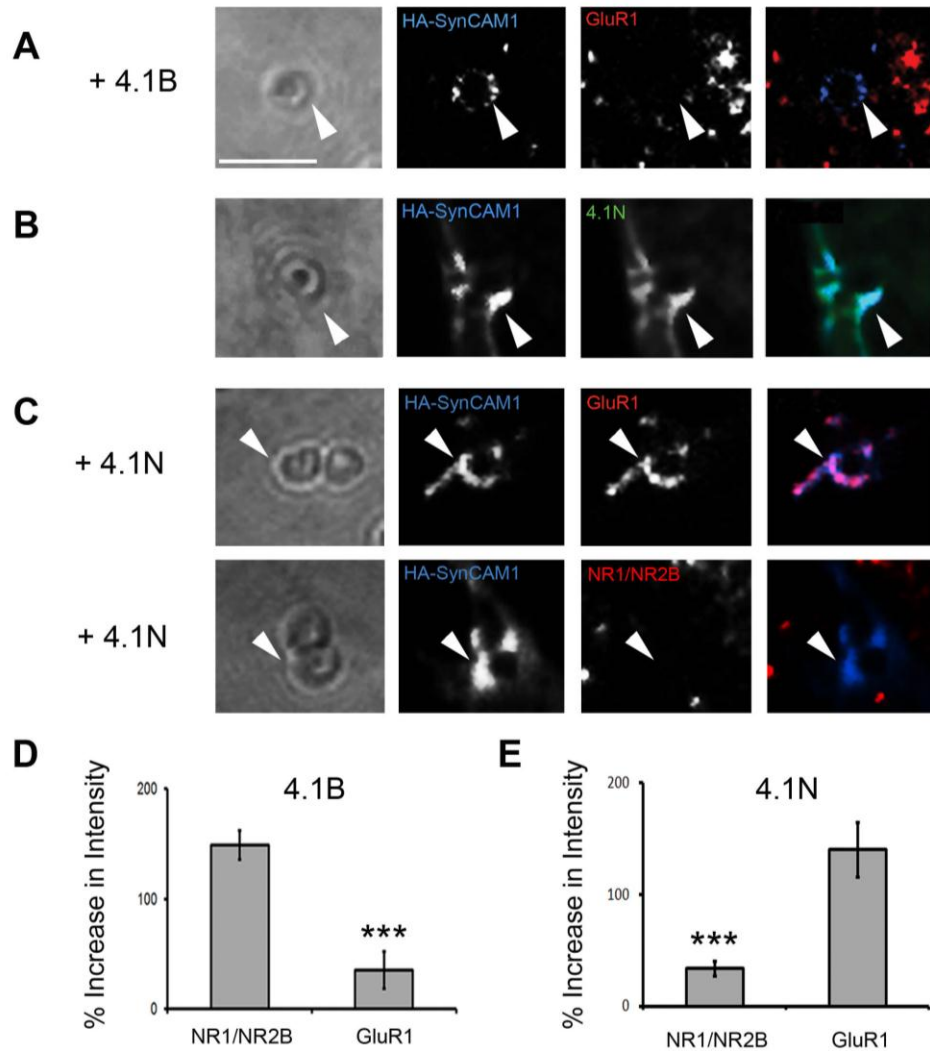


Figure 5. Specificity of 4.1 effector proteins to glutamate receptor recruitment. **(A)** Protein 4.1B did not significantly enhance recruitment of AMPA type receptors (GluR1) as compared to NR1/NR2B type receptors (arrowhead). Scale bar equals 2 μ m. **(B)** Protein 4.1N was recruited to sites of HA-SynCAM1 accumulation in contact with microspheres (arrowheads). **(C)** Protein 4.1N induced significant recruitment of GluR1, but not NR1/NR2B, containing receptors to adhesion sites at microspheres (arrowheads). **(D)** Quantification of GluR1 recruitment vs. NR1/NR2B recruitment via protein 4.1B ($34.9 \pm 16.8\%$ vs. $148.7 \pm 13.3\%$, $p < 0.001$, $n = 15$). **(E)** Quantification of GluR1 recruitment vs. NR1/NR2B recruitment via protein 4.1N ($139.8 \pm 24.4\%$ vs. $33.4 \pm 6.95\%$, $p < 0.001$, $n = 15$). Error bars represent s.e.m.

Synaptic localization of protein 4.1B

Intrigued by these initial observations in the COS7 and HEK293 cell culture assays, we sought to complete a series of experiments to determine the relevance of protein 4.1B function in the neuronal context. Previous biochemical studies have reported that 4.1B is detected in PSD fractions prepared from rat forebrain, and could therefore be localized to excitatory synapses *in vivo* (Scott et al., 2001). To confirm synaptic localization of 4.1B, we immunolabeled cultured hippocampal neurons with antibodies to 4.1B and the markers Synapsin I and PSD-95 at 4, 8 and 12 days *in vitro* (DIV). Synapsin I is a protein that associates with synaptic vesicles and is thus located in presynaptic terminals, while PSD-95 is located in the glutamatergic postsynaptic density (Cho et al., 1992; Fletcher et al., 1991; Hunt et al., 1996). The immuno-labeling of protein 4.1B revealed a highly punctate distribution at all ages examined (Fig.6A). At 4DIV, an age at which very few synapses have formed (Washbourne et al., 2002), protein 4.1B was localized in distinct puncta (3.7 ± 0.5 puncta/20 μ m, n = 10), some of which ($3.4 \pm 1.2\%$ of total 4.1B puncta) were colocalized with the few synapses present, i.e. sites of colocalization of Synapsin I and PSD-95. The vast majority (81.9 ± 4.9 puncta/20 μ m, n = 10) were not colocalized with either Synapsin I or PSD-95 (Fig.6A,C) as 4.1B puncta far outweighed the presence of either Synapsin or PSD-95 puncta. However, almost all synapses present in the cultures at 4DIV (and at all other time points examined) demonstrated colocalization of protein 4.1B immunoreactivity ($84.6 \pm 7.7\%$, $98.5 \pm 0.8\%$, $91.6 \pm 2.1\%$ of synapses at 4, 8 and 12 DIV, respectively: Fig.6B). Thus, as the number of synapses increased during development *in vitro*, the distribution of 4.1B puncta switched from not being associated with either pre- or postsynaptic markers to being colocalized with both Synapsin I and PSD-95 (Fig.6C). Interestingly, the intensity of the puncta decreased with age (Supplementary Figure 2), suggesting that the presence of protein 4.1B at synapses decreases with increasing maturity. Taken together, these results strongly suggest a function for 4.1B at synapses, and that protein 4.1B may play an important role during the early phases of synapse formation.

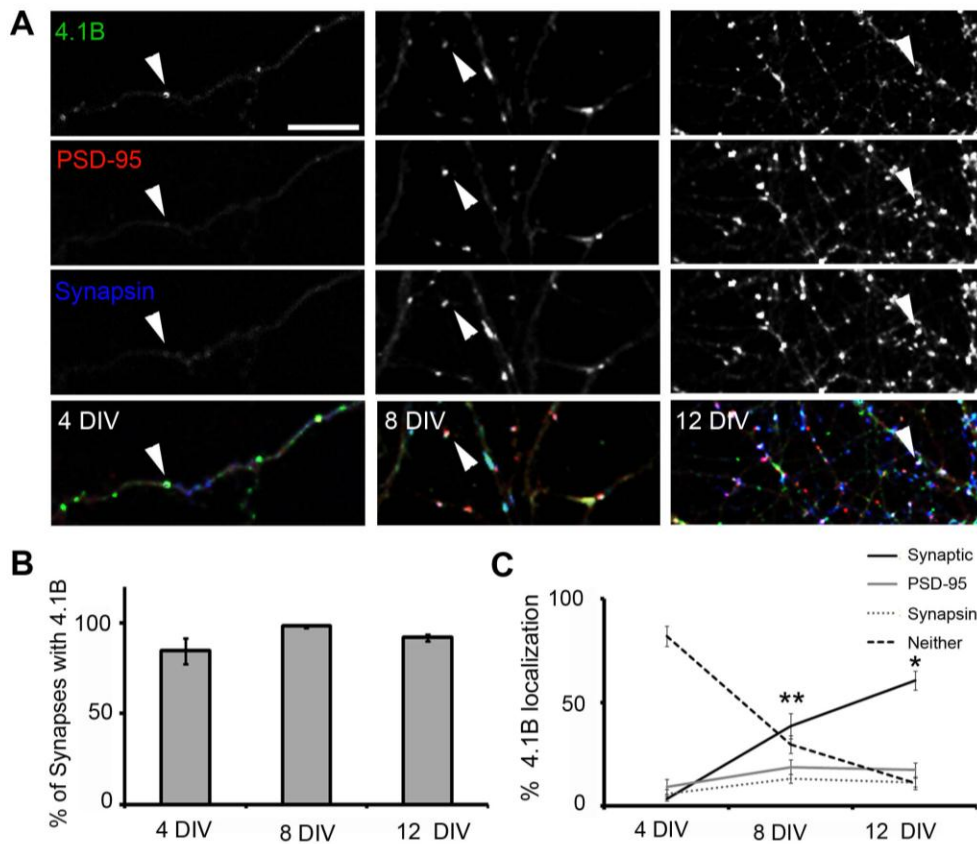


Figure 6. Localization of endogenous protein 4.1B in cultured hippocampal neurons. **(A)** Immunolabeling of protein 4.1B (green) with the synaptic markers PSD-95 (red) and Synapsin I (blue) at 4, 8 and 12 DIV. Arrowheads indicate examples of protein 4.1B localization. Synaptic sites, areas enriched in all three proteins are white in the merged image (bottom row). Scale bar equals 10 μ m. **(B)** Quantification of the percentage of synapses that show protein 4.1B localization over time in culture. Error bars represent s.e.m. **(C)** Quantification of the distribution of protein 4.1B puncta as determined by colocalization with synapsin I, PSD-95, both (Synaptic) or neither markers. Error bars represent s.e.m. (* $p < 0.05$, ** $p < 0.01$, $n = 10$).

Protein 4.1B enhances synaptic localization of NMDARs in hippocampal neurons

Because protein 4.1B is localized to synapses in hippocampal neurons (Fig.6), it was interesting to examine whether 4.1B could recruit NMDARs to “true” synapses, analogously to recruitment seen in the CAMRA and in HEK293/CGC co-cultures (Fig.2 and 4). To specifically label surface exposed NMDARs, we transfected cultured hippocampal neurons at 7 DIV with a plasmid to express GFP-tagged NMDAR subunit 2B (GFP-NR2B). We also cotransfected expression plasmids for 4.1B or a short hairpin

RNA (shRNA) construct to 4.1B, to manipulate the expression levels of protein 4.1B. 24 hours later, we labeled GFP-NR2B subunits present at the neuronal surface by exposing live, transfected neurons to GFP antibodies at 4°C (Washbourne et al., 2004b). Subsequently, neurons were fixed and permeabilized to visualize total GFP-NR2B (Fig.7A) and synaptophysin.

We first characterized the effectiveness of the shRNA. Expression of the 4.1B shRNA resulted in a 25% decrease in the intensity of 4.1B puncta 24 hours after transfection (from 9216 ± 621 a.u. to 6895 ± 423 a.u. for ctl and 4.1B shRNA, respectively, $n = 11$, $p < 0.05$). This may be an underestimation of knock-down as we did not take into account diffuse dendritic and cell body levels. Furthermore, knockdown was only performed for 24 hours, a relatively short time period. This short time period was important as we did not want high levels of GFP-NR2B expression to compromise trafficking pathways to synapses. Additionally, we attempted to target a time period in development when 4.1B production would be high to compensate for the short expression period of the shRNA. Despite the relatively weak reduction in 4.1B levels with this shRNA protocol, we measured a significant reduction in the normalized intensity of punctate surface GFP-NR2B at synapses, as determined by colocalization with synaptophysin, when compared to mismatch (Ctl) shRNA ($71.8\% \pm 10.6$ of ctl, $n = 11$, $p < 0.05$; Fig. 7B). This reduction in NR2B surface intensity was not apparent at non-synaptic sites ($83.1\% \pm 10.2$ of ctl, $n = 11$, $p = 0.3$; Fig.7B). We also measured the ratio of surface to total GFP-NR2B to determine whether 4.1B was involved in delivery of NMDARs to the plasma membrane, as has been suggested for 4.1N (Shen et al., 2000). The ratio of surface-labeled to total GFP-NR2B subunits was unchanged in all conditions ($n=11$ per condition, $p > 0.05$), suggesting that 4.1B specifically recruits NMDARs to synapses including both internal and surface pools.

In contrast to knock-down with shRNA, overexpression of protein 4.1B resulted in an enhancement of the surface localization of GFP-NR2B at synapses ($163.4\% \pm 9.7$ of ctl, $n = 11$, $p < 0.05$; Fig.7B). The increase in surface localization of NR2B to synapses was abrogated by deletion of the FERM domain (Δ FERM, $122.4\% \pm 10.1$, $n = 11$, $p = 0.064$; Fig. 7B). These results suggest that protein 4.1B plays an important role in the

delivery of NMDAR subunits to synapses in hippocampal neurons, and that the FERM domain through which it may interact with SynCAM1 is necessary for this function.

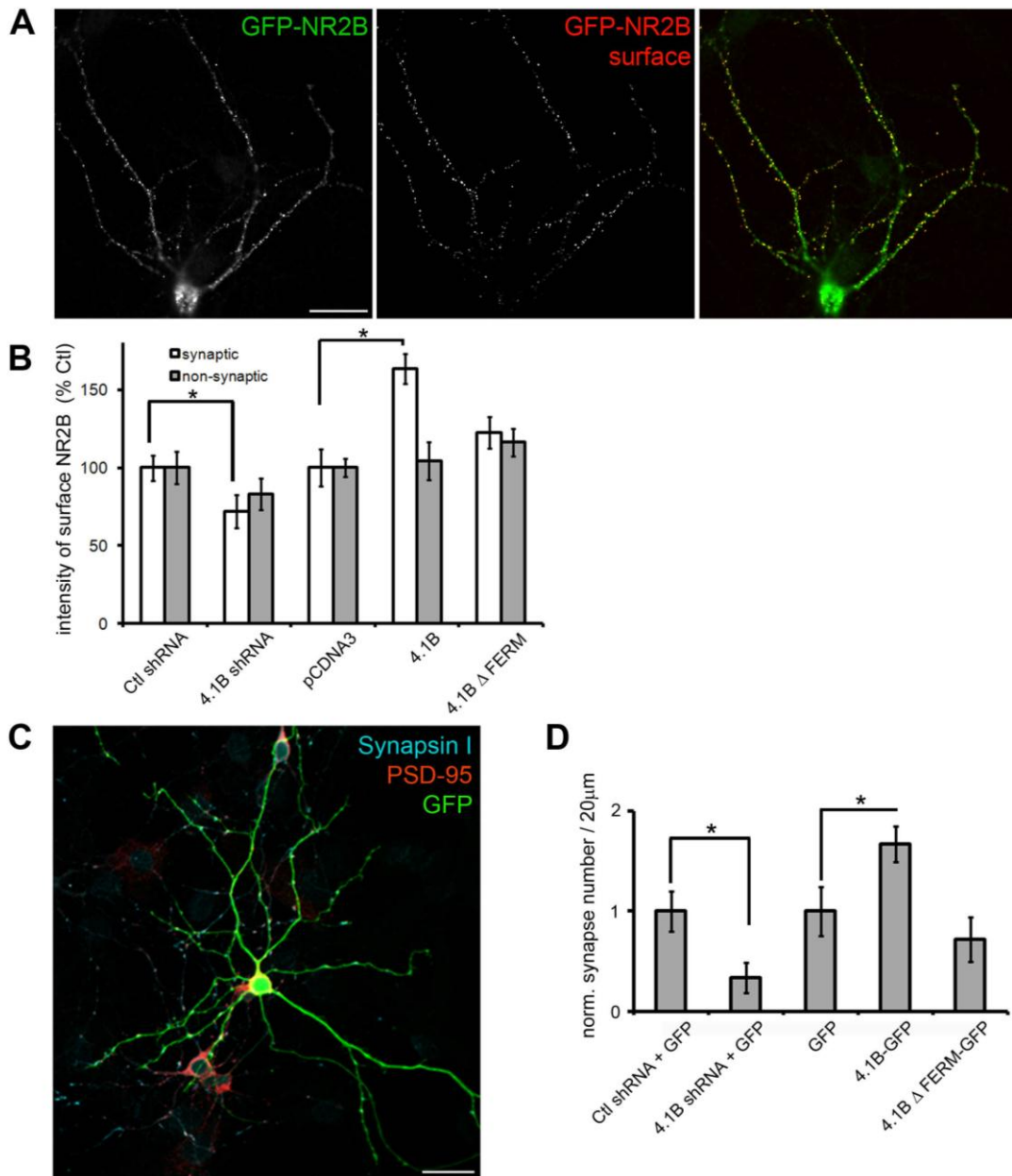


Figure 7. Protein 4.1B enhances NMDAR localization at synapses. **(A)** Transfected hippocampal neurons were incubated with antibodies to GFP (rb) at 4°C to label surface GFP-NR2B (surface, red) and subsequently fixed, permeabilized and reincubated with GFP antibodies (ms) to reveal total GFP-NR2B (total, green) and antibodies to synapsin I (not shown). Scale bar = 50 μm. **(B)** Quantification of the intensity of surface GFP-NR2B puncta at synaptic and non-synaptic sites in hippocampal neurons expressing shRNA to 4.1B (4.1B shRNA), control shRNA (Ctl shRNA), 4.1B and 4.1B ΔFERM and empty

vector (pCDNA3) for 24 hours. Error bars represent s.e.m. (* $p < 0.05$). (C) Neurons expressing shRNA to 4.1B (4.1B shRNA) and GFP, control shRNA (Ctl shRNA) and GFP, 4.1B-GFP, 4.1B Δ FERM-GFP or GFP alone for 48 hours were immunolabeled with antibodies to synapsin I and PSD-95. Scale bar = 50 μ m. (D) Quantification of the numbers of synapses per 20 μ m of dendrite as determined by the colocalization of synapsin I and PSD-95. Error bars represent s.e.m. (* $p < 0.05$, $n = 11$).

Protein 4.1B enhances synaptogenesis in hippocampal neurons

In our co-culture experiments between CGCs and HEK293 cells, we noted a significant increase in both NMDAR mEPSC frequency and percentage of cells with recordable mEPSCs with cotransfection of protein 4.1B and SynCAM1, suggesting a great facilitation of functional synapse formation between neurons and HEK293 cells. (Fig.4). To test whether protein 4.1B exhibited a similar effect on functional synapse formation in neurons, we either increased or decreased 4.1B expression levels for two days (from 6 DIV to 8 DIV) and immunolabeled neurons with antibodies to the pre- and postsynaptic markers SynapsinI and PSD-95, respectively (Fig.7C). Quantification of the numbers of synapses, i.e. sites of colocalization of SynapsinI and PSD-95, revealed that a reduction in protein 4.1B expression levels due to shRNA expression results in a 3-fold decrease in synapse number (from 1.13 ± 0.2 synapses/20 μ m to 0.38 ± 0.06 synapses/20 μ m for ctl and 4.1B shRNA respectively, $n = 11$, $p < 0.05$; Fig. 7D). In contrast, increasing 4.1B expression levels by expressing 4.1B-GFP increased synapse number 1.7-fold (from 0.88 ± 0.2 synapses/20 μ m to 1.48 ± 0.3 synapses/20 μ m for GFP and 4.1B-GFP, respectively, $n = 11$, $p < 0.05$; Fig.7D). Synapse number was normalized to control conditions. This increase in synapse number was completely abolished by deletion of the FERM domain (4.1B Δ FERM-GFP, 0.64 ± 0.1 synapses/20 μ m, $n = 11$, $p > 0.05$; Fig.7D). This suggests that 4.1B is sufficient and necessary to drive the formation of synapses between hippocampal neurons in culture and that this activity is dependent on the FERM domain.

Protein 4.1B specifically enhances NMDAR currents in hippocampal neurons

To further characterize the potential role of protein 4.1B on NMDAR recruitment in neurons, we analyzed the functional consequences of manipulating protein 4.1B expression levels in dissociated hippocampal neuronal culture. We were interested in whether protein 4.1B exerted effects analogous to those observed in our other assays. We recorded NMDA-mEPSCs in the presence of TTX, NBQX and BMR in a solution lacking Mg^{2+} , as previously described in detail (Fu et al., 2005). To minimize variability due to cell heterogeneity and to measure synaptic currents with optimal space clamp and resolution, we selected hippocampal neurons with relatively small cell body size (15-20 μ m) and simple dendritic arborization. We compared recordings from neurons expressing either GFP, 4.1B-GFP, 4.1B Δ FERM-GFP or 4.1B shRNA with GFP at 12-14 DIV (Fig.8). Protein 4.1B overexpression significantly increased both mean frequency (0.09 ± 0.02 Hz in GFP cells, 0.17 ± 0.01 Hz in 4.1B-GFP expressing cells, $p < 0.05$; $n > 30$) and amplitude of NMDA-mEPSCs as compared to GFP expressing cells (19.2 ± 3.3 pA in GFP cells, 26.4 ± 2.7 pA in 4.1B-GFP cells, $p < 0.05$; $n > 30$; Fig.8A-C), whereas the deletion of the FERM domain in 4.1B prevented the increase in frequency and amplitude (0.12 ± 0.03 Hz, 18.4 ± 2.3 pA, respectively). The expression of 4.1B shRNA significantly decreased the frequency of NMDAR mEPSCs (0.05 ± 0.02 Hz), but not peak amplitude (15.6 ± 3.7 pA, $p = 0.09$, $n > 30$). It is possible that the knock-down by the 4.1B shRNA was not sufficient to significantly reduce the NMDAR mEPSC peak amplitude. However, our results are consistent with the idea that 4.1B plays a role in recruiting NMDARs to synapses in cultured hippocampal neurons.

The NR2B subunit of the NMDAR has been shown to be more prevalent at synapses during development, with NR2A gradually taking over at mature synapses (Tovar and Westbrook, 1999). NR2B subunits cause a slow decay time component in NMDAR current kinetics (Kohr and Mody, 1994; Kohr and Seeburg, 1996; Monyer et al., 1994). Upon analysis of the decay time constant of NMDA-mEPSCs (τ_w) from our 4.1B-expressing cultured hippocampal neurons, we noticed that decay was significantly prolonged when compared to control transfected cells (212.5 ± 32.9 ms in GFP control cells, 275.6 ± 25.2 ms in 4.1B expressing cells, $p < 0.05$; $n > 30$; Fig.8D). No significant

effect on τ_w was seen in neurons expressing 4.1B Δ FERM or 4.1B shRNA (198.6 ± 21.8 ms in 4.1B Δ FERM cells, 188.3 ± 38.4 ms in 4.1B shRNA cells, $p = 0.58$; Fig.8D). The effect on τ_w indicates that protein 4.1B might specifically increase the recruitment of NR2B-containing NMDARs to synaptic sites. To further test this hypothesis, we recorded mEPSCs in the presence of ifenprodil ($10 \mu\text{M}$), as it is a specific antagonist of NR1/NR2B-containing NMDARs (Mott et al., 1998). Changes in our measures in the presence of ifenprodil should then reflect the proportion of the NMDARs containing only NR1 and NR2B subunits. Application of ifenprodil to neurons overexpressing 4.1B resulted in a 73% ($73 \pm 5\%$, $n = 12$) decrease in mEPSC frequency compared to before ifenprodil application (Supplementary Fig. 3). This inhibition was only marginally decreased in the GFP only expressing neurons ($69 \pm 2\%$, $n = 12$, $p > 0.05$). This suggests a potentially small increase in the NR2B only population of NMDARs when 4.1B is overexpressed. However, we did measure a significant difference between 4.1B overexpression and 4.1B knock-down with shRNA ($60 \pm 4\%$, $p = 0.03$). Taken together, the small changes in ifenprodil sensitivity might reflect the presence of heterotrimeric NR1/NR2A/NR2B NMDARs containing, which are likely not as sensitive to ifenprodil as NR1/NR2B NMDAR subtypes. Nevertheless, our results are consistent with the idea that protein 4.1B enables the recruitment of NMDARs containing NR2B subunits to synapses.

To test whether the effects of protein 4.1B were specific to NMDARs and not to AMPARs, we recorded from transfected hippocampal neurons in the presence of BMR and TTX. No significant effects were seen for AMPAR-mEPSC mean frequency (0.48 ± 0.08 Hz in GFP cells, 0.56 ± 0.14 Hz in 4.1B-GFP overexpressing cells, $p = 0.79$; $n = 16$) or amplitude of mEPSCs (40.1 ± 10.3 pA in GFP cells, 57.8 ± 13.7 pA in 4.1B-GFP cells, $p = 0.51$; $n = 16$; Fig.8E-G). Taken together, these results demonstrate that protein 4.1B exhibits the same glutamate receptor specificity as characterized in our CAMRA and HEK293 co-culture assays.

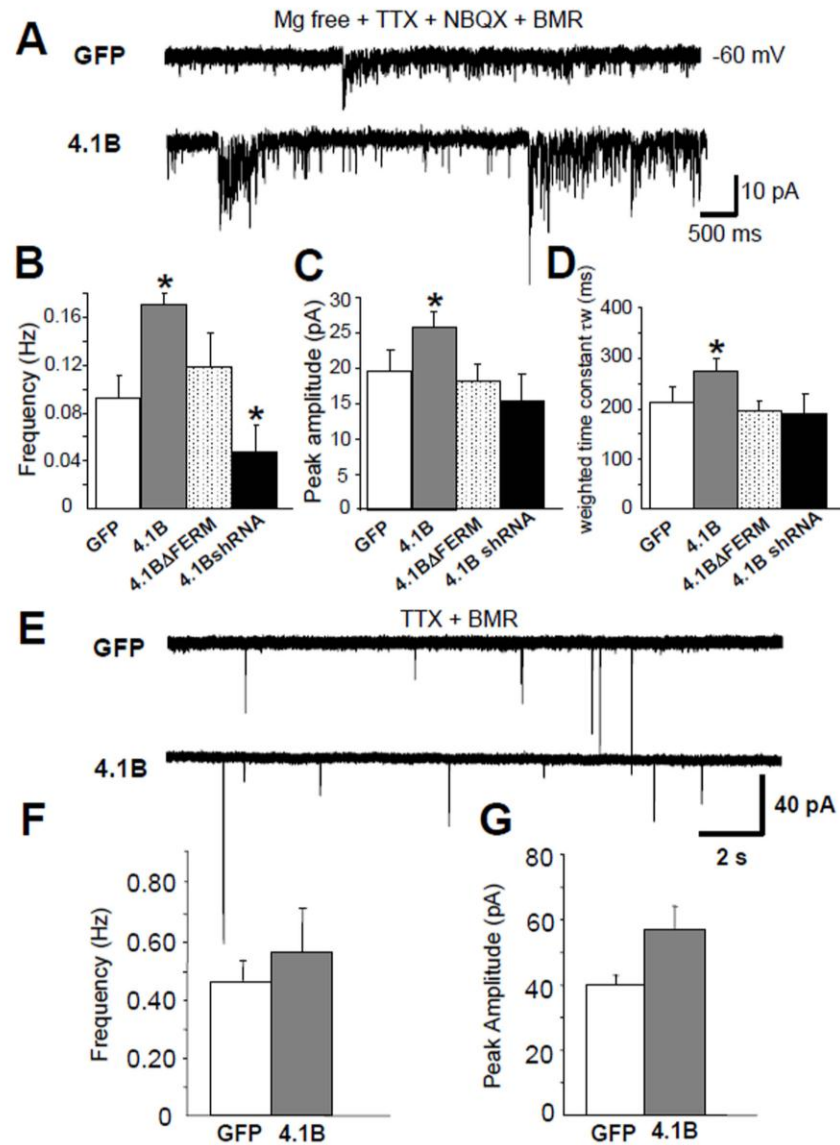


Figure 8. Protein 4.1B enhances NMDAR mediated synaptic events in cultured hippocampal neurons. **(A)** Representative traces of isolated NMDA-mEPSCs recorded from hippocampal neurons (12-14 d.i.v) in Mg²⁺ free solution with TTX (0.5 μM), NBQX (5 μM) and BMR (50 μM) under different transfection conditions. **(B)** Overexpression of protein 4.1B increases and knock-down of 4.1B with shRNA decreases NMDA-mEPSC frequency (p < 0.05, n >30) **(C)** amplitude (p < 0.05, n >30) and **(D)** τ_w (p < 0.05, n >30) in hippocampal neurons. **(E)** Representative traces of isolated AMPA-mEPSC recordings in hippocampal neurons in presence of TTX (0.5 μM) and BMR (50 μM) in regular ECS with Mg²⁺ **(F)** 4.1B-GFP did not significantly affect the frequency of AMPA-mEPSCs (p = 0.79, n=16) or **(G)** amplitude (p = 0.51, n=16). Error bars represent S.E.M.

3. DISCUSSION

While a large number of proteins have been localized to the postsynaptic density and are thought to contribute towards its development and function (Reviewed in (Dillon and Goda, 2005; Feng and Zhang, 2009), it remains unclear which molecular interactions are sufficient to recruit glutamate receptors to synaptic sites early in synapse development. In particular, the relatively novel synaptic cell adhesion molecule SynCAM1 has yet to be shown important for postsynaptic development and, thus, even less is known about its potential interactions leading to receptor recruitment. In this series of studies, we have used a microsphere-based assay, the CAMRA, and an HEK293-neuronal co-culture assay as effective tools to screen potential SynCAM1 effector molecules sufficient to induce glutamate receptor recruitment. We identified protein 4.1B as a specific and potent effector of NMDAR recruitment to SynCAM1 adhesion sites. We also observed that other potential effectors could interact with SynCAM1 (CASK, Syntenin1), but these molecules did not impact NMDAR recruitment to the extent of 4.1B in our assays. Negative results in the case of these experiments do not completely rule out the possibility that these molecule do not play any role in NMDAR trafficking. For example, it was recently discovered that CASK plays a significant role in trafficking of NMDARs to the membrane surface and their localization to synapses in cultured hippocampal neurons (Jeyifous et al., 2009). However, it is clear that this activity of CASK requires that it work in tandem with SAP97, and that manipulations of CASK do not impact measures of synapse formation independently of changes in levels of NR1 at synaptic sites in neurons (Jeyifous et al., 2009). Thus, our assay may truly reflect whether any one type of molecule is sufficient to interact with SynCAM1 to recruit glutamate receptors. Furthermore, in an attempt to determine the degree of specificity that SynCAM1 and protein 4.1B have on the recruitment of glutamate receptor types, we identified 4.1N as an additional SynCAM1 effector molecule sufficient to differentially recruit AMPA type receptors.

In this set of studies we were able to demonstrate three key findings regarding the function of protein 4.1B. Specifically, protein 4.1B facilitated the direct aggregation of NMDARs at sites of contact and adhesion, enhanced morphological measures of presynaptic differentiation, and specifically enhanced the frequency of NMDAR, not

AMPA, mediated mEPSCs. Thus, this is the first report of a role for protein 4.1B at excitatory synapses and is the first demonstration of a potential mechanism by which SynCAM1 may directly participate in the early developmental process of postsynaptic differentiation. The results obtained in COS7 cells and the HEK293 cell/neuron co-culture help clarify that protein 4.1B largely promotes the development of functional postsynaptic structures in neurons containing NMDARs with a very specific composition. First, overexpression of protein 4.1B in neurons enhanced localization of NMDARs to synapses (Fig.7), and increased the peak amplitude of NMDAR-mediated mEPSCs (Fig.8), but not that of AMPAR-mediated mEPSCs. In keeping with this, knock-down of 4.1B with shRNA resulted in a decrease in synaptic levels of NMDARs (Fig.7), however, surprisingly it had no significant effect on peak amplitude (Fig.8). These results suggest specific and potent effects of protein 4.1B specifically on NMDAR recruitment. The significant effect on the peak amplitude of mEPSC in cultured neurons is in line with the direct recruitment effects observed in the CAMRA, while it is surprising that we did not observe a significant increase in peak amplitude of mEPSCs from co-cultured HEK293 cells expressing SynCAM1 and protein 4.1B. As discussed previously, this particular measure in the HEK293 cell co-culture may be more sensitive to the particular levels of NMDARs present in transfected cells, which is a factor that cannot be strictly controlled in the assay. Therefore, we consider this feature a limitation to determining the exact localization and levels of NMDARs in transfected HEK293 cells. However, this limitation is addressed if the other measures obtained in the assay are interpreted in light of the direct recruitment measurements calculated in the CAMRA, where we can more specifically measure localization and levels of NMDARs at sites of adhesion.

For example, the increase in frequency of mEPSCs and percentage of HEK293 cells with recordable synaptic events seen when protein 4.1B is co-expressed with SynCAM1 suggests that either 4.1B is increasing the localization of NMDARs to release sites that would otherwise have been undetectable and/or that 4.1B is enhancing the formation of presynaptic terminals onto HEK293 cells. We conclude that this enhancement of frequency is only partially explained by an increase in presynaptic stabilization onto transfected cells which we quantified by labeling presynaptic terminals in co-culture (Fig.4E &F). However, the enhanced localization of NMDARs specifically

to synaptic release sites presumably augments the detection of NMDAR mediated mEPSCs and contributes significantly to the observed effects of protein 4.1B, especially given that 4.1B does not similarly enhance the detection of AMPAR mediated mEPSCs in co-culture nor hippocampal culture.

Indeed, we do find that the combined data from our assays strongly support that protein 4.1B also has a role in the stabilization of functional presynaptic terminals via trans-synaptic interactions. Our studies using the HEK293 cell / neuronal co-culture assay and the overexpression studies in hippocampal neurons suggest that postsynaptically localized protein 4.1B exerts an effect on presynaptic differentiation or release in addition to its effects on receptor recruitment. The increase in mean mEPSC frequency in hippocampal neurons suggests either an increased number of presynaptic contacts or enhanced vesicle release at existing contacts. This result is supported by labeling of presynaptic terminals in the HEK293cell/neuron co-culture study. However, we repeatedly fail to observe an increase in AMPA mediated mEPSCs in every assay, suggesting that protein 4.1B largely exerts its effect via its NMDAR specific recruitment capabilities postsynaptically. Regardless, protein 4.1B may either (1) act to enhance the adhesive nature of SynCAM1 contact sites, resulting in more release sites, or (2) modulate vesicle release properties in a retrograde fashion through SynCAM1 adhesion to mediate presynaptic differentiation. Thus, protein 4.1B plays a partial role in stabilization or function of presynaptic structures, but further experimentation will be needed to clarify its trans-synaptic role in neurons.

Given that protein 4.1B, a molecule most notably involved in cytoskeletal organization (Sun et al., 2002), exerted such a direct and strong effect on NMDAR recruitment to synapses, it is interesting to consider how it may perform its role at the postsynaptic density. 4.1 family proteins regulate actin dynamics via direct binding through their spectrin-actin binding (SAB) domain. Furthermore, NMDAR localization to synaptic sites requires significant actin stabilization, while non synaptic clusters of NMDARs can be maintained even when the actin cytoskeleton is destabilized (Allison et al., 1998). Moreover, spectrin has even been reported to directly bind NMDARs in the brain (Wechsler and Teichberg, 1998). As our assay revealed differential receptor recruitment activity of two 4.1 family members, 4.1B and 4.1N, their functions at the

synapse are not simply explained by the possession of a single protein-protein binding region such as the SAB domain. It will be important in future studies to determine which domains differentially modulate NMDAR versus AMPAR recruitment and which processes are actin dependent and independent.

The specificity of the recruitment of NR2B subunit containing NMDARs, as measured by the weighted decay constant τ_w (Fig.8), is particularly interesting, as recruitment of the NR2B subunit is especially relevant to early developmental processes. NR2B subunits are more prevalent at synapses than NR2A during early development (Stocca and Vicini 1998)(Tovar and Westbrook, 1999). Furthermore, scaffolding molecules such as SAP102 and PSD-95 appear to mediate the NR2B to NR2A switch that is a key feature of synaptic maturation (van Zundert et al., 2004). It is possible that 4.1B must now also be considered in playing a role in this process. However, consistent with the role for protein 4.1B at “young” developing synapses, we found that the endogenous localization of protein 4.1B to excitatory synapses in neuronal culture appeared very early (4 DIV) and the intensity at synapses dropped off with time though its localization did not (Supplemental Fig.2). Previous *in situ* hybridization studies in newborn mouse brain show specific protein 4.1B expression in the purkinje cell layer of the cerebellum, regions CA1 and CA3 of the hippocampus and throughout the cortex (Parra et al., 2000). Many of these regions are primarily the targets of major glutamatergic inputs and so it is interesting to speculate that protein 4.1B regulates excitatory postsynaptic differentiation in these areas before or near birth.

The protein structure of the 4.1 family proteins has been intensively studied, and it is clear that in addition to the FERM, CTD and SAB domains, critical Ca^{2+} -sensitive and insensitive calmodulin binding domains regulate the association between 4.1 proteins and transmembrane proteins in erythrocyte membranes (Nunomura et al., 2000). Ca^{2+} /calmodulin is known to be a key regulator of processes underlying synapse formation such as actin cytoskeleton dynamics (Konur and Ghosh, 2005; Oertner and Matus, 2005; Saneyoshi et al., 2008) and glutamate receptor activity and localization (Ehlers et al., 1996; Wyszynski et al., 1997). This suggests that a 4.1 family member's activities and dynamics would be subject to the specific regulatory mechanisms known to affect glutamate receptor recruitment to the synapse and subsequent synaptic maturation.

Such dynamics have not yet been reported for 4.1 molecules as they have been for other synaptic proteins (Sharma et al., 2006), but would further support the idea that protein 4.1B could act as a regulated developmental signal central to the specific localization of glutamate receptors.

Interestingly, we demonstrated that both family members (4.1B and 4.1N) were readily recruited to adhesion sites via SynCAM1. We assume that 4.1N also binds to SynCAM1 through its FERM domain, as it is about 73% identical to the FERM domain of 4.1B (Parra et al., 2000). However, 4.1N and 4.1B show completely opposite specificities for glutamate receptor subtypes (Fig. 5). 4.1N is known to bind to GluR1 through the CTD (Shen et al., 2000), a domain that is also 73% identical to the CTD of 4.1B (Parra et al., 2000). This means that enough amino acids have changed between 4.1N and 4.1B in the CTD to switch binding from AMPAR subunits to NMDAR subunits. Alternatively, the ~30% amino acid difference between 4.1B and 4.1N can simply abrogate binding of 4.1B to AMPARs and other domains have acquired the ability to bind NMDARs directly or indirectly. 4.1B has at least three additional domains (U1, U2 and U3) that show significant sequence differences compared with other 4.1 proteins. These domains have no identified protein interaction or regulatory roles as yet. We hypothesize that these U domains might play a role in positively regulating the interaction of 4.1B with NMDARs but not with AMPARs. Future studies investigating the effects of 4.1B deletion constructs will provide insight into these possibilities

4. METHODS

Expression Vectors and Constructs

Human 4.1B cDNA was obtained from Irene Newsham (University of Texas, Houston, TX). Deletions of the FERM domain (Δ FERM; amino acids 106-302) and the C-terminal domain (Δ CTD; amino acids 894-1097) were performed by PCR. Full length and the deletion mutants were subcloned into pEGFP-N1 (Clontech, Mountain View, CA) and pCDNA3. To generate shRNA to mouse 4.1B, the following sequence of 4.1B was subcloned into the pSuper vector (Brummelkamp et al., 2002): 5'-CGTGACCGGCTTCGAATAA-3'. For control shRNA, the following sequence was used: 5' – GATCTGAAGGCGCCTATAC – 3'. HA-SynCAM1 was obtained by PCR

from mouse cDNA using the following primers: gccgaagcttatggcgagtgctgtgctgccg and tcgggaattcctagatgaagtactctttcttctcgg. An HA tag and SalI site were inserted using the megaprimer PCR technique: cttctccttcaatcaactgtagcgtagctctgggacgtcgtatgggtagtcgactttag taaacagattctgtcc. Deletion of the FERM binding domain (Δ FERMb; amino acids 376-389) was performed by megaprimer PCR: ggccgctattttgccgccaaggagccgatgac. The PDZ binding domain (Δ PDZIIb; amino acids 415-418) was generated by PCR. The resulting HA-tagged constructs were transferred to pCDNA3. 4.1N-GFP was a gift from Richard Huganir (Johns Hopkins University, Baltimore, MD). GFP-NR2B was provided by Anne Stephenson (University College London, UK). Syntenin1-GFP was provided by Jeremy Henley (University of Bristol, UK). Myc-CASK was a gift from Ben Margolis (University of Michigan, Ann Arbor, MI) and GRIP1-GFP was obtained from Casper Hoogenraad (Erasmus Medical Center, Rotterdam, NL). GluR1-GFP has been described previously (Washbourne et al., 2002).

COS7 Cell Culture and Transfection

COS7 cells (ATCC[®] Manassas, VA) were plated at a density of 50,000 cells per ml onto poly-L-lysine (Sigma, St. Louis, MO) coated glass coverslips and maintained in DMEM, 10% FCS, 25 units Penicillin and 25 μ g streptomycin/ml. 24 hours later, or approximately at 60-70% confluency, cells were transiently transfected with 3.5 μ g total DNA per well of a 12 well plate using lipofectamine 2000 (Invitrogen). Transfection reagent was added to wells containing DMEM, 10% FCS without pen/strep and incubated for 4-5 hours at which time the media was replaced by fresh DMEM, 10% FCS and 2mM kynurenic acid. Microsphere clustering is performed on live cells 28-30 hours later.

Microsphere Preparation

100 μ l of ProteinA coated microspheres (~1 μ M diameter; Bangs laboratory, Inc) were resuspended in 750 μ l of protein A/G buffer (0.1 M TE and 0.15 M NaCl, pH 7.5) and then centrifuged at 4°C, 10,000xg for 5 minutes. The supernatant was discarded and microspheres were washed similarly two more times. After the final wash, microspheres were resuspended in 50 μ l protein A/G buffer and 50 μ l COS7 maintenance media with

target IgG (10 μ g α -HA, rabbit polyclonal, Bethyl Laboratories Inc., Montgomery, TX). Microspheres were incubated with antibody solution for 1hr at 4°C with gentle agitation and vortexing every 5-10 minutes. After incubation microspheres, were washed three times in the same manner as before using protein A/G buffer.

Microsphere Application and Surface Immunolabeling

6-9 μ l of prepared microsphere suspension was added to transfected COS7 cells in 1 ml of fresh media and plates were swirled gently to distribute microspheres. Microspheres were incubated with cells for 35-45 minutes at 37 °C. Live cells were then rinsed 2x gently with warmed 1xPBS, then fixed for 8 minutes in 1.5% PFA, 4% sucrose at 4°C. After fixation, coverslips were blocked with 10%BSA, 1% blocking reagent (Roche) for 30 minutes at room temperature. Primary solution, antibodies against HA (anti-mouse IgG1, 1:1000, Covance, Emeryville, CA) and GFP (chicken polyclonal, 1:1000, Chemicon-Millipore, Billerica, MA) in 5% BSA, 0.5% blocking reagent, was added for 45 minutes (to not more than 1 hour) at room temperature. Coverslips were washed and incubated in secondary antibodies for 35-40 minutes at room temperature (Alexa Fluor® 633 goat α -mouse IgG1 1:800, Alexa Fluor® 546 goat α -chicken IgG 1:800 Molecular Probes Eugene, OR). A control stain on cells with only internal GFP (GFP-NR2B alone without NR1 co-transfection or a GFP tagged-effector) was always performed in parallel to the described experiments. In the experiments where surface receptor accumulation was measured, the effectors were not GFP tagged. Additionally, CAM - Effector colocalization experiments were conducted independent of CAM – Effect or - Receptor experiments.

Hippocampal Cell Culture and Immunolabeling

Medium density hippocampal cultures were prepared from embryonic day 19 Sprague Dawley rat pups as described (Brewer et al., 1993), with minimal modifications. Briefly, neurons were plated in plating media (10% FCS, 20 mM dextrose, 25 units Penicillin and 25 μ g streptomycin in MEM (Invitrogen/GIBCO)) at a density of 40,000-60,000 cells/ml on 12 mm coverslips coated with poly-L-lysine (Sigma, St. Louis, MO) and incubated for 4-5 hours. This media was changed for the remainder of culturing to a

maintenance medium (Neurobasal medium (Invitrogen, Carlsbad, CA), 1x B-27 (Invitrogen), 0.5 mM Glutamax-I (Invitrogen), 50 units Penicillin/ 50µg Streptomycin (Sigma) and 0.07% beta-Mercaptoethanol). Neurons were fed fresh maintenance media in half changes every three days in culture. This protocol was slightly modified in the preparation of the hippocampal neurons for the electrophysiology where neurons were derived from P1 mice. Endogenous staining of protein 4.1B (goat polyclonal to EPB41L3/DAL-1, 1:500 Abcam Inc. Cambridge, MA), PSD-95 (mouse monoclonal IgG2A clone 28/43, 1:250, James Trimmer – UC Davis/NIMH NeuroMab Davis, CA) and SynapsinI (rabbit polyclonal 1:800, Chemicon-Milipore, Billerica, MA) were performed on hippocampal neurons from 4 to 12 d.i.v. Cells were fixed 10 minutes in 4% PFA + 4% sucrose at 4°C and then 5 minutes in 100% MeOH at -20 °C, permeabilized in 0.25% Triton X-100 for 5 minutes at room temperature and blocked for 1 hour in 10% BSA + 1% Blocking reagent (BR; Roche). Cells were incubated in primary solution (antibodies + 3% BSA + 0.3% BR) for 3 hours at room temperature and then in secondary antibodies for 45 minutes at room temperature (Alexa fluor® 546 Goat anti-mouse IgG2A and 633 Goat anti-rabbit 1:600 Molecular Probes® Eugene, OR and Cy™ 2 Donkey anti-Goat 1:600 Jackson Immuno Research, West Grove, PA).

Surface Immunolabeling of GFP-NR2B in Hippocampal Cell Culture

Hippocampal neuronal cultures were prepared as described previously, and then transfected at 7 d.i.v. with a 1:5 mixture of GFP-NR2B to untagged target plasmid: either control shRNA, 4.1BshRNA, 4.1B full length, 4.1B ΔFERMb or plasmid vector. A total of 4-5µg of plasmid DNA was transfected using the Calcium Phosphate transfection kit, ProFection® (Promega, Madison, WI). Neurons were incubated in precipitate for up to 1 hour and then placed back into fresh media with pen/strep and allowed to express for 24 hours. To label surface GFP-NR2B, total GFP-NR2B and presynaptic structures, transfected neurons were washed gently 2 times in fresh ACSF at room temperature and then fresh media without pen/strep plus anti-GFP antibody (rabbit polyclonal, 1:1000 Chemicon-Milipore, Billerica, MA) was added for 15-20 minutes at 4°C. Cells were gently washed afterwards 3x in 4°C PBS and then fixed with 4% PFA for 20 minutes at 4°C. Fixed cells were treated with 0.25% tritonX-100 for 5 minutes at room temperature,

blocked in 10% BSA+1% Roche Blocking medium for 1 hour at room temperature. Secondary for the surface labeled GFP was added for 30 minutes at room temperature (Alexa fluor® 546 Goat anti-rabbit). After washing, primaries against GFP (chicken polyclonal, 1:1000, Chemicon-Millipore, Billerica, MA) and Synaptophysin (mouse monoclonal 1:1,500, SIGMA, Saint Louis, MO) were added for 1 hour at room temperature. Cells were washed again and then secondary against the primaries for total GFP and synaptophysin was applied for 45 minutes at room temperature (Alexa fluor® 488 Goat anti-chick and Goat anti-mouse IgG1,1:600 Molecular Probes® Eugene, OR). To confirm that we label surface GFP specifically in each experiment, we ensured that GFP only, and/ or GFP-4.1BFL controls did not have significant immune label in the 546 channel. Further all puncta that had signal in the 546 channel also contained 488 signal, confirming that we label both surface and total GFP.

All studies were conducted with approved protocols from both the University of Oregon Animal Care and Use Committee and the Georgetown University Animal Care and Use Committee, in compliance with NIH guidelines for the care and use of experimental animals.

Imaging, Quantification and Statistical Analysis

COS7 cells were imaged on an inverted Nikon TU-2000 microscope with an EZ-C1 confocal system (Nikon) with a 100x oil-immersion objective (1.45 NA). Cells were imaged blind to specific co-transfection conditions. Cells were chosen for analysis if there were clear examples of microspheres with accumulations of the target CAM at site of contact (an average of a $110 \pm 11.8\%$ increase in intensity of HA-NLG1 of HA-SynCAM1 was measured at microspheres relative to background levels in the cell where visible accumulation was scored). 14-15 microspheres from 14-15 individual cells were chosen from three independent experiments in each condition. All channels were scanned sequentially and in the same plane of focus as apparent CAM aggregation. Images obtained in a given channel were obtained at constant laser intensities and the gain adjusted to just below intensity saturation. Images were converted to bitmaps and average intensity was analyzed surrounding an individual microsphere in each channel

using Image Pro Plus[®] software. Briefly, average intensity increase at a given microsphere was calculated as follows: $(I_{\text{microsphere}} - I_{\text{background}}) / I_{\text{background}} * 100\% = \text{“\% increase in intensity at microsphere”}$ (Fig.1B). $I_{\text{microsphere}}$ is the average intensity in an annulus immediately surrounding the microsphere that is equal in width to the radius of the microsphere (annulus 1 in Fig.1B). $I_{\text{background}}$ is the average intensity in an annulus surrounding the first around the microsphere (annulus 2 in Fig.1B) plus the average intensity in the area of the microsphere itself. The data are expressed in percent intensity above background, and given our conservative estimates of what is signal we are more likely to have underestimated total protein accumulation rather than overestimated. We did not assume a normal distribution of our CAMRA data and given the sample size in each experimental condition, we applied the non-parametric Mann Whitney test in all comparisons. Bonnferroni’s correction was applied to correct for multiple comparisons in the NMDAR and effector CAMRA experiments. Ten planned comparisons were made among the control and treatment groups. Given this number of multiple comparisons, comparison-level significance was tested at an alpha level of 0.0051 for an experimental-level Type I error rate of 0.05. Significance is depicted in graphs as asterisks: * is $p < 0.05$, ** is $p < 0.01$ and *** is $p < 0.005$. The non-parametric Mann Whitney-U was also used to test for significance in the comparisons of neuronal expression data unless otherwise noted. All data are expressed as mean \pm standard error of the mean.

Immunoprecipitation and Western Blotting

COS7 cells were transfected with the plasmids of interest and cultured for 24 hours. Cells were lysed in 250 μ l of lysis buffer (150mM NaCl, 50mM Tris-HCl, 0.5mM EDTA, 0.2% Triton X-100 and protease inhibitor tablets, pH7.4) for 45 minutes at 4°C with agitation. This mixture was centrifuged at 14,000 x g for 5 minutes at 4°C and the supernatant collected. 20 μ l of the supernatant was used as the input sample. 115 μ l was incubated with 3 μ g of anti-HA (mouse monoclonal; Bethyl Laboratories) overnight at 4°C with rotation, and 115 μ l was incubated without antibody. The following day, 50 μ l of protein-A-sepharose beads in lysis buffer was added to both samples and incubated for 2 hours at 4°C with rotation. Protein-A-sepharose beads were collected by centrifugation and washed 3 times in lysis buffer. Bound proteins were eluted with 100 μ l Laemml

sample buffer, boiled, separated on an SDS-PAGE gel, transferred to nitrocellulose membranes and probed with either anti -HA rabbit (1:1000; Bethyl Laboratories) or anti -GFP rabbit (1:1000; Invitrogen).

CGC and HEK293 Cell Co-culture and Transfection

Primary cultures of mouse cerebellar granule cells (CGC) were prepared from postnatal day 5-7 (P5-7) from C57Bl6 mice. Mouse pups were sacrificed by decapitation in agreement with the guidelines of the Georgetown University Animal Care and Use Committee. The cerebella were dissociated as described in (Gallo et al., 1987). Cells were dispersed with trypsin (0.25 mg/ml, Sigma, St. Louis, MO) and plated at a density of 1.1×10^6 cells/ml on glass coverslips (Fisher Scientific, Pittsburgh, PA) coated with poly-L-lysine (10 μ g/ml; Sigma) in 35 mm Nunc dishes. The cells were cultured in basal Eagle's medium supplemented with 10% bovine calf serum, 2 mM glutamine, and 100 μ g/ml gentamycin (all from Invitrogen Corporation Carlsbad, CA), and maintained at 37°C in 5% CO₂. The final concentration of KCl in the culture medium was adjusted to 25 mM (high K⁺). To achieve functional synapse formation, at 5 d.i.v. the medium was replaced with the low (5 mM) potassium medium (MEM supplemented with 5 mg/ml glucose, 0.1 mg/ml transferrin, 0.025 mg/ml insulin, 2 mM glutamine, 20 μ g/ml gentamicin, Invitrogen, and cytosine arabinofuranoside 10 μ M, Sigma) as previously described (Chen et al., 2000; Prybylowski et al., 2002). Human embryonic kidney 293 cells (HEK293; American Type Culture Collection, Rockville MD, ATCC No. CRL1573) were grown in Minimal Essential Medium (Gibco BRL, Gaithersburg, MD), supplemented with 10% fetal bovine serum, 100 units /ml penicillin (Gibco BRL), and 100 units/ml streptomycin (Gibco BRL), in a 5% CO₂ incubator. Exponentially growing cells were dispersed with trypsin, seeded at 2×10^5 cells/35-mm dish in 1.5 ml of culture medium and plated on 12 mm glass cover slips. HEK293 cells after transfection were dispersed with trypsin and plated on CGC cultures at a density of 1×10^4 cells/12-mm coverslip. HEK293 cells were transfected as described in (Vicini et al., 1998) using a modification of the calcium phosphate precipitation technique. Briefly, mixed plasmids (3 μ g total) were added to the dish containing 1.5 ml MEM culture medium for 12-16

hours at 37°C under 5% CO₂. Greater than 80% of cells expressed all the plasmids transfected as assessed independently with pEGFP, pDsRED2 and pECFP plasmids (not shown; Clontech).

HEK293 Cell/Cerebellar Co-culture for Synaptic Labeling

Human embryonic kidney 293 cells were grown in Minimal Essential Medium (Gibco), supplemented with 10% fetal bovine serum in a 5% CO₂ incubator. Exponentially growing cells were dispersed with trypsin, seeded at 2×10^5 cells/35-mm dish in 1.5 ml of culture medium. HEK293 cells were then transfected within 24hrs after splitting as described Fu et al. (2003). Briefly, mixed plasmids (3 µg total) were added to the dish containing 1.5 ml MEM culture medium for 12–16 h at 37°C. HEK293 cells after transfection were dispersed and plated on CGCs cultures (DIV5) at a density of 2×10^4 cells/12-mm coverslip. 2 days later, live cultured HEK293-neuron co-culture was fixed with 4% paraformaldehyde, 4% sucrose in PBS for 10 min, and washed three times in PBS. Fixed neurons were permeabilized with 0.25% Triton X-100/PBS for 5 min, washed several times with PBS (5min per wash), and incubated in 10% bovine serum albumin in PBS for 1 hr to block non-specific staining. Cells were then incubated overnight (4°C) with the following primary antibodies: rabbit anti-synapsin1 antibody (1:1000; Chemicon, Temecula, CA), mouse anti-PSD-95 antibody (1:100, abcam) and mouse anti-gephyrin (1:1000; mAb7α; Synaptic Systems). After washing with PBS, cells were incubated with goat anti-rabbit indocarbocyanine (Cy3)-conjugated secondary antibodies (1:1000; Jackson ImmunoResearch, West Grove, PA) and goat anti-mouse Alexa Fluor 647 –conjugated secondary antibodies for 1hr at RT. Prepared cells were imaged on an inverted Nikon TU-2000 microscope with an EZ-C1 confocal system (Nikon) with a 100x oil-immersion objective (1.45 NA). Cells were imaged blind to specific co-transfection conditions and specific criteria for chosen cells were set as per (Biederer and Scheiffele, 2007). Briefly, the measure taken and compared was percent of HEK293 cell surface area covered by synapsin I label where PSD95 and Gephyrin signal were absent. Each channel was scanned sequentially at constant laser intensities and gain was set just below saturation. Images were processed and analyzed using Image Pro Plus[®] software. Briefly, images were thresholded to subtract background in a

semiautomatic fashion to obtain average intensity and area of labeled regions. Data is expressed as mean \pm s.e.m. and a two-tailed unpaired Student's t test was employed to determine significant differences between target comparisons (* = $p < 0.05$).

Electrophysiology

The recording chamber was continuously perfused at 5 ml/min with ECS composed of (in mM): NaCl (145), KCl (5), MgCl₂ (1), CaCl₂ (1), HEPES (5), glucose (5), sucrose (25), phenol red (0.25mg/l) and D-serine (5 μ M) (all from Sigma) with pH adjusted to 7.4 with NaOH. All experiments were performed at room temperature (24-26°C). The recording solution contained (in mM): potassium gluconate (145), HEPES (10), ATP.Mg (5), GTP.Na (0.2), and BAPTA (10), adjusted to pH 7.2 with KOH. Electrodes were pulled in two stages on a vertical pipette puller from borosilicate glass capillaries (Wiretrol II, Drummond, Broomall, PA). Pipette resistance ranged from 5 to 7 M Ω . NMDA-mEPSCs were pharmacologically isolated using bicuculline methiobromide (BMR, 50 μ M), TTX (0.5 μ M) and 2,3-Dihydro-6-nitro- 1,2,3,4-tetrahydrobenzo[f]quinoxaline-7-sulfonamide (NBQX, 5 μ M) (all from Sigma) in a Mg²⁺-free solution, while AMPA-mEPSCs were recorded in presence of BMR (50 μ M) and TTX (0.5 μ M) in regular extracellular solution (ECS) with Mg²⁺. Solutions and drugs were delivered locally with a Y-tube device (Murae et al., 1989). Whole-cell voltage-clamp recordings from neurons and HEK293 cells were made at -60 mV and performed at room temperature using an Axopatch 200 or an Axopatch-1D amplifier (Axon Instruments, Union City, CA). A transient current response to a hyperpolarizing 10 mV pulse was used to assess resistance and capacitance throughout the recordings. Currents were filtered at 2 kHz with a low-pass Bessel filter (Frequency Devices, Haverhill, MA), digitized at 5-10 kHz using an IBM-compatible microcomputer equipped with Digidata 1322A data acquisition board and pCLAMP9 software (both from Molecular Device Co., Sunnyvale CA).

Off-line data analysis, curve fitting, and figure preparation were performed with Clampfit 9 (Molecular Device) software. NMDA-mEPSCs' decay was fit using Clampfit 9 (Molecular Device) from averages of at least 20 events selected with Minianalysis (Synaptosoft Inc, Fort Lee). The decay phase of currents was fit using a simplex algorithm for least squares exponential fitting routine with a double exponential equation of the form

$I(t) = I_f \times \exp(-t/\tau_f) + I_s \times \exp(-t/\tau_s)$, where I_x is the peak current amplitude of a decay component and τ_x is the corresponding decay time constant. To allow for easier comparison of decay times between experimental conditions, the two decay time components were combined into a weighted time constant $\tau_w = [I_f/(I_f+I_s)] * \tau_f + [I_s/(I_f+I_s)] * \tau_s$. All data are expressed as mean \pm standard error of the mean, P-values represent the results of analysis of variance (ANOVA) for multiple comparisons or two-tailed unpaired Student's t tests.

CHAPTER III

THE INTRACELLULAR REGION OF NL1 REGULATES BEHAVIORAL AND SYNAPTIC MATURATION

The work described in this chapter was submitted to *Neuron* and contains co-authored material. I am first author as I worked in close collaboration with P. Washbourne to develop the main hypotheses addressed in this work, and analyze and interpret the data. I also composed the manuscript with advisement from P. Washbourne, and with vital editing provided by J. Constable, R. Arias, R. Chebac, M. Kyweriga and M. Wehr. R. Arias was instrumental in the organization, collection and analysis of behavioral data. R. Chebac was vital in the organization and collection of the immunostaining staining data. M. Kyweriga under advisement from M. Wehr gathered the data on sensory-evoked responses in auditory cortex, initially screened mouse lines in basic behavioral tests and aided in the development of our behavioral analysis methods. L. Davis aided significantly in the development of necessary analytical methods.

1. INTRODUCTION

While the development of neural systems and behavior certainly requires an appropriate balance between synaptic stabilization and flexibility, it is unclear how such an equilibrium may be achieved. It is possible that certain molecular factors specifically facilitate, or permit, potentiation and stabilization of glutamatergic synapses at precise stages of development, while other factors may serve to limit, or prevent, forms of plasticity that would potentiate a synaptic connection and preclude it from serving a future role in encapsulating experience. Such mechanisms could mark specific subsets of synapses for modification during developmental periods characterized by heightened rates of specification and stabilization, and preserve a second immature population that retained a more dynamic state such as that more prevalent during early development. Studies of the expression and function of the NMDA receptor subunits NR2A, NR2B and NR3A, reveal that such mechanisms may exist (Carmignoto and Vicini, 1992; Crair, 1999; Crair and Malenka, 1995; Perez-Otano and Ehlers, 2004; Roberts et al., 2009; Sheng et al., 1994).

A clear picture of the regulatory molecules that underlie immature synaptic states versus more mature states does not exist. For example, higher levels of the NMDAR subunit NR2B and the scaffolding protein SAP102 exist earlier in mammalian development and are thought to underlie the dynamic nature of newly formed synaptic structures, or rather, immature synaptic structures (Washbourne et al., 2004b; Zheng et al., 2010; Zheng et al., 2011). Conversely, levels of the NMDAR subunit NR2A and the scaffolding molecules SAP97 and Shank increase as a synapse matures and higher levels of these proteins are associated with the larger, more stable synaptic structures that are found in mature adult mammals (Fu et al., 2005; Petralia et al., 2005; Sala et al., 2001). While the eventual increase in NR2A at excitatory synapses appears to be activity dependent, it remains unclear which molecules expressed at excitatory synapses are necessary to orchestrate this important developmental progression *in vivo*. It is also unknown how such developmental switches in protein localization at excitatory synapses impact the maturation of complex forms of behavior such as learning and memory.

Neurologin1 (NL1) is a well characterized synaptic cell adhesion molecule that plays a prominent role in activity-dependent synaptic maturation *in vitro* (Chubykin et al., 2007; Wittenmayer et al., 2009). Moreover, manipulations of NL1 function *in vivo* also suggest that it is required to stabilize memory in adult animals (Jung et al., 2010; Kim et al., 2008), while ubiquitous overexpression causes a deficit in learning and an increase in the preponderance of highly potentiated synapses that are limited in plasticity (Dahlhaus et al., 2010). Previous *in vitro* studies of the intracellular signaling capabilities of NL1 suggest that it may regulate such crucial processes via its PDZ and WW binding domains (Barrow et al., 2009; Chih et al., 2005; Iida et al., 2004; Meyer et al., 2004; Tallafuss et al., 2010), while others suggest that synaptic targeting and its enhancement of glutamate receptor mediated synaptic transmission may be independent of this intracellular signaling (Dresbach et al., 2004; Prange et al., 2004; Shipman et al., 2011). This implies that NL1 may exact its effect on the maturational status and plasticity of glutamatergic synapses via proteins capable of interacting with these domains, but its specific role at the synapse *in vivo* is still a matter of debate. Importantly, NL1, as well as related family members such as NL3, and scaffolding molecules purported to interact with NL1 via the C-terminus, have been implicated in developmental disorders such as autism (Bourgeron,

2009; Durand et al., 2007; Glessner et al., 2009; Jamain et al., 2003; Pampanos et al., 2009). One hallmark of such disorders is an abnormality in the structure and modifiability of dendritic spines, the cellular site of the majority of glutamatergic synapses (Penzes et al., 2011). This suggests that resolving the mechanisms by which NL1 may regulate the relative stability of mature synapses *in vivo* may facilitate our ability to understand the proper development of important behaviors.

Here, we compared the behavioral and synaptic phenotypes of mice overexpressing the full length version of NL1 (HA-NL1FL) versus a version missing the terminal 55 amino acids (HA-NL1 Δ C) in order to determine which molecular factors mediated NL1's influence on the state of glutamatergic synapses *in vivo*. We observed that full length NL1 overexpressing animals showed deficits in learning and increased perseverance in reversal tasks, while mice expressing NL1 with the intracellular deletion were more flexible in behavior, similar to juvenile animals. Furthermore, we found key changes in spine morphology and synaptic protein content that were consistent with the idea that we induced the large scale maturation of synapses in the full length NL1 animals, while delaying key developmental milestones of synapse maturation in animals with the truncated form. Comparison of the two lines of mice illuminate the significance of NL1 C-terminus signaling *in vivo*, and point towards a richer understanding of the key molecular targets that potentially gate the maturation of glutamatergic synapses and complex behavior.

2. RESULTS

Generation of HA-NL1FL and HA-NL1 Δ C transgenic mice

The intracellular C-terminus of NL1 contains both the PDZ binding and WW binding motifs which are thought to underlie important aspects of glutamatergic postsynaptic development. To understand the contribution of these signaling domains to behavioral and synaptic maturation within known mnemonic neural systems *in vivo*, we employed a genetic system to target our manipulations to the forebrain. We generated mice that express the coding region for either Neuroligin1 full length (NL1FL) or Neuroligin1 missing the terminal 55 amino acids (NL1 Δ C) under the tetO promoter that is induced by the tetracycline transactivator protein (tTA). Both versions of NL1 were

tagged with the hemagglutinin (HA) peptide sequence on the N- terminus to facilitate localization and quantification of transgene expression *in situ* (HA-NL1FL and HA-NL1ΔC, **Figure 1A**). After generation of the founder groups, mice were backcrossed to the C57BL/6J strain of mice prior to being crossed to mice that expressed tTA driven by the CaMKIIα promoter (Mayford et al., 1996). Double transgenic progeny from these crosses were obtained at the expected Mendelian frequencies in both cases (HA-NL1FL and HA-NL1ΔC), and were subsequently examined for basic health, behavior, fertility, morbidity and mortality rates (Moy et al., 2006; Moy et al., 2004) . No overt changes in health, nor gross behavior were found (data not shown).

To effectively compare and contrast the behavioral and synaptic profiles between the two lines of mice, we needed to confirm that the expression patterns of the transgenes in both lines of animals were similar. We characterized the expression patterns by performing immunocytochemistry on brain sections, and found comparable expression levels of the transgenes in similar cell types within both transgenic lines.

Immunolabeling for the HA tag demonstrated that in both lines of animals, the transgenes were expressed in a subset of the expected forebrain nuclei and neural circuits based on employing the CaMKIIα-tTA driver line. This included the amygdala (Amg) and specific cell populations within the neocortex such as the retrosplenial granular (RSG) formation and layers II/ III & V of the somatosensory cortex (SS1) and other primary sensory areas, though notably, we did not observe high levels in visual cortex (**Figure 1B**). Neither transgene was detected in the striatum (data not shown). Importantly, HA expression in both lines of mice was observed within the hippocampal circuit, the system primarily associated with the explicit forms of learning and memory behaviors previously shown to rely on NL1 function (Blundell et al., 2010; Dahlhaus et al., 2010) (**Figure 1B, red box**). HA expression was also primarily confined to cell populations within CA1, while no significant levels of HA were observed in cell bodies within region CA3 or the dentate gyrus (**Figure 1C & 1D**). Accordingly, subcellular localization of HA, dendritic localization, within the hippocampal circuit was restricted to the stratum oriens (SO), stratum radiatum (SR) and stratum lacunosum moleculare (SLM) of CA1.

Surprisingly, we noticed an approximately 2 fold increase in levels of HA-NL1FL and HA-NL1ΔC in the SLM relative to the SR (SLM:SR intensity ratio 2.1 ± 0.3 vs. 2.5

± 0.4 , HA-NL1FL and HA-NL1 Δ C respectively, n.s., **Figure 1B lower right, 1C & 1D**). This relative increase in HA levels in the SLM vs. the SR, does not parallel the relative intensity levels of PSD95 between SLM and SR (SLM:SR ratio of PSD95: 0.75 ± 0.04 vs. 0.80 ± 0.04 respectively, n.s. **Figure 1C & 1D**). It is unlikely that this difference in localization is due to differences in trafficking between NL1FL and NL1 missing the PDZ and WW domains as both of our lines show these same localization effects. Also, we observed that both transgenes, when imaged at higher magnification in the SLM and SR, primarily localized to sites positive for PSD95 immunolabeling and were far less frequently observed to co-localize with GABA-AR α 1 (**Figure 1E & 1F**). This is consistent with previous reports that NL1 trafficking to synapses is independent of C-terminus signaling (Dresbach et al., 2004; Prange et al., 2004).

Finally, labeling of the HA-tag together with cell nuclei (DAPI) in hippocampal sections showed that approximately $35.2\% \pm 2.3\%$ of CA1 cells expressed the HA-NL1 Δ C within the cell body at higher levels than surrounding cells. We did not see this effect in the HA-NL1FL mice (**Figure 1C & 1D**). However, overall cell densities in the CA1 regions of both lines were not different from each other. This suggests that this difference did not appear to enhance non-specific effects such as cell death. Therefore, the expression patterns present in the two lines of mice are comparable and allowed for a straightforward comparison of behavioral and synaptic profiles.

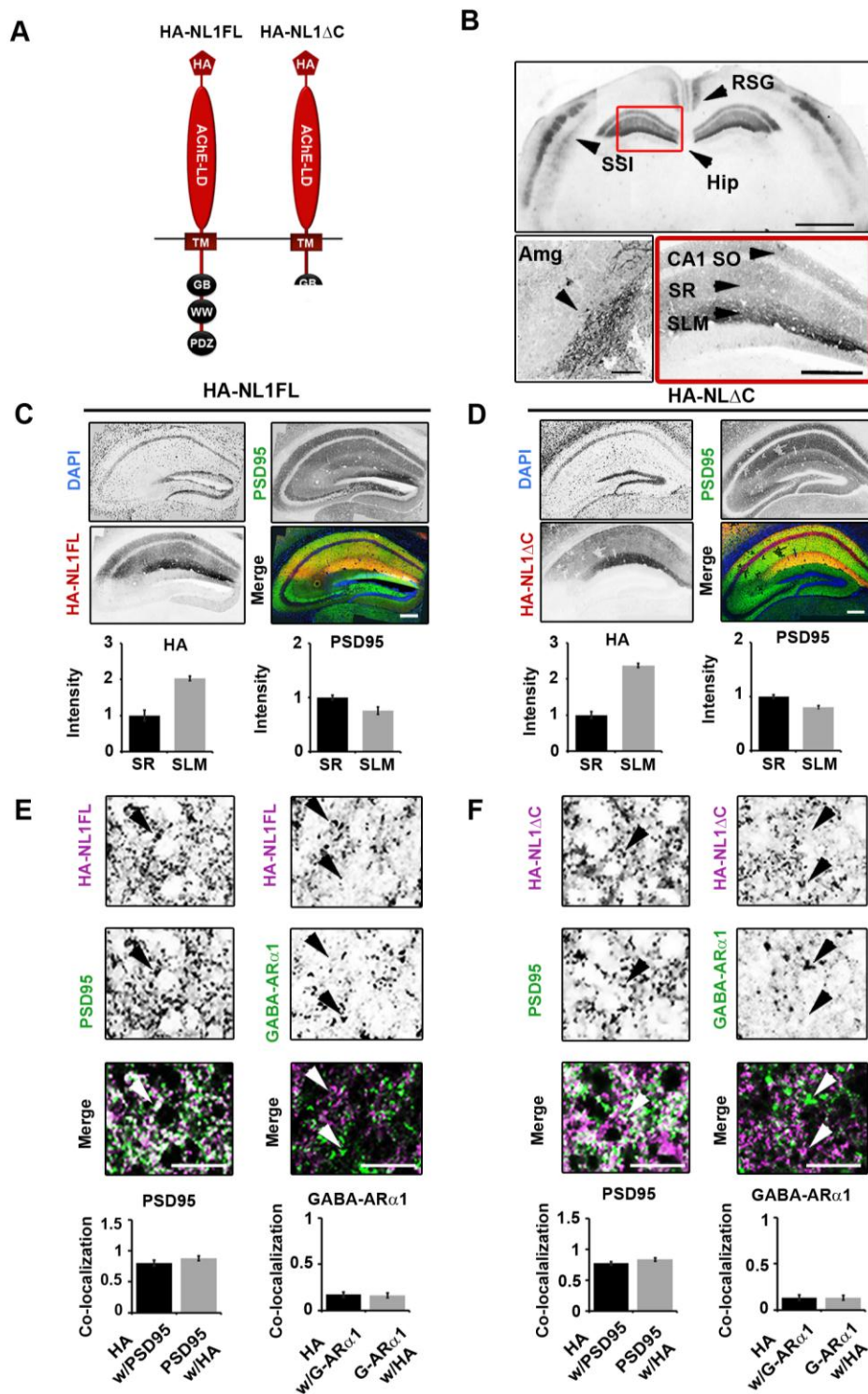


Figure 1. Expression of HA-NL1FL and HA-NL1ΔC in transgenic mice. (A) Schematic of the protein structure of HA-NL1FL and HA-NL1ΔC encoded by the constructs that were used to generate transgenic mice. Abbreviations: Hemagglutinin epitope tag (HA), transmembrane domain (TM), purported gephyrin binding motif (GB), WW binding

domain (WW), PDZ type II binding domain (PDZ). **(B)** Immuno-labeling of HA shows localization patterns of the HA-NL1 constructs. Top panel: retrosplenial angular gyrus (RSG), layers II/III and V of somatosensory cortex (SS1) and the hippocampus (Hip), arrow heads, scale bar equals 2 mm. Lower left panel: Expression in the amygdala (Amg), arrow head, scale bar equals 300 μ m. Lower right panel: Expression in specific strata of the hippocampus, arrow heads, stratum oriens (SO), stratum radiatum (SR), stratum lacunosum moleculare (SLM). Scale bar equals 200 μ m. Dark areas reflect positive labeling. Sections analyzed were between -1.58 mm and -2.30 mm of bregma. **(C & D)** Immunolabeling of PSD95 (green), DAPI (blue) and HA epitope tag (red) for HA-NL1FL **(C)** and HA-NL1 Δ C **(D)**, scale bar equals 200 μ m. Quantification of both HA and PSD95 intensity levels between SLM and SR. All intensities normalized to SR levels. **(E & F)** Higher magnification and quantification of co-localization between HA and markers of excitatory (PSD95) vs. inhibitory (GABA-AR α 1) synaptic markers, **(E)** HA-NL1FL mice and **(F)** HA-NL1 Δ C mice. See **Supplemental Figure 1** for discussion of imaging processing. Differences in co-localization patterns in all cases were not significant. Error bars represent SEM, significance determined by Student's t-test, n = 3 pairs and * = p < 0.05, ** = p < 0.01 and *** = p < 0.001.

Manipulation of NL1 intracellular signaling distinctly alters behavioral performance in learning and memory tasks

We reasoned that distinct behavioral differences during complex behavior between these two lines would argue for a significant role for NL1 intracellular signaling domains at synapses. Given that global manipulations of NL1 function have been found previously to impact explicit learning and memory behaviors (Blundell et al., 2010; Dahlhaus et al., 2010), we first characterized the behavioral performance of our transgenic lines employing the Morris water maze. Using this task, we gauged learning and memory behaviors in four separate phases. First, a two-day visually cued learning acquisition phase assessed gross changes in sensory processing and abilities to grasp the task goals. Second, acquisition training to find the location of a hidden platform using visual cues in the surrounding environment was applied to measure learning rates over many trials. Third, we administered a probe trial where the platform was removed and the searching pattern of the mice was analyzed over a 60 second time window to assess recall behavior. Finally, reversal training to find a new location measured flexibility by determining how quickly searching behavior would adjust when the location of the platform was changed.

HA-NL1FL mice took longer than littermate controls to reach the location of a hidden platform in the Morris water maze over six days of training (RMANOVA, main effect of genotype: $F_{(1,17)} = 63.2$, $p < 0.001$, and main effect of genotype x day interaction: $F_{(5,107)} = 2.78$, $p < 0.05$, $n = 10$ pairs), while visually cued performances, were indistinguishable from control littermates (**Figure 2A - 2A''**). Analysis of probe trial performance after acquisition training revealed a significant increase in the distance to first cross the former platform location in the HA-NL1FL mice relative to controls (147.4 ± 29.3 cm vs. 79.3 ± 6.8 cm, respectively, $p < 0.05$, $n = 10$ pairs, student's t-test, **Figure 2B and 2B'**). The HA-NL1FL mice also made fewer crosses over the former platform location (3.6 ± 0.4 vs. 5.7 ± 1.2 crosses, $p < 0.05$, student's t-test, $n = 10$ pairs). However, both groups similarly preferred searching within the target quadrant relative to the other quadrants (**Figure 2B, 2B'' and Supplemental Figure 1A**). These results support the idea that learning and recall behaviors in this spatial task are impaired relative to controls in the absence of gross changes in visual processing and motor skills.

In addition to the specific changes in learning and memory behavior as gauged by the first portion of water maze testing, HA-NL1FL mice also took longer to efficiently localize the reversed platform location than controls in the last phase of the water maze task (RMANOVA main effect of genotype: $F_{(1,17)} = 5.21$, $p < 0.025$ and main effect of genotype x day interaction: $F_{(5,107)} = 2.51$, $p < 0.05$, $n = 10$ pairs, **Figure 2C-2C''**). On day two of reversal training the HA-NL1FL mice made more crosses of the former platform location than controls (3.4 ± 0.5 vs. 1.4 ± 0.4 , respectively, $p < 0.05$, student's t-test $n = 10$ pairs, **Supplemental Figure 1B**), while the controls spent less time in the quadrant that formerly contained the platform (13.7 ± 0.7 % vs. 39.2 ± 3.2 %, controls vs. HA-NL1FL mice respectively, $p < 0.01$, **Supplemental Figure 1B**). Therefore, the overall behavioral profile of the HA-NL1FL mice in reversal training reflects an increase in perseverance for previously trained information and general lack in flexibility. These results suggest that in addition to learning and memory behavior, flexibility in these behaviors was also sensitive to overexpression of NL1.

To understand whether there was a general deficit to acquire explicit information, we also examined learning and recall behavior in the object recognition task. In this task, an animal is allowed to explore two identical objects over a single exposure period and is

then removed from the environment with a specific delay period while one of the objects is replaced with a novel one. Spending more time with the novel object when they are put back into the environment is interpreted as accurate learning and recall performance. We administered this task with two delay periods between exposures, 1 hour and 24 hours, to assess short term and long term recall respectively. We observed a lack of preference for a novel object after a 1 hour delay between object exposures in the novel object task ($49.9 \pm 5.4\%$ time with new object vs. 50%, n.s., Wilcoxon-signed rank test, $n = 10$ pairs, **Supplemental Figure 1C**). This result precluded testing for recall after a 24hr delay. These results strengthen the idea that the HA-NL1FL mice exhibit a distinct reduction in their ability to learn and recall explicit forms of information in the absence of a more general deficit in sensory processing.

The behavioral profile observed in the HA-NL1FL mice sharply contrasted that observed in the HA-NL1ΔC mice during water maze testing and object recognition. The HA-NL1ΔC mice displayed no deficits in the acquisition training phase of the task (**Figure 2D and 2D'**). Surprisingly, we observed a significant difference in behavior during the visually cued portion of training. There was a significant decrease in the distance to reach the platform location by the fourth trial of visually cued training on the first day accounting for a significant decrease in latency to reach the cued target (309.4 ± 81.3 cm vs. 539.0 ± 74.3 cm, HA-NLΔC mice vs. controls respectively, $p < 0.05$, Student's t-test, $n = 10$ pairs, **Figure 2D''**; Average Latency: 29.9 ± 4.8 s vs. 42.4 ± 3.9 s, respectively, $p < 0.05$). Together, these results show that there were no deficits in strict measures of learning, but rather there may have been an advantage in learning the task goals during the visually cued trials. During the probe trial, HA-NL1ΔC mice showed no difference in the distance they took to first cross the location of the former platform as compared to controls (**Figure 2E and 2E'**), nor any difference in the number of crosses of the former platform location (5.0 ± 0.5 vs. 4.1 ± 0.8 , n.s.). Interestingly, the HA-NL1ΔC mice spent less time in the target quadrant than controls over the entire trial, though they still retained more of a preference for the target quadrant than would be predicted by chance ($41.7 \pm 4.0\%$ vs. 64.9 ± 7.3 , HA-NL1ΔC mice vs. controls respectively, $p < 0.01$, **Figure 2E and 2E''**). These results suggest that they showed less persistence in searching the former location, but showed no significant deficits in strict

measures of recall during this phase of testing. During reversal training, HA-NL1 Δ C mice located the position of the new target faster than controls (main effect of genotype: $F_{(1,19)} = 11.56$, $p < 0.001$, main effect genotype x day interaction: $F_{(5,119)} = 3.01$, $p < 0.025$, $n = 10$ pairs, **Figure 2F**) and more directly on the fourth trial (222.3 ± 36.6 cm vs. 434.6 ± 82.4 cm, $p < 0.05$, $n = 10$ pairs, Student's t-test, **Figure 2F'**). We may therefore conclude that this group of animals is more flexible in this task.

Investigation of recall behavior in the object recognition task confirmed that the HA-NL1 Δ C mice showed no learning difference over a short, 1 hour, delay as their novelty preference was similar to controls (**Supplemental Figure 1C**). However, we observed impairment for recall after a single exposure with a delay of 24 hours (Novelty preference: $49.9 \pm 8.8\%$ vs. 50% , $p < 0.05$, $n = 10$ pairs, Wilcoxon-signed rank test, **Supplemental Figure 1D**). This suggested that object recognition learning over the short term occurred similarly to controls in this task, but that the memory was less stable over 24 hours with a single trial exposure. Similar results were achieved in a spatial version of the object recognition task (data not shown), suggesting that the change in recall behavior generalized to multiple forms of explicit memory formation, but may not have been observed in the Morris water maze due to high repetition in training with short delays in a single day.

Overall, examination of behavior in the Morris water maze suggests an absence of learning and recall deficits such as those observed in the NL1FL animals. Instead, we see evidence that they have improved performance in the visually cued phase of training, and that they show enhanced flexibility as evidenced by less persistence in searching the location that formerly contained the platform during the probe trial, and locating the new target location faster than controls during reversal. These results suggest that NL1's intracellular signaling plays a significant role in the execution of learning and memory behaviors.

Due to the potential role of the C-terminus of NL1 in the maturation of synapses, we hypothesized that the behavioral enhancement in flexibility might be the result of retention of juvenile behavioral traits. To address this idea, we had to first characterize juvenile performance in C57BL/6J mice in the Morris water maze. One month old mice were able to perform the task and showed no significant difference in their learning

acquisition curve as compared to 3 month old adult mice (**Figure 2G and 2G'**). Similar to the HA-NL1 Δ C mice, we found a significant decrease in the distance to reach the visually cued platform on the fourth trial of training (243.9 ± 29.7 cm vs. 99.8 ± 68.7 cm, juveniles vs. adults, respectively, $p < 0.05$, $n = 9$ pairs, Student's t-test, **Figure 2G''**). During the probe trial, distance to first cross the former target location as well as the number of crosses made over 60 seconds (4.3 ± 0.7 vs. 5.0 ± 0.6 , n.s.), were not different from adults (**Figure 2H and 2H'**). Juveniles and mature adults spent more time in the target quadrant than would be expected by chance, but differed in their degree of preference ($43.9 \pm 2.9\%$ vs. $54.9 \pm 3.3\%$, respectively, $p < 0.05$, **Figure 2H and 2H''**). Finally, during reversal training, adults took longer to find this novel location than the juveniles (**Figure 2I**) and they were less direct than juveniles (537.4 ± 102.5 cm vs. 280.1 ± 40.6 cm, $p < 0.05$, $n = 10$, Student's t-test, **Figure 2I'**). The juveniles also showed a lack of persistence in searching the former target area in the fourth trial of the first day of reversal training as compared to the adults (former platform location crosses: 1.49 ± 0.02 vs. 3.43 ± 1.30 , respectively, $p < 0.05$). It is important to note that we observed such changes in flexibility in the absence of changes in direct measures of recall such as path length to platform location, similar to the observations we made for NL1 Δ C mice. Thus, the characteristics of the behavioral profile of juvenile mice in the Morris water maze are decidedly similar to those of the HA-NL1 Δ C animals, suggesting that expression of the NL1 deletion is not only distinct from full length expression, but also maintains learning and memory related behavior in a more juvenile state.

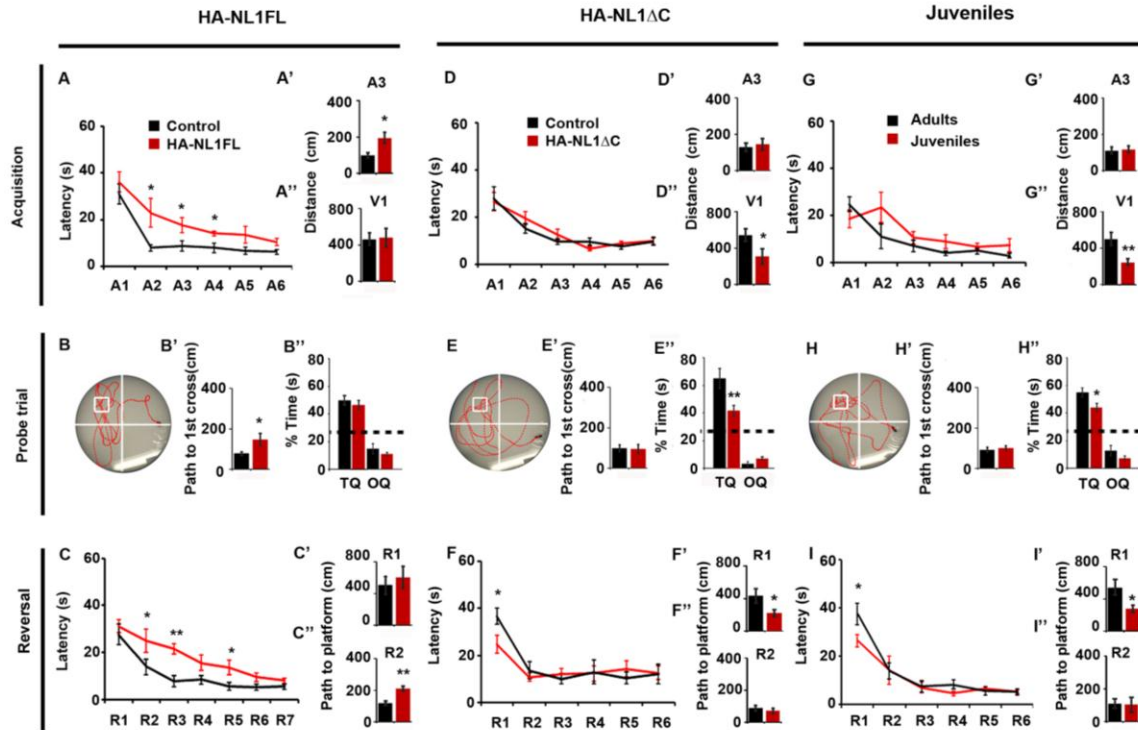


Figure 2. Manipulations of NL1 intracellular signaling distinctly alters behavioral performance in learning and memory behaviors. **(A, D & G)** Mean latency in seconds (s) of transgenic or juvenile mice (red) and their controls (black) during the acquisition phase of training to reach a hidden platform location. A difference in latency was only detected for the HA-NL1FL mice ($p < 0.001$, $n = 10$). Days of training labeled A1 through A6. **(A', D' & G')** Differences in distance measures were consistent with differences found from latency measures. Mean path length in centimeters (cm) to reach the hidden platform on the first trial of day 3 (A3) were different between only the HA-NL1FL mice and their controls ($p < 0.05$, Student's t-test). **(A'', D'' & G'')** Mean path lengths to reach visually cued platform on the fourth trial of the first day (V1) were different between both the HA-NL1 Δ C mice and their controls ($p < 0.05$, Student's t-test, $n = 10$), and the juveniles vs. adults ($p < 0.01$, Student's t-test, $n = 9$). **(B, E & H)** Exemplary search path of an HA-NL1FL, HA-NL1 Δ C and juvenile mouse, respectively, during the probe trial. White box indicates former location of the platform and white lines divide the pool into quadrants analyzed. **(B', E' & H')** Mean path length to first cross the target was different between groups for only the HA-NL1FL mice ($p < 0.05$, Student's t-test). **(B'', E'' & H'')** Total time in the target quadrant (TQ) was similar to controls for the HA-NL1FL mice but different for both the HA-NL1 Δ C and juvenile mice ($p < 0.01$ and $p < 0.05$, respectively), OQ: opposite quadrant. **(C, F & I)** Mean latencies (s) to find a new platform location, days of training are labeled as R1 through R7. Reversal training performance was different for all groups, with HA-NL1FL mice taking more time over days to reach the new target location ($p < 0.001$), while the HA-NL1 Δ C and juvenile mice found the new location faster on the first day of training ($p < 0.05$ and $p < 0.05$ respectively). **(C', F' & I')** Mean path lengths to the new target on the fourth training trial of day 1 (R1) were similar between the HA-NL1FL mice and their controls, but

different for the HA-NL1 Δ C and juvenile mice relative to their controls ($p < 0.05$ and $p < 0.05$). (C'', F'' & I'') Path length to new target was longer between only the HA-NL1FL mice and their controls during the first training trial of the second day (R2, $p < 0.01$, Student's t-test). See **Supplemental Figure 2** for additional behavioral measures and control data. Error bars equal SEM, significance determined with RMANOVA with Tukey's *post hoc*, $n = 10$ pairs unless otherwise noted, * = $p < 0.05$, ** = $p < 0.01$ and *** = $p < 0.001$.

NL1 intracellular signaling regulates morphological characteristics of spines and synapses in the SLM

Previous *in vivo* studies of NL1 function suggest that this gene facilitates the maturation of excitatory synapses (Dahlhaus et al., 2010). Therefore, we hypothesized that the behavior observed in our mice may have been driven by a change in the relative proportion of mature to immature synapses. To determine whether we could identify the predicted shifts in the synaptic population, we measured both spine morphology and the presence of mature excitatory and inhibitory synaptic markers in the hippocampus of both HA-NL1FL and HA-NL Δ C mice. Given the expression pattern of our transgenes, we were afforded the opportunity to examine how such alterations may have been specific to targeted layers within the hippocampus (**Figure 1C and 1D**). We labeled CA1 neurons in the hippocampus with DiI and imaged dendrites and spines from the SLM and SR target layers at high magnification. In HA-NL1FL mice, there is a greater than 2 fold increase in the average area of spine heads in the SLM ($220.4 \pm 25.0\%$ vs. $100 \pm 8.3\%$, respectively, $p < 0.01$, $n = 36$, Student's t-test), but no significant change in density (**Figure 3A**). Interestingly, we did not see significant changes in spine head area ($100 \pm 9.9\%$ vs. $119.8 \pm 8.2\%$, n.s.) nor density ($100 \pm 4.1\%$ vs. $110.0 \pm 8.2\%$, n.s.) in the SR of HA-NL1FL animals. This is consistent with the idea that the region with the highest level of transgene expression was the most impacted. When spine parameters were measured and compared in HA-NL1 Δ C animals relative to their controls, we found a significant 21% increase in the density of spines in SLM ($100 \pm 10.0\%$ vs. $121.0 \pm 6.2\%$), and a trend toward a decrease in spine head area ($100 \pm 8.5\%$ vs. $85.9 \pm 14.1\%$, $p = 0.08$, $n = 36$, Student's t-test, **Figure 3B**). No significant difference in density ($100 \pm 8.7\%$ vs. $114.1 \pm 4.9\%$, n.s.) nor spine head area ($100 \pm 16.8\%$ vs. $115.1 \pm 10.9\%$, n.s.) were

found in the SR. Given that increases in spine head size parallel increases in maturation and synaptic potentiation with experience-dependent remodeling (Kasai et al., 2010a; Kasai et al., 2010b; Wilbrecht et al., 2010), it is noteworthy that we see a significant shift towards an increase in the size of spine heads in the HA-NL1FL mice. Importantly, no such change was brought about by HA-NL1 Δ C, but rather we observed an increase in the number of spines and a decrease in their size relative to controls specifically in the SLM, suggesting a retention of immature spine characteristics in this region.

As another measure to characterize the maturity of synapses as a function of transgene expression, we quantified the area, intensity and density of Synapsin I puncta, a marker of mature presynaptic terminals, and PSD95-positive puncta, a marker of mature postsynaptic densities, in the SLM. In HA-NL1FL mice, we found significant changes consistent with an increase in the prevalence of mature synaptic structures in SLM. The average area and intensity of Synapsin I puncta was increased relative to littermate controls (area: 158.5 ± 5.4 % vs. 100 ± 11.5 %, $p < 0.01$, **Figure 3C**, intensity: 130.5 ± 9.7 % vs. 100 ± 5.4 %, $p < 0.05$), while the average area of PSD95 puncta was enhanced without significant changes in intensity (area: 173.2 ± 15.0 % vs. 100 ± 16.1 %, $p < 0.01$, **Figure 3C**, intensity: 111.2 ± 4.7 % vs. 100 ± 12.6 %, n.s.). These changes are consistent with an increase in the proportion of mature synaptic structures present, however, we failed to observe a significant increase in the frequency of co-localization between PSD95 and Synapsin I (123.5 ± 9.8 % vs. 100 ± 13.5 %, n.s.). This corroborates the idea that HA-NL1FL overexpression in this line altered the state of the synapses present, but that we could not detect a significant increase in synapse number in the SLM.

Remarkably, we observed distinct changes in Synapsin I and PSD95 labeling in the HA-NL1 Δ C mice that were consistent with the presence of more immature synaptic structures. In this line of mice, we detected a significant decrease in the area of Synapsin I positive puncta (area: 72.9 ± 4.9 % vs. 100 ± 5.8 %, $p < 0.05$, **Figure 3D**) and a non-significant trend towards a decrease in the area of PSD95 puncta (70.1 ± 6.12 % vs. 100 ± 12.2 %, $p = 0.0991$, **Figure 3D**). No significant changes in Synapsin I, nor PSD95 intensity were observed (SynapsinI: 113.4 ± 1.6 % vs. 100 ± 7.9 %, n.s., PSD95: 113.2 ± 1.7 % vs. 100 ± 5.8 %, n.s.). Consistent with the changes in spine numbers, we also observed a significant increase in the density of PSD95 puncta (137.8 ± 4.4 % vs. $100 \pm$

7.8%, $p < 0.05$, **Figure 3D**) but not a matching increase in Synapsin I puncta density ($110.5 \pm 4.9\%$ vs. $100 \pm 5.8\%$, n.s.), nor change in the density of puncta that are positive for both PSD95 and Synapsin I ($90.5 \pm 10.9\%$ vs. $100 \pm 8.8\%$, n.s.). Previous studies have reported that PSD95 may play a role in recruiting mature forms of glutamate receptors to synapses and it is certainly present at mature synapses. However, other studies have found PSD95 associated with highly mobile clusters of postsynaptic proteins that are in transport to newly formed and nascent synapses (Gerrow et al., 2006). Our discovery of a significant increase in the number of PSD95 only puncta (without Synapsin I), may therefore be consistent with the idea that the number of newly formed/immature synaptic structures able to initially recruit low levels of PSD95 is increased in the HA-NL1 Δ C animals, but that the lower levels of PSD95 present may not be sufficient to stimulate the other features of synaptic maturation such as an increase in markers of mature presynaptic terminals such as Synapsin I.

Finally, the relative intensity of PSD95 to Gephyrin was also measured in order to test the possibility that changes in NL1 function altered the relative balance of excitation to inhibition, as changes in this measure mark important developmental transitions in plasticity and could partially account for the observed changes in behavior (Hensch, 2004; Hensch and Fagiolini, 2005; Southwell et al., 2010). Changes in the relative excitation to inhibition have also been reported in mice overexpressing NL1 more ubiquitously (Dahlhaus et al., 2010). Surprisingly, we observed a trend towards a decrease in the ratio of PSD95 to Gephyrin in HA-NL1FL mice relative to controls ($56.9 \pm 10.8\%$ vs. $100 \pm 10.8\%$, $p = 0.076$). This was supported by an increase in Gephyrin intensity in the HA-NL1FL mice as well as a slight decrease in PSD95 intensity (Normalized Gephyrin Intensity: $146.2 \pm 16.6\%$ vs. $100 \pm 22.7\%$, $p = 0.1139$). We observed no significant changes in the ratio of PSD95 to Gephyrin in the HA-NL1 Δ C mice ($75.5 \pm 13.5\%$ vs. $100 \pm 11.2\%$, n.s.). Our results suggest that overexpression of NL1 in the hippocampus, specifically in SLM, results in an increase in the mature characteristics of excitatory synapses and tips the balance of excitation to inhibition in regions of CA1. In contrast, expression of the C-terminal deletion protein leads to an increase in the number of smaller postsynaptic structures and fails to change the relative ratio of excitation to inhibition that can be detected by our measures. This supports the

idea that NL1's terminal region is required to elicit key hallmarks of synaptic maturation, and that NL1 Δ C maintains a synaptic state more commonly associated with earlier stages of development.

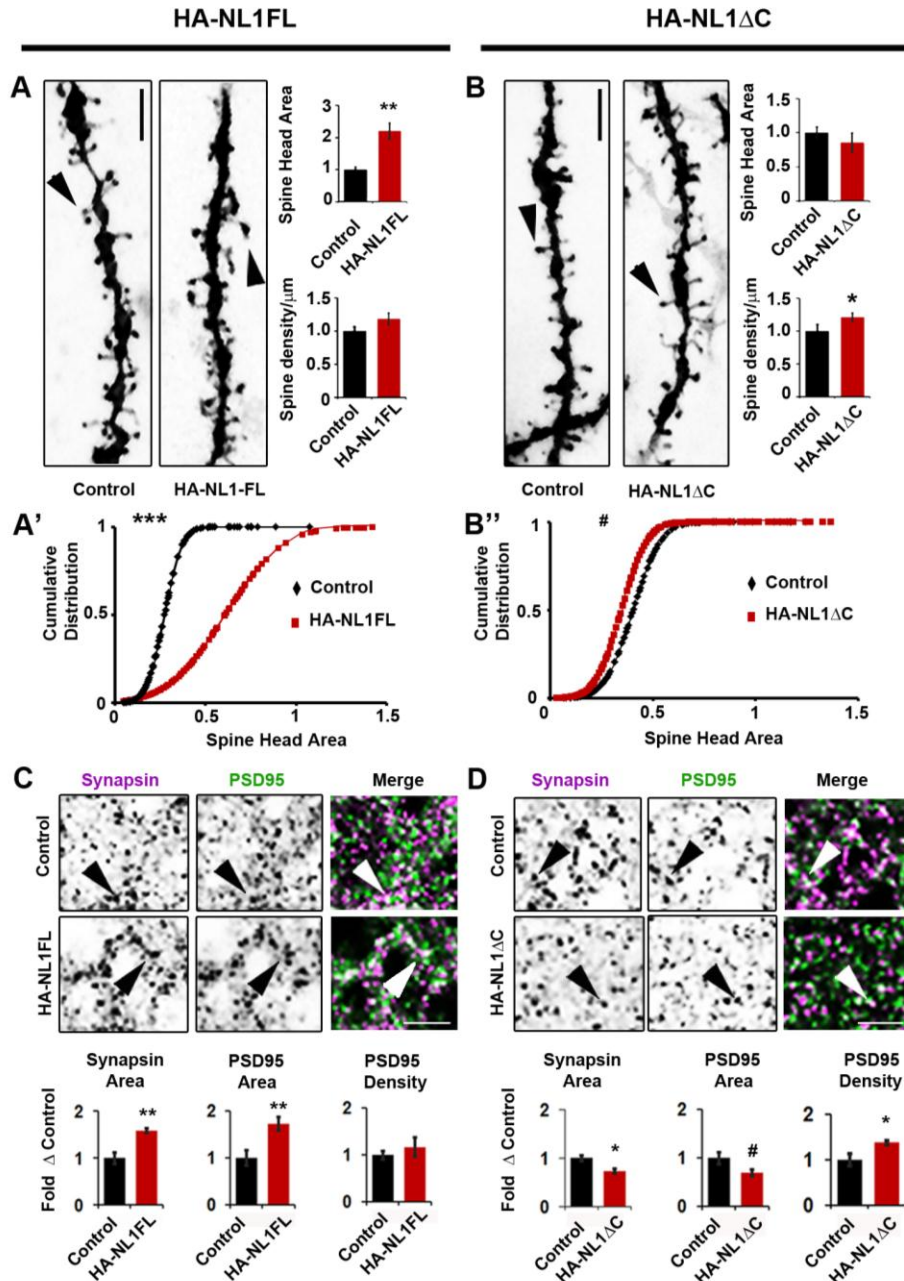


Figure 3. NL1 intracellular signaling regulates the morphological characteristics of spines and synapses in SLM. (**A & B**) Exemplary images of dendritic spine segments of (**A**) control vs. HA-NL1FL mice and (**B**) control vs. HA-NL1 Δ C mice, scale bar equals 2.5 μ m. The mean spine head area was increased for only the HA-NL1FL mice, while spine density was only increased in the HA-NL1 Δ C mice ($p < 0.05$, Student's t-test, $n = 36$ pairs). (**A' & B'**) Cumulative distributions of spine head sizes across 36 dendritic

segments from each group were shifted in the HA-NL1FL mice ($p < 0.00001$, Kolmogorov-Smirnov test), while the difference in the cumulative distributions of spine head size between controls and HA-NL1 Δ C mice suggested a trend towards a decrease in area ($p = 0.077$, Kolmogorov-Smirnov test). **(C & D)** Representative images and quantification of Synapsin I and PSD95 positive puncta characteristics of **(C)** controls vs. HA-NL1FL mice and **(D)** controls vs. HA-NL1 Δ C mice. The average areas of Synapsin I and PSD95 puncta were larger in HA-NL1FL mice than controls, but there was no significant difference in PSD95 density. In the HA-NL1 Δ C mice, the average area of Synapsin I puncta was decreased, with a trend towards a decrease in average PSD95 puncta area ($p = 0.0512$) and an increase in PSD95 density. Areas positive for immunostaining are black (see Supplemental Experimental Procedures and Supplemental Figure 4). The merge image is shown in color, with Synapsin I in purple, PSD95 in green and areas of overlap appearing white. Arrows highlight Synapsin I and PSD95 co-localization, scale bar equals 2.5 μ m. Error bars are SEM, Student's t-test performed in all cases unless otherwise noted, $n = 4$ pairs. # = $p < 0.08$, * = $p < 0.05$, ** = $p < 0.01$ and *** = $p < 0.001$.

Distinct changes in synaptic protein composition in HA-NL1FL versus HA-NL1 Δ C mice

Studies characterizing the molecular state of excitatory synapses across development have found activity-dependent changes in the prevalence of specific isoforms of postsynaptic scaffolding molecules and glutamate receptors at distinct developmental stages (Petralia et al., 2005; van Zundert et al., 2004; Zheng et al., 2011). We therefore predicted that manipulation of NL1 function should impact the postsynaptic scaffolding molecules and glutamate receptors associated with progression through development and synaptic maturation and potentiation. For example, synapses in an immature state would be predicted to have higher levels of NR2B and SAP102, and their prevalence should decrease with development. In contrast, synaptic structures in a mature state would show high levels of NR2A, GluR1 and SAP97, and the prevalence of these markers should increase over development as entire systems mature. To understand how NL1 exerted its effects on synaptic state, we examined the protein composition of synapses in both the HA-NL1FL and HA-NL1 Δ C animals via quantitative immunoblotting of isolated synaptosomal fractions from hippocampal tissue. Overexpression of NL1FL within restricted regions of the hippocampal formation led to a significant increase in synaptic levels of Synapsin I, NR2A, and SAP97, with trends towards an increase of large effect size in NR1 and Shank family members (**Figure 4A**)

and GluR1 and GluR2 (**Supplemental Figure 2**). We observed no significant changes in the synaptic levels of PSD95, nor the key inhibitory synaptic marker Gephyrin. In contrast, expression of HA-NL1 Δ C resulted in enhanced levels of NR2B and SAP102 in synaptosomal fractions, and a small, but significant increase in PSD95 was measured (**Figure 4B**). Notably, HA-NL1 Δ C was not able to facilitate an increase in Shank family members, nor NR2A levels as its full length counterpart did, but rather yielded a significant decrease in SAP97 (**Figure 4B**). These changes are consistent with the idea that there was an overall enrichment of mature synaptic markers in the hippocampi of the HA-NL1FL animals, and that there was an enrichment of immature synaptic markers in the HA-NL1 Δ C animals. Furthermore, these results suggest specific scaffolding molecules, namely SAP97 and Shank, and SAP102, may have played a significant role in determining the observed differential synaptic states, respectively.

To confirm that the changes in synaptic protein levels directly related to the level of expression of our transgenes, we analyzed immunostaining characteristics of a few key synaptic proteins specifically within the SR versus the SLM, as we noted a significant difference in transgene localization between these target layers. The intensity and area of NR2B puncta specifically within the SLM of HA-NL1 Δ C animals was enhanced relative to controls (Intensity: 136.8 ± 3.8 vs. $100 \pm 9.4\%$, $p < 0.05$, Area: 143.5 ± 7.4 vs. 100 ± 8.3 , $p < 0.01$, **Figure 4D**). We also noted a trend towards an increase in levels of NR2B within the SR as well (Intensity: 130.8 ± 11.5 vs. 100 ± 7.6 , $p = 0.071$, Area: 132.2 ± 16.9 % vs. 100 ± 7.0 %, $p = .1937$), but no significant change in levels within the molecular layer of CA3 were detected (Intensity: $100 \pm 9.6\%$ vs. $111.3 \pm 7.1\%$, n.s.). We failed to identify any changes in measures of NR2B immunofluorescence within the hippocampus of HA-NL1-FL mice (**Figure 4C**).

Immunolabeling with an antibody to all three Shank family members (panShank) revealed that levels of one or all members were specifically increased in the SLM of the HA-NL1FL mice relative to controls (Intensity: 135.2 ± 1.6 % vs. 100 ± 2.7 %, respectively, $p < 0.01$, Area: 131.7 ± 18.9 % vs. 100 ± 12.6 %, $p < 0.05$, **Figure 4E**) and not increased in the HA-NL1 Δ C mice (**Figure 4F**). No significant changes in intensity nor area of panShank labeled puncta were found in the SR. Our results demonstrate that we induced the largest changes in maturation in regions with higher levels of transgene

expression in the hippocampus, specifically, the SLM. Thus, we conclude that the intracellular C-terminal region of NL1 aids in the maturation of excitatory synapses, i.e. transitioning from an NR2B-rich and Shank-poor state to one with high Shank levels and low NR2B.

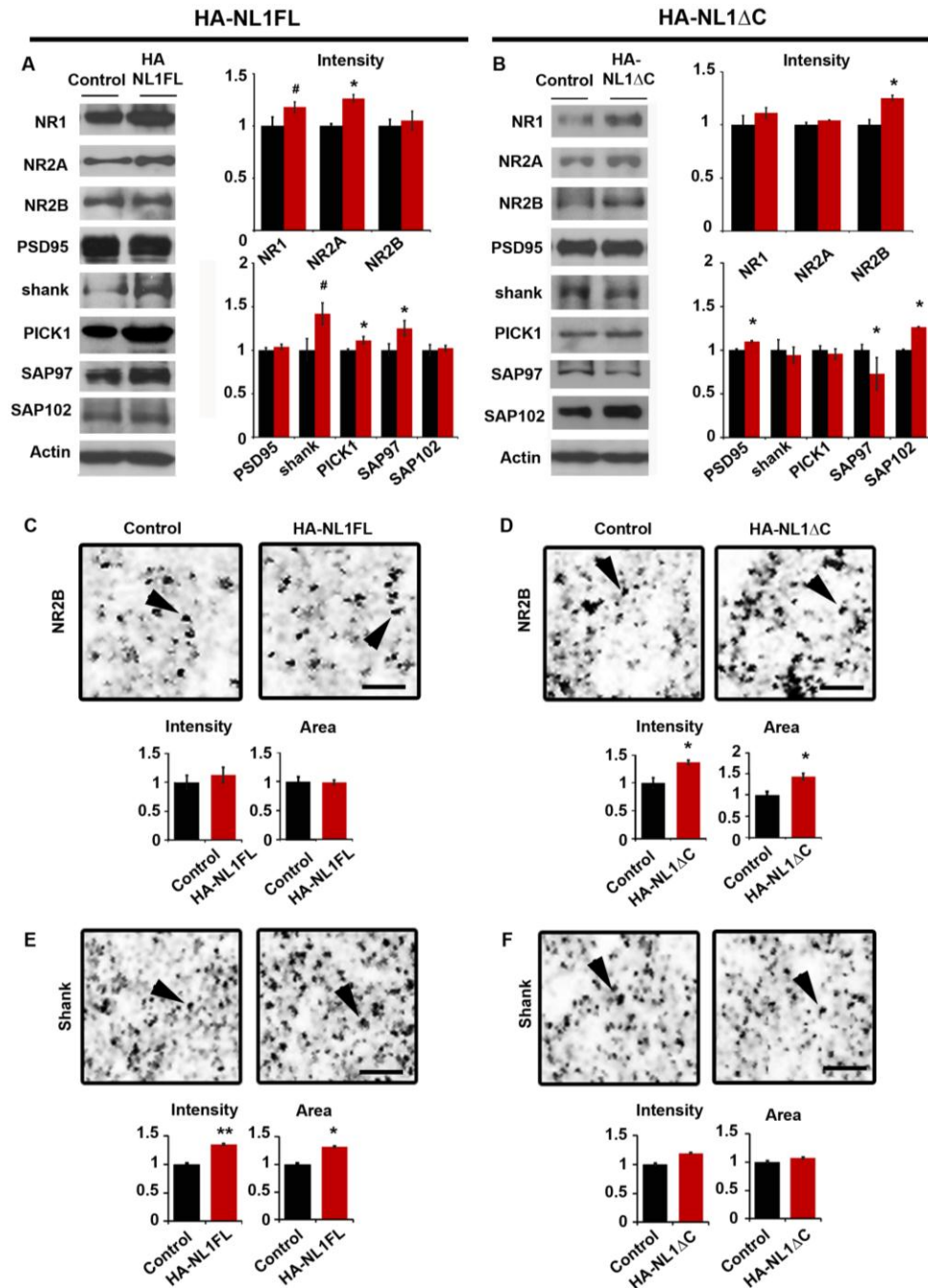


Figure 4. Distinct changes in synaptic protein composition in HA-NL1FL versus HA-NL1ΔC mice. (**A & B**) Representative western blots of synaptosomal fractions from the hippocampus of (**A**) controls vs. HA-NL1FL mice and (**B**) controls vs. HA-NL1ΔC mice. Synaptosomes from the same mouse in each group are shown for every blot, with the group mean intensity plotted on the right normalized to control levels. The HA-NL1FL mice (red) expressed higher levels of the glutamate receptor NR2A, and the scaffolding molecule SAP97 and trended towards an increase in Shank family members as compared to controls, while the HA-NL1ΔC mice expressed higher levels of NR2B and SAP102, with a small increase in PSD95, and a decrease in SAP97 as compared to their controls

(See **Supplemental Figure 3** for detailed statistics and additional data). **(C & D)** Representative images of a $36\mu\text{m}^2$ region of SLM from sectioned tissue immunolabeled for NR2B from **(C)** controls vs. HA-NL1FL mice and **(D)** controls vs. HA-NL1 Δ C mice. Average intensity and area of puncta from the two groups is graphed below. No differences were detected between HA-NL1FL mice and their controls, while there was a significant increase in NR2B intensity and area of puncta specifically in the SLM of HA-NL1 Δ C mice as compared to their controls. Scale bar equals $2\mu\text{m}$, and arrows highlight puncta for comparison. **(E & F)** Representative images of a region of SLM labeled for panShank from **(E)** controls vs. HA-NL1FL mice and **(F)** controls vs. HA-NL1 Δ C mice. There was an increase in the average intensity and area of panShank puncta in the HA-NL1FL mice specifically in the SLM, but there was no difference in measures of panShank intensity, nor area of puncta in the SLM between the controls and HA-NL1 Δ C mice. Scale bar equals $2\mu\text{m}$, and arrows highlight puncta for comparison. Significance was determined with Student's t-test in all cases, $n = 4$ pairs and $\# = p < 0.104$ * = $p < 0.05$, ** = $p < 0.01$, *** = $p < 0.001$.

The changes in synaptic protein levels correlate with specific aspects of behavioral performance

We were surprised at how closely maturation of behavior matched that of excitatory synapses. To determine whether there was indeed a significant correlation between synaptic changes and the degree to which behavior shifted, we compared NR2B levels in the HA-NL1 Δ C mice and controls to the degree of flexibility exhibited during their reversal training (**Figure 2 & Figure 5**). First, we compared NR2B intensity levels to distance to reach the new location on the fourth training trial on the first day of reversal training. We examined this trial as we noticed that the largest time differences to reach the new location occurred here. Additionally, most of the HA-NL1 Δ C mice failed to visit the former location of the target first before finding the new location during this trial, shortening the distance they traveled before reaching the new location and reflecting a lack of persistence in searching the previous location (**Figure 2F'**). We included both control and HA-NL1 Δ C mice in this analysis to determine whether NR2B levels in the SLM were related to the behavioral performance independent of the presence of the transgene. That is, we wanted to know whether the natural variation in this behavior present in the control group was also related to NR2B levels. Increased levels of NR2B correlated with shorter distances to reach the new target location on a mouse-by-mouse basis (**Figure 5A**). Importantly, NR2B levels did not correlate with distance to first reach

the former target location in the probe trial, a more direct measure of recall accuracy (**Figure 5B**), suggesting that NR2B levels in the SLM do not reflect recall *per se*.

Another robust phenotype that we noticed in the HA-NL1 Δ C mice was a lack in persistent searching of the target quadrant and a strikingly different spatial distribution in their search patterns during the probe trial preceding reversal training. We therefore tested whether dwell time in the target quadrant also negatively correlated with NR2B levels and reflected an increase in flexibility. Comparisons of target quadrant dwell times to NR2B levels only yielded a relationship that approached significance (**Figure 5C**.) It was possible that substantial information about the distribution of the search path was lost in only accounting for time spent in the target quadrant. For example, analyzing only dwell time in the target quadrant artificially constrains what is a "targeted searching behavior" since it discounts locations and visits to neighboring quadrants (which may still reflect persistent searching if those locations are near the border of the target). Therefore, we derived a metric based on the distribution of radial distances between any two points of the search path to more specifically describe the localization of the search path (see Experimental Procedures). "Path Dispersion", or the full-width at half-maximum (FWHM) of the two-point radial distance distribution, increases as searching expands over the area of the pool and decreases as searching becomes more localized to a confined region (**Figure 5D**, compare the path of mouse X vs. Z). Path dispersion was highly correlated to NR2B levels (**Figure 5E**), suggesting that it may serve as a valid complementary method for assessing important changes in searching behavior during the probe trial. To validate the idea that the degree of dispersion may have facilitated finding the new location faster, or rather, also reflected enhanced flexibility, we compared path dispersion to distance to reach the new location on the fourth training trial. This directly showed that if a mouse had a more distributed search pattern during the probe trial, it also located the new target location more directly at the end of the first day of reversal training regardless of genotype (**Figure 5F**). Together, this series of comparisons suggests that higher NR2B levels in the SLM are tied to enhanced performance during reversal training and more dispersed search patterns during the probe trial.

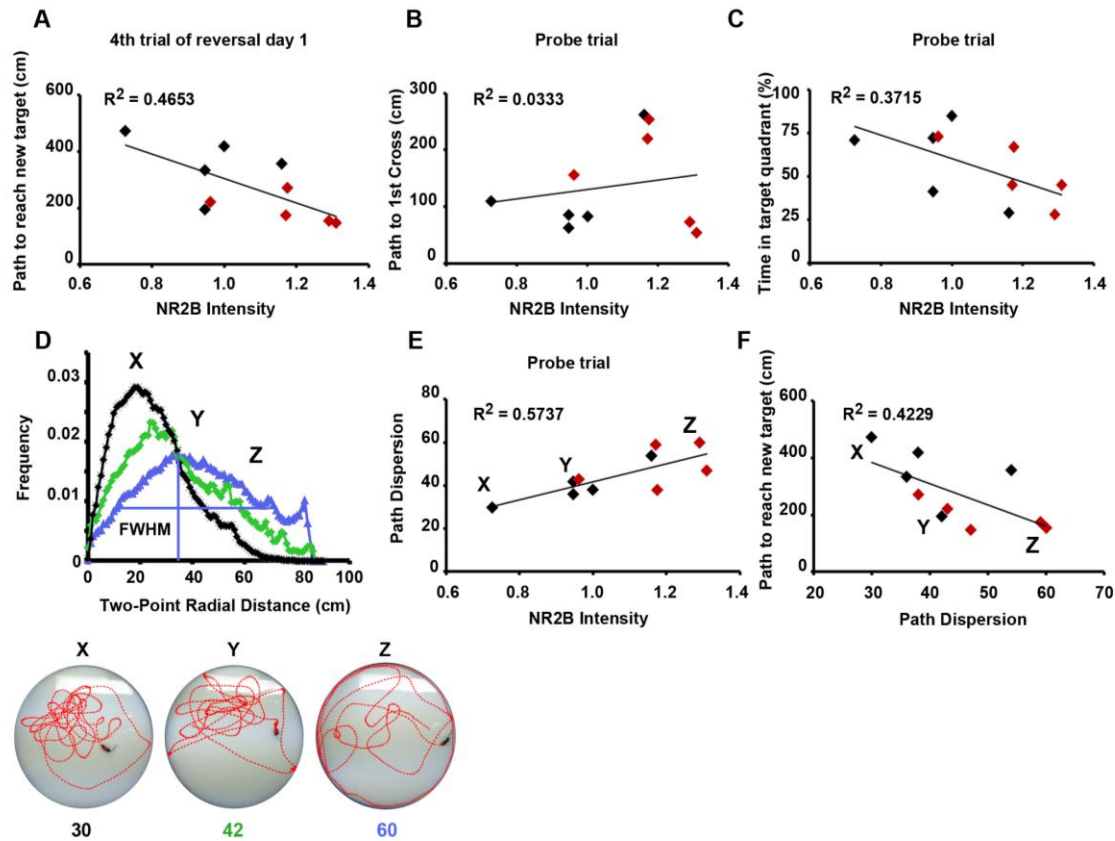


Figure 5. Correlation between levels of NMDAR subunit NR2B in the SLM and flexibility behavior. **(A)** NR2B intensity in the SLM correlated with the distance to reach the platform in the fourth training trial of reversal day 1 on a mouse by mouse basis ($p < 0.05$, $n=10$, 5 controls and 5 $NL1\Delta C$ mice). **(B)** NR2B levels did not correlate with distance to first cross the former platform location the probe trial, suggesting specificity in the relationship between SLM NR2B levels and measures of flexibility. **(C)** The correlation between NR2B levels and percent time spent in the target quadrant during the probe trial approached significance for a negative correlation ($p = 0.0617$, $n = 10$). **(D)** Exemplary two-point radial distance distributions for three search paths from mouse X (black), Y (green) and Z (blue). The full width at half max (FWHM) of each distribution was taken as the defining characteristic of the distribution, called “Path Dispersion”, and used as the metric for cross correlation analyses (see Experimental Procedures for detailed description of measure). The individual search paths and the color-coded path dispersion score in cm are shown below for mouse X, Y and Z. **(E)** The more NR2B in the SLM, the more “Dispersed” the search area during the probe trial of water maze testing ($p < 0.025$, $n = 10$). **(F)** The path dispersion measure also correlated with distance to reach the new target location during reversal training ($p < 0.05$).

Manipulations of NL1 intracellular signaling impact social behavior and sensory evoked responses in the cortex.

NL1 function has been linked to social behavior as well as learning and memory in studies where genetic manipulations were more ubiquitous (Blundell et al., 2010) Moreover, it is unclear which neural circuits may process social information (Insel and Fernald, 2004) We therefore studied whether our manipulations could also impact social behavior in order to address the relevance of NL1-mediated synaptic maturation on this complex form of behavior. First, the three chambered social preference test allowed us to gauge basic social preferences (Moy et al., 2004) In the first phase, the test animal is given a choice to interact with either an inanimate object or an age and sex matched stranger mouse. In the second phase, the test animal is given a choice of the previously introduced mouse and a novel social partner. Typically, mice of our background strain prefer social interaction over that with an object, and interaction with a novel partner over that of a familiar (Moy et al., 2004). We observed no significant differences in the behavior of the HA-NL1FL mice relative to the controls, which performed as expected in this task (**Figure 6A**). We thus conclude that there is an absence of a significant deficit in basic social behavior in this line of mice.

As more complex forms of social interaction could have still been impaired, we also measured aggression and dominance behavior in male mice employing both the resident-intruder task and dominance tube test (Duncan et al., 2004; Messeri et al., 1975; Moy et al., 2004) In the resident-intruder task male mice are separately housed for up to 7 days in order to establish a home territory and then an age, weight and sex matched intruder is introduced and several measures of basic social interaction and more aggressive acts are scored. Introduction of an intruder mouse under these conditions typically induces overt acts of aggression in our background strain of mice. We also saw no significant difference between the HA-NL1FL mice and controls in their interaction during this task (**Supplemental Figure 4A, left graph**). The dominance tube test can also be used to confirm differences in dominance, as it pits two mice against each other in a confined tube in which a more dominant male would force the less dominant to retreat. This test assesses more subtle levels of dominance that may be present, but may not result

in more aggressive acts such as mounting or fighting. We again found no difference in this behavioral test between the HA-NL1FL mice and their controls (**Supplemental Figure 4A, right graph**).

In contrast, HA-NL1 Δ C mice were different from controls on many measures of sociability. They failed to show a characteristic preference for social novelty, while still displaying a strong preference for social interaction in general in the three chambered social preference test (**Figure 6B**). This lack of preference for a novel partner is unlikely to be due to the previously described differences in learning and memory as similar tests for novel objects revealed a preference for novel objects with a delay between exposures of up to an hour. In these tests for social novelty, the delay between different phases of testing is only 10-15 minutes. Therefore, we observe selective changes in social novelty preference versus a change in preference for novelty per se. This implies that the HA-NL1 Δ C mice either had a specific deficit in their ability to detect social novelty, or did not prefer novel social partners to the familiar if they could discriminate. Interestingly, we found that juvenile mice of the same background strain (C57BL/6J) also lacked a preference for social novelty without lacking preference for social interaction, as compared to adult mice (**Figure 6C**). This suggests that more complex features of social interaction are affected in the HA-NL1 Δ C mice and that the effects are similar to the normal social behavior exhibited by juvenile mice.

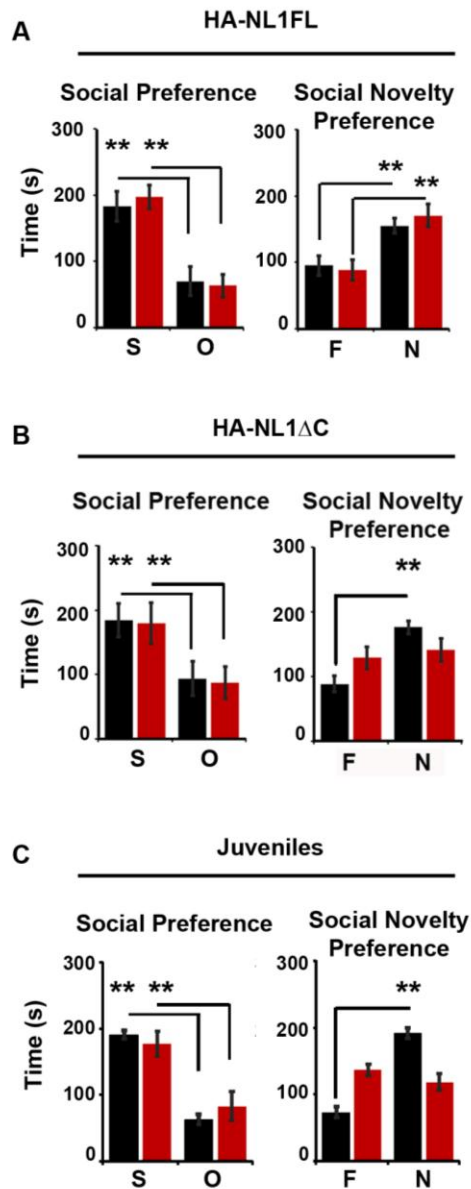


Figure 6. Manipulations of NL1 intracellular signaling affect social behavior. **(A)** Performance in the three chambered social preference task. Mean time in seconds (s) spent in the chamber with either a social partner (S) or an object (O), is depicted for both controls (black bars) and HA-NL1FL mice (red bars) in the left graph. Mean time spent in a chamber with either a familiar social partner (F) or a novel social partner (N) is depicted in the graph to the right. Both controls and HA-NL1FL mice preferred to spend time with a social partner vs. an object and a novel partner vs. a familiar (n =10 pairs). **(B)** There was no difference in preference for social interaction over interaction with an object for HA-NL1ΔC mice (red bars in left graph). However, the HA-NL1ΔC mice did not show the characteristic preference for a novel social partner and instead were equally engaged with a familiar (F) and novel (N) mouse (red bars in right graph, n = 10). **(C)**

Juvenile mice preferred social interaction to investigating an inanimate object, but also did not display preference for social novelty ($n = 9$). See **Supplemental Figure 4** for additional behavioral measures. Error bars are SEM, significance was determined with RMANOVA, with Tukey's *post hoc* and $* = p < 0.05$, $** = p < 0.01$, $*** = p < 0.001$.

We also observed strong changes in aggressive and dominant social behavior in males. In measures of social interaction employing the resident-intruder paradigm, our transgenic mice were less likely to engage in a fight (**Supplemental Figure 4B, left graph**, $56.7 \pm 3.3\%$ vs. $16.7 \pm 1.1\%$ vs. controls vs. HA-NL1 Δ C mice, $p < 0.025$, $n = 9$ pairs). However, there are no significant effects in other forms of social interactions during this test including dominant mounting behaviors (data not shown). The HA-NL1 Δ C mice were more likely to be submissive when pitted against group housed control mice in the dominance tube test (**Supplemental Figure 4B, right graph**). The performance of our controls in this task indicates that group housed mice are equally likely to exhibit dominant or submissive behavior, while the HA-NL1 Δ C transgenics lost more bouts than would be predicted by chance if only half of the group were submissive to opponent mice. Overall, these results suggested that expression of HA-NL1 Δ C resulted in a decrease in overt acts of aggression in addition to the lack of preference for social novelty.

While the changes in social behavior were surprising given the restricted expression pattern, recent studies of likely downstream targets of NL1 such as Shank family members suggested that altered synaptic transmission from the cortex may partially contribute towards changes in social behaviors (Peca et al., 2011) Interestingly, we found highest levels of our transgenes in the SLM of the hippocampus, a region that receives direct input from the entorhinal cortex via the perforant pathway and may critically support the coordinated cortical-hippocampal dynamics that are thought to support many forms of behavior apart from learning and memory (Gordon, 2011; Hasselmo and Schnell, 1994; Hasselmo et al., 1995) Furthermore, we found similarly high levels of expression of our transgenes in specific regions of cortex (**Figure 1B**). Therefore, we measured sensory-evoked responses in the auditory cortex to determine whether we could detect functional changes in the cortex that were consistent with the previously observed synaptic changes thoroughly characterized in the hippocampus

(**Figure 3 and Figure 4**). We could not detect a significant change in the relationship between neuronal firing rates and stimulus strength in the auditory cortex of HA-NL1FL mice (**Figure 7A**). In contrast, we found a significant shift in the threshold for evoking sensory responses in the HA-NL1 Δ C transgenic mice as compared to controls (**Figure 7B**). However, basic auditory responses such as the startle reflex were unaffected (data not shown). Interestingly, such a shift in the threshold for sensory evoked responses is a characteristic developmental milestone in the auditory cortex, where a decrease in the threshold to elicit a change in firing rate accompanies developmental progression (de Villers-Sidani et al., 2007; Moore and Irvine, 1979). Furthermore, the higher threshold for sensory-evoked responses seen in both typical juveniles as well as our NL1 Δ C mice is consistent with the idea that there is a decrease in synaptic strength within auditory cortex, or within other regions that provide input to the auditory cortex, relative to normally developed adults.

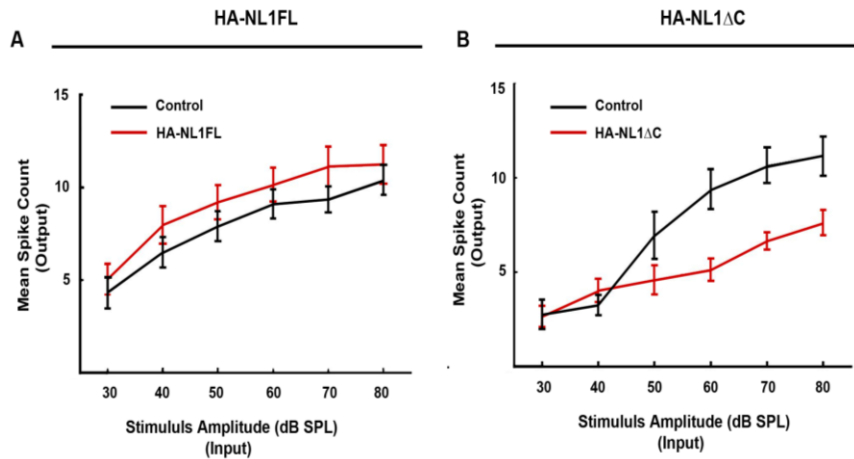


Figure 7. Manipulations of NL1 affect sensory evoked responses in cortex. (**A**) Mean spike counts for neurons in the auditory cortex activated by differing levels of stimulus strength (white noise clicks) are plotted for both controls (black) and HA-NL1FL mice (red). No significant changes in sensory-evoked responses were found in the HA-NL1FL mice relative to controls. (**B**) HA-NL1 Δ C mice showed an increase in the stimulus threshold necessary for eliciting an increase in firing rate ($p < 0.001$, $n = 11$ pairs). Error bars are SEM, and significance was determined by RMANOVA.

3. DISCUSSION

In this study, we present concrete evidence for the importance of the intracellular C-terminal region of NL1 in the maturation of synapses *in vivo* and evidence that this synaptic maturation within discrete forebrain nuclei is correlated with a maturation of complex behaviors. Specifically, we showed that overexpression of NL1FL in the hippocampus results in memory deficits and perseverance for already learned targets, whereas expression of truncated NL1 improved flexibility, highly reminiscent of juvenile behavior. In addition, social behaviors were tipped towards a juvenile-like state in HA-NL1 Δ C mice, and sensory-evoked responses in the auditory cortex confirmed that at least one feature of neural circuit function was maintained in a more immature state when HA-NL1 Δ C expression was spatially restricted to regions of the forebrain. At the cellular level, we examined synaptic spines and the localization of key proteins to synapses in the hippocampus; NL1FL expression resulted in a bias towards mature synapses, i.e. large spine heads containing more NR2A, Shank, SAP97 and GluR1, and NL1 Δ C expression resulted in immature synapses, i.e. smaller spines containing more NR2B and SAP102. This suggests that the manipulations of NL1 that we introduced were sufficient to alter the maturational states of glutamatergic synapses and that such changes correlated with developmentally relevant changes in behavior and brain function.

We propose a simple model whereby NL1 C-terminal signaling facilitates a series of molecular steps that act to enhance the recruitment of Shank family members and SAP97 which in turn promote the maturation and potentiation of excitatory synaptic structures (**Figure 8**). The data suggest that activities carried out by the last 55 amino acids lead to the replacement of juvenile synaptic scaffolding molecules with a more mature complement of proteins, as expression of NL1 Δ C could not induce the increase in factors that characterize mature synaptic structures. Furthermore, expression of NL1 Δ C led to retention of immature synaptic markers such as SAP102 and NR2B while repelling SAP97. This suggests that this molecule enacted a dominant negative activity that prevented the accumulation of mature synaptic factors. Such a molecular process could have prevented the activity-dependent synaptic elimination of early born synapses that is known to accompany development and simultaneously halted their maturation. This mechanism could account for the observed increase in the number of synapses found with

an immature synaptic protein complement in the HA-NL1 Δ C mice (**Figure 4B and 4D**). Interestingly, recent *in vitro* studies in organotypic cultures have found a novel regulatory region within the C-terminal region of NL1 that was necessary to enhance several features of synapse formation and function (Shipman et al., 2011). This implies that non-PDZ intracellular domains within NL1 may also play a significant role in synaptic development, however our results clearly suggest that long term *in vivo* manipulation of NL1 signaling via the PDZ domains impacts synaptic and behavioral maturation. Therefore, future studies dissecting the intracellular activities of NL1 *in vivo* are necessary to illuminate whether NL1 may play mechanistically distinct roles during initial synapse formation versus maturation.

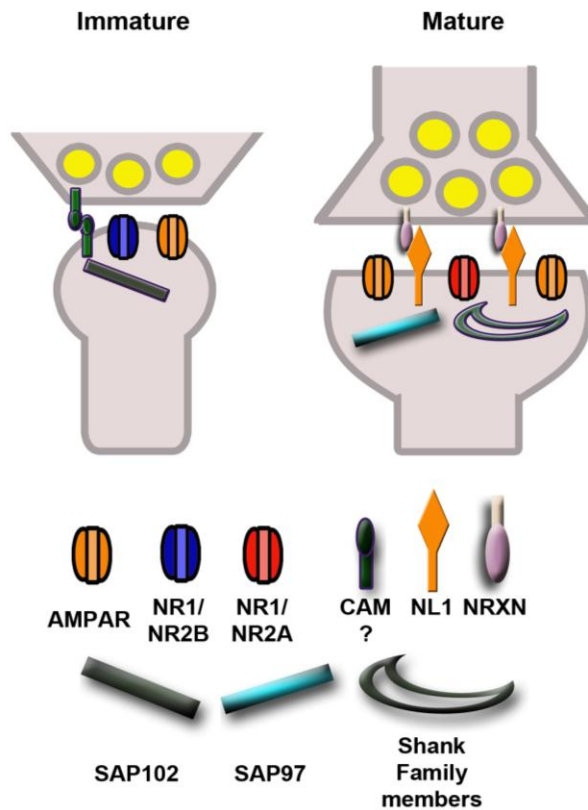


Figure 8. Model for NL1's role in late phases of synaptic maturation. NL1 mediates the transition from an immature synaptic state to a mature synaptic state via its intracellular signaling. NL1 C-terminus signaling is required for the replacement of immature scaffolding molecules such as SAP102 with mature forms such as SAP97 and Shank family members. This change brings about the replacement of NR2B containing

NMDARs with those composed of NR2A, which may ultimately underlie the observed changes in spine morphology induced by overexpression of the full length NL1.

The last 55 amino acids of NL1 support crucial features of synaptic maturation that are linked to developmentally regulated changes in synaptic stability.

The expression level of an array of postsynaptic scaffolding molecules and glutamate receptors have been observed to change as a function of developmental progression and the gradual accumulation of stronger, more stable glutamatergic synapses. Scaffolding molecules such as SAP102, PSD95, PICK1, SAP97, Shank1 and 3 are known to interact with the PDZ binding motif of NL1 and each have been implicated in mediating a subset of the synaptic changes that parallel the development of neural circuits (Meyer et al., 2004; Petralia et al., 2005; Tallafuss et al., 2010; van Zundert et al., 2004; Zheng et al., 2011) Individually, several of these molecules have also recently been reported to impact learning, memory and social behaviors. Our study of NL1 overexpression is the first to investigate the effects of this manipulation on key scaffolding molecules as well as behavioral progression (Dahlhaus et al., 2010) Therefore, our results clarify and extend our understanding of NL1 synaptic recruitment capabilities *in vivo*.

Shank protein family members and SAP97 synaptic localization were up-regulated by the overexpression of full length NL1. It is therefore possible that these proteins partially facilitated the observed increase in mature synaptic structures and deficits in spatial learning observed in the HA-NL1FL animals. Shank1 and 3 contain PDZ domains that can bind to the C-terminus of NL1 and they form an integral part of the postsynaptic density (Sheng and Kim, 2000) Further, both family members have been suggested to support increases in spine head size, and other critical features of synapse maturation such as AMPA receptor trafficking to synapses and enhanced synaptic potentiation (Sala et al., 2001) A study examining the phenotype of Shank1 null mice found an increase in the number of smaller, weaker spines in the hippocampus that correlated with a specific enhancement in spatial learning and memory behaviors (Hung et al., 2008). Shank3 also regulates the size and density of dendritic spines, but is more highly expressed in distinct regions of the brain as compared to Shank1. Interestingly,

knockout, or other reductions, of Shank3 function spares learning and memory behaviors while altering social behavior (Bangash et al., 2011; Bozdagi et al., 2010; Peca et al., 2011) Overall, this suggests that Shank family members affect the potentiation of glutamatergic synapses throughout the brain, and that this cellular process impacts complex behaviors such as learning, memory and social interaction.

Like Shank proteins, SAP97 has been reported to enhance the mature characteristics of synapses, namely the size and complexity of dendritic spines (Kim and Sheng 2004, Poglia 2010). It is thought that its ability to target NR2A and GluR1 type subunits to synapses directly mediate its ability to potentiate glutamatergic synapses (Gardoni et al., 2003; Mauceri et al., 2007; Nakagawa et al., 2004; Sans et al., 2001; Schluter et al., 2006). Enhancements to the levels of both GluR1 and NR2A accompany maturation of synapses and neural circuits through development and insertion of GluR1 at synapses has been equated with synaptic potentiation and increases in synaptic strength (Malinow and Malenka, 2002) Our model posits that it is primarily through these scaffolding molecules that NL1 drives increases in levels of NR2A and GluR1, such as those observed in this study. It is possible that these events then lead to an enhancement in the proportion of large spines in the SLM, limiting the substrate available for modification during experience. This could account for impaired spatial learning and enhanced behavioral perseverance for learned information.

We did not see a decrease in Shank localization at synapses in the HA-NL1 Δ C mice, but did observe a highly significant decrease in SAP97 and an increase in SAP102 (**Figure 4B**) This suggests that opposing levels in SAP97 and SAP102 proteins may account for the larger population of smaller, immature synaptic structures discovered in the HA-NL1 Δ C mice. SAP102 is a scaffolding protein that is highly motile early in development, and believed to underlie the early organization of glutamatergic synapses. It is possible that such a molecule partially defines the state of a glutamatergic synapse as immature by limiting or selectively enhancing the availability of key receptor subtypes such as the NMDAR subunits NR2B and NR2A. Consistent with this idea, culture studies show that SAP102 is part of an NMDAR transport packet (Washbourne et al., 2004b) and differentially affects the recruitment of NR2B and NR2A to synaptic contacts, biasing towards a preferential trafficking of NR2B (van Zundert et al., 2004;

Zheng et al., 2011). Further, the relative ratio of NR2B to NR2A at synapses has important functional consequences for the strength and plasticity of those synapses. It is thought that the eventual replacement of NR2B with NR2A facilitates mature forms of plasticity that lead to the long term stabilization of synaptic connections (Vicini et al., 1998). In support of this idea, this switch occurs just prior to developmental periods characterized by rapid synaptic specification (van Zundert et al., 2004). Moreover, artificially elevating NR2B levels in the adult causes enhanced spatial learning thus validating the idea that it supports a bias towards plasticity and away from rigid stabilization (Tang et al., 1999). Therefore, we propose that our manipulations of NL1 impacted levels of key scaffolding molecules that induced a developmentally relevant change in the complement of glutamate receptors present at the synapses in our lines of mice.

Alterations of NL1 function within specific neural circuits supported developmentally relevant shifts in behavior

Previous manipulations of NL1 function *in vivo* implicate the molecule in specifically altering long term synaptic potentiation and stabilization (Blundell et al., 2010; Dahlhaus et al., 2010; Kim et al., 2008), a process mechanistically tied to those involved in the activity-dependent validation of synapses during critical periods of sensory system development. Accordingly, these modifications in NL1 function in the adult also impaired acquisition and long term retention of a variety of forms of memory. Therefore, prior to our study, it was an open question as to how NL1 function may specifically impact the development of mnemonic systems. Studies of learning and memory behaviors in rats suggest that explicit mnemonic systems and behavior undergo a substantial transformative period early in juvenile development where the capacity to learn and remember changes dramatically (Brown and Kraemer, 1997; Rossier and Schenk, 2003; Rudy, 1994). More recent evidence suggests that less stable hippocampal place fields can be found in juveniles as compared to the adult rat, and it is known that the long term stability of hippocampal place fields rely on NMDAR-mediated activity (Kentros et al., 1998; Langston et al., 2010; Scott et al., 2011). However, creating a clear picture of the molecular processes that underlie this developmental transition, and

whether they rely on developmentally relevant shifts in NMDAR activity, requires the genetic access that is currently only afforded by studies in mice. Here, we provided some of the first evidence that explicit forms of learning in juvenile mice may be accomplished in a manner similar to adults by at least one month of age (Figure 2G – 2I’). This suggests that potential sensitive periods for the development of this complex behavior may take place between eye opening (conferring the ability to visually explore an environment) and one month of age, and that the more subtle aspects of this behavior are still being shaped after one month postnatal in mice. Our results in the NL1 Δ C mice are consistent with the idea that specific perturbations of NL1 function may have prevented typical developmental advancement of both learning and memory behavior.

The correlation between NR2B and flexibility, such as the one we found with NR2B levels (**Figure 5**), would help explain our other observations regarding synaptic and behavioral changes in both our lines of mice. We predicted, based on previous studies, and subsequently confirmed, that the full length version of NL1 would enhance the proportion of mature synaptic structures present in the forebrain relative to controls, thus limiting the number of synapses subject to further potentiation and modification with experience (**Figure 3A, 3A’, 3C, Figure 4A and 4E**). This activity would then bear out in a deficit to modify behavior with repeated experience as few synapses would be available for event related potentiation, resulting in learning and memory deficits and a general lack in flexibility. Further, we had anticipated that expression of the truncated version of NL1 would simply fail to elicit the enhanced proportion of synapses in a highly potentiated state, resulting in a failure to induce the changes in behavior seen with NL1FL. However, this manipulation resulted in mice that were more similar to juveniles than to that of age matched adults (**Figure 2D – I’**). The HA-NL1 Δ C mice exhibited short term learning and flexibility enhancement, with a slight deficit in long term memory retention with a single trial exposure. This behavioral profile would be consistent with an increase in the proportion of synapses in a highly modifiable state that were more difficult to maintain in a highly potentiated form. Studies of NR2B function suggest that a difference in NR2B levels could support such a change in state. Conversely, studies of NR2A function also seem to suggest that specifically enhancing the levels of this subtype, could strengthen and stabilize synaptic contacts facilitating many of the

morphological and functional hallmarks of synaptic maturation, while limiting bi-directional synaptic modification. Therefore, the changes in the proportion of NMDAR subunit types that we observed in our mice are likely to underpin many of the concomitant changes in synaptic morphology, function and behavior that were measured.

Finally, it is unclear how varying states of synaptic maturation may impact social behavior, but the behavioral data examining NL family function *in vivo* suggests that there may be a link between the cellular processes governed by NLs and social interaction (Blundell et al., 2009; Dahlhaus and El-Husseini, 2010; Hines et al., 2008; Jamain et al., 2008). Studies that seek to understand social interaction in mice often center on studies of play in young male animals and aggression in older males. It is unclear what developmentally related synaptic mechanisms may account for the observation that these behaviors appear differentially prevalent between young and mature male mice. Interestingly, NMDAR hypofunction has been linked to enhanced aggression in male mice, further implicating changes in glutamate-mediated signaling over development as a process that underlies important aspects of complex social behavior (Duncan et al., 2009). This suggests that age-specific aspects of NMDAR signaling could regulate the development of social interaction. This idea is consistent with our observations that we find reduced aggression and enhanced flexibility in social preference in the HA-NLΔC mice when we also find enhancement in juvenile forms of scaffolding proteins and NMDAR subunit composition. Therefore, it is interesting to speculate that these changes in social behavior also reflect maintenance of more juvenile like characteristics, and that such changes may be linked to the state of modifiability of glutamatergic synapses within specific neural systems (**Figure 1B**). Taken together, this set of studies validates the role of NL1-mediated processes in the maturation of complex behaviors, and hones in on the molecular pathways that may specifically regulate flexibility in such behaviors.

These results validate the idea that specific NL1 intracellular signaling domains regulate late stages of synaptic maturation *in vivo*, and provide the first evidence, that artificially manipulating the relative proportion of glutamatergic synapses in one state versus another *in vivo*, within specific neural systems, alters behavioral traits that change as a function of development.

4. METHODS

All studies were conducted with approved protocols from the University of Oregon Institutional Animal Care and Use Committee, in compliance with NIH guidelines for the care and use of experimental animals.

Transgenic Mouse Generation and DNA Constructs

Neurologin1 was amplified and GFP tagged as described in (Fu et al., 2003). The GFP was replaced with an HA epitope tag sequence via PCR and was inserted into pTRE-tight (Clontech) via the vector pCDNA3 using HindIII and XhoI and then HindIII and XbaI sites. The TetO-HA-NL1FL was linearized with XhoI and injected into embryos. The HA-NL1 Δ C was similarly created except that the last 55 amino acids were deleted via PCR with the following reverse primer (NL1- Δ C:

ggtctcgagctacctcctcatagcaagagtataatctggg). Constructs were confirmed with sequencing and successful transgenesis was confirmed via genomic PCR and Western blot of forebrain homogenate for the HA tag

All single transgenic mice (TetO-HA-NL1 Δ C positive or TetO-HA-NL1FL positive) as well as double transgenic mice (CamKII α -tTA /TetO-HA-NL1 Δ C positive) were first examined for basic health and behavior according to standard methods (Moy et al., 2004). No overt changes in health, reproduction and behavior were observed. Further, single transgenics were used as controls in all experiments to exclude nonspecific effects of transgenesis resulting in the changes observed.

Immunocytochemistry, Microscopy and Image Processing

In most cases, brains from 4 animals of each genotype were dissected immediately from animals euthanized by decapitation with isoflurane anesthesia and flash frozen with liquid nitrogen. Brains were stored at -80°C for up to 3 weeks until sectioned. For the animals used in the NR2B and behavioral comparisons, samples from 5 mice in each group were prepared. Frozen tissue was cryosectioned to 8 μ m thickness. Sections on slides were then fixed with 4% PFA solution in phosphate buffered saline (PBS) for 30 minutes at 4 °C, followed by 3 5-minute rinses in PBS with gentle agitation.

Antigens were made accessible with a 0.05% trypsin wash for 5 min at room temperature and washed with PBS. Slides were then blocked, incubated in specified primaries, washed and followed with appropriate secondary antibody (See Supplemental Experimental Procedures for details of procedures).

Images were taken on an inverted Nikon TU-2000 microscope with an EZ-C1 confocal system (Nikon) with either a 10x or 100x oil immersion objective (1.45 NA). Sections were imaged blind to specific conditions. Images were processed and quantified in Image Pro Plus® (Media Cybernetics). Briefly, three 100 μm^2 regions within each hippocampal area per section was selected for analysis, automatically thresholded and puncta selected with the automatic bright objects feature. Measures of mean intensity and area were recorded for each punctum and average densities of puncta per 100 μm^2 were calculated. The process was repeated for three separate sections from each mouse analyzed, with 3 mice analyzed in each condition. Staining in CA1 SR, SLM and the molecular layer of CA3 were measured. Group means were compared and statistical significance was determined using the Student's t-test with α level set at 0.05.

Synaptosomal Preparations and Western Blotting

The hippocampal formation, including the subiculum, was dissected from experimental mice and homogenized in 1.5ml of buffer (4mM HEPES, 320mM Sucrose, protease inhibitor tablets (Roche), pH7.4) using a Potter-Elvehjem tissue grinder. Homogenate was centrifuged for 10 minutes at 850xg, the supernatant was removed and centrifuged at 12000xg for an additional 10 minutes. Pellet was resuspended in 2ml buffer and centrifuged for 10 minutes at 14000xg. The final pellet was resuspended in 500 μl of buffer. Protein concentration was determined using the BioRad D_C Protein Assay kit. Samples were diluted in sample buffer (312mM Tris-HCl, pH6.8, 50% glycerol, 10% SDS, 0.05 Bromophenol blue and 25% β -Mercaptoethanol) to a final concentration of 0.3 $\mu\text{g}/\mu\text{l}$. A total of 3 μg was loaded onto an SDS-PAGE gel, with samples from 4 animals per genotype, transferred to nitrocellulose membranes and probed with the antibodies shown at a dilution of 1:1000 (see Supplemental Experimental Procedures for sources of antibodies).

Behavior

Basic reflex and health assessment follows (Moy et al., 2004). Briefly, mice were screened for weight differences, coat condition, abnormal tooth length, reproductive capability, gross visual functions such as forepaw reaching towards a distant object, and basic motor capabilities such as climbing rates and clinging times to an inverted wire cage lid.

Morris Water Maze

The Morris water maze task was based on the standard methods for spatial learning in rodents (Vorhees and Williams, 2006). Each transgenic cohort consisted of 10 double positive male mice and 10 control males positive for one of the two transgenes. In the juvenile analysis, 8 juvenile males and 8 adult males from a previous breeding by the same parents were compared. Briefly, the mice were tested for their ability to find an escape platform (diameter = 12 cm) on four different components in the following order: 1) a two day visible platform acquisition, 2) a six day hidden (submerged) platform acquisition phase with the target moved to a different location, 3) a subsequent probe trial in the absence of the platform and 4) a hidden platform training in a new location (reversal training). In each case except the probe trial, the criterion for learning was an average latency of 15 s or less to locate the platform across a block of four consecutive trials per day separated by rest periods of 3-5 minutes (see Supplemental Experimental Procedures for further details of training and measures). All data were analyzed with repeated measures ANOVA (RMANOVA), followed by Tukey's *post hoc* test to compare means of interest, with α level set at 0.05.

Path Dispersion Metric

To characterize the spatial distribution of search paths relative to locations searched by the animal (animal centric) as opposed to regions more generally defined by the location of the target and the observers perception of the task goals (observer/task centric), we developed a strategy to calculate and describe the spatial relationship between all the points in a track (Figure 5D). We first built the two-point distance distribution of the track, $P(r)$. This is done by measuring the distance, r , from each point

in the track to every other point in the track, binning the distances into 0.5cm bins centered at, $r = 0.5, 1.0, 1.5 \dots n$, and then counting the number of measured distances that fall into each bin. We then normalized the bin counts to the total number of distances measured, equal to $\frac{(N-1)(N-2)}{2}$, where N is the number of points in the track (Figure 5D).

Therefore, highly localized search patterns will have narrow distributions shifted toward smaller r , while more dispersed search paths will have wider distributions shifted toward larger r . In order to condense this clustering information into a single number, we measured the full width at half max (FWHM) of $P(r)$. The HM of $P(r)$ is calculated as the maximum value of $P(r)/2$ and the two r values, r_+ and r_- for which $P(r) = \text{HM}$ are then found from the distribution. The FWHM is then calculated as $\text{FWHM} = r_+ - r_-$. Note that it is not necessarily accurate to interpret $P(r)$ as a probability distribution, that is using $P(r_i)$ to calculate the probability of finding a second track point within $\pm 0.5\text{cm}$ of a radius, r_i measured from an initial track point. This interpretation fails due to the finite size of the maze pool. The finite size of the pool constrains the area the animals are able to explore, and thus width of the measured $P(r)$ distributions. Despite this limitation, the FWHM values can still be employed as a direct measure of track localization, or rather, the clustering of locations visited within the animal's search path. We define FWHM as "Path Dispersion" because the measure increases with an increase in the distribution of the path taken by the animal over a larger area of the pool.

Object Recognition

The experiment was performed as described in (Bevins and Besheer, 2006) Briefly, mice were individually habituated to an open-field round container (30 cm in diameter x 30 cm in height) for 15 minutes. The training session followed the habituation session by 10 minutes. During the training session, two novel objects were placed in the open field, and the animal was allowed to explore for 20 min. All trials were recorded by video, and measures of time spent exploring each object, time to first make contact with an object, percent thigmotaxis, and which object was first approached were scored. Criteria for active exploration included sniffing, touching and circling the objects. After a delay from initial exploration of one hour, the animal was placed back into the same box in which one of the familiar objects during training was replaced by a novel object

and allowed to explore freely for 15 min. A preference index, a ratio of the time spent exploring the novel object (retention session) over the total time spent exploring both objects, was used to measure recognition memory. Data were calculated as mean \pm SEM. Significant differences from chance performance were determined by Wilcoxon-signed rank test, with α level of 0.05. Chance performance was assumed to be 50% time at each object.

Three Chambered Social Preference Test

This test was performed as described in (Moy et al., 2004) The test was performed in three phases: (A) *Habituation*. The test mouse was first placed in the middle chamber and allowed to explore for 10 min, with the doorways into the two side chambers open. Each of the two sides contained an empty wire cage. The wire cages were 11 cm in height, with a bottom diameter of 10.5 cm. A weight was placed on the top of each cage to prevent movement. Wire cages were cleaned with EtOH between trials and washed thoroughly at the end of each testing day. (B) *Sociability*. After the habituation period, the test mouse was enclosed in the center compartment of the social test box, and an unfamiliar mouse (a group housed “stranger” mouse), was placed in one of the wire cages of the side chambers chosen semi-randomly. This insured a mixture of right and left locations were tested within each group and accounted for potential biases in side preference. After the stranger mouse was in place, the test mouse was allowed to explore the entire social test box for a 10-min session. Sessions were recorded by video and scored by two blinded and trained observers. Number of approaches of stranger and object were scored. Total time and track distribution within each chamber was calculated using Image Pro Plus, and percentage of time spent near either cup was the metric displayed in Figure 6. (C) *Preference for social novelty*. Immediately following the sociability test, each mouse was tested in a third 10-min session with a choice of the familiar stranger vs. a novel group housed stranger mouse of the same strain, age and sex. The same measures as mentioned above were calculated and social novelty preference could be calculated by comparing time differences in the interactions with the familiar and novel mouse. Significance was determined by repeated measures ANOVA and the α level set at 0.05.

Spine Density and Morphology Quantification

Brains from 3 animals of each genotype were sectioned immediately after euthanasia by isoflurane followed by decapitation. 150 μ M thick coronal sections were cut at room temp on a vibratome and placed into 2% PFA for 30 minutes. Sections were then placed on slides and covered in 1xPBS. DiI crystals (Sigma-Aldrich®) were sparsely inserted into stratum oriens of region CA1 in the dorsal hippocampus as well as directly in the synaptic target layer SLM or SR. Tissue was monitored for distribution of DiI labeling between 1-5 days. 4-5 serial sections containing both hemispheres from each animal were labeled with DiI. 12 well isolated dendrites from both proximal Sr, and SLM were imaged at 100x magnification using a Nikon C1 confocal microscope (see above) and quantified. Results were averaged across three animals for each genotype, yielding a total of 36 individual dendrites analyzed per hippocampal layer, per genotype (see Supplemental Experimental Procedures for details on dendritic branch selection criteria). Composite images were created from 10-20 μ m thick z-stacks taken at 0.2 μ m increments with a small pinhole. Spine density, number of spines per 10 μ m of dendrite, and spine head area were measured using ImageJ. Prior to outlining spines for analysis, images were converted to 8-bit greyscale, deconvolved and thresholded until individual spines were clearly dissociable.

Auditory Cortex Electrophysiology

Briefly, each mouse was anesthetized and the left temporal cortex was surgically exposed (craniotomy and durotomy) and covered with 1.5% agarose in 0.9% saline. Tungsten electrodes, with 1-2 M Ω impedances were employed to find cortical regions with strong multiunit responses to click trains, determined audio-visually. Click trains were presented at 80 dB SPL, for 25 ms in duration with inter-stimulus intervals of 500 or 1000 ms. Each mouse had 1-4 recording sites in layer 3-5 of auditory cortex (*Mean depth* = 419 μ m, *Range*: 314-580 μ m, *n* = 21). The rate level function measures neural spike counts driven by increasing sound amplitude in dB (SPL) for white noise (WN) clicks. The number of spikes were summed from a 50 ms window, beginning at the stimulus onset using a spike detection threshold of 3 SD over 40 trials. Subjects: 5 control

male mice with 11 recording sites (range of 1-4) and 4 transgenic male mice with 10 recording sites (range of 1-3) were used for these experiments. Significance was determined with repeated measures ANOVA with the α level set at 0.05.

CHAPTER IV CONCLUSIONS

PARALLEL MECHANISMS FOR INITIATING THE EARLY STAGES OF GLUTAMATERGIC SYNAPSE FORMATION MAY EXIST

Using a cell adhesion molecule receptor recruitment assay or CAMRA we have identified the 4.1 proteins, protein 4.1B and 4.1N, as postsynaptic effector molecules of the recently discovered cell adhesion molecule SynCAM1. My studies have revealed three important and novel findings: 1) SynCAM1 interacts with protein 4.1B to directly recruit NMDARs shortly after synaptic-like contact; 2) Postsynaptic protein 4.1B enhances presynaptic differentiation through SynCAM1; and 3) proteins 4.1B and 4.1N differentially regulate glutamate receptor recruitment to sites of adhesion. Studies in cultured hippocampal neurons suggest that 4.1B plays an important role in the recruitment of NR2B-containing NMDARs to synapses during development. Thus, these studies delineate a novel function for 4.1 proteins in the recruitment of specific glutamate receptor types to synapses. This result adds 4.1B proteins to the panoply of proteins that impact the trafficking of the early arriving glutamate receptor subunit NR2B, suggesting that some functions of SynCAM1 are redundant or act in parallel with other cell adhesion molecules that are expressed over similar time periods in order to ensure that building a functional synapse occurs properly. Interestingly however, SynCAM1 only knockout mice do exhibit a behavioral phenotype (Takayanagi et al., 2010). This result suggests that there are some functions of SynCAM1 that change the properties of the synapse in ways that have important consequences on behavior, but cannot be compensated for in its absence. It is also not uncommon that a single protein may play distinct functional roles at multiple stages of development. Perhaps SynCAM1's early roles are redundant with other proteins, but it may serve later functions at the synapse for which compensatory mechanisms do not exist. As synaptic function is critically dependent on the complement of glutamate receptors present, it will be interesting to identify the full array of receptor types that are affected by manipulations of SynCAM1 levels. Therefore, determining how SynCAM1 may perform both similar and unique molecular functions at the synapse

relative to other adhesion molecules is important to understanding the development of the brain and behavior.

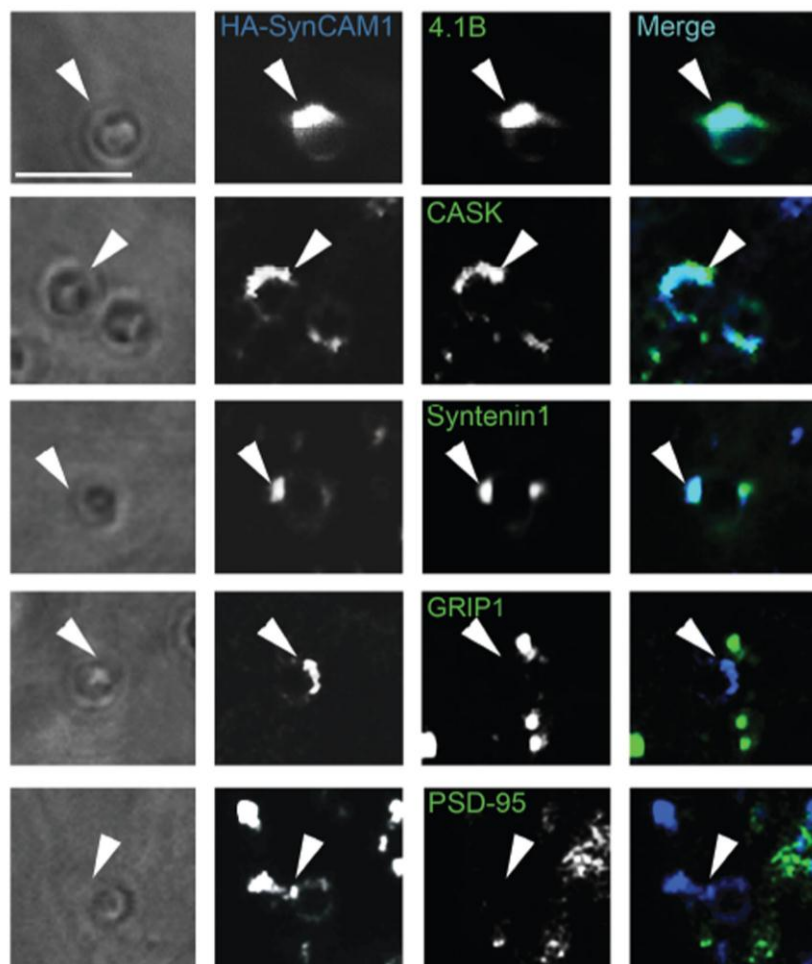
THE DEVELOPMENT OF COMPLEX FORMS OF BEHAVIOR CRITICALLY RELY ON SYNAPTIC MOLECULES THAT SUPPORT THE MODIFICATION OF SYNAPSES WITH EXPERIENCE

Our results validate that specific NL1 intracellular signaling domains regulate late stages of synaptic maturation *in vivo*, and provide the first evidence to our knowledge, that artificially manipulating the relative proportion of glutamatergic synapses in one state versus another *in vivo* within specific neural systems alters behavioral traits that change as a function of development. NL1 has been implicated in the NMDAR and activity dependent synaptic elimination that shapes the development of complex features of sensory processing (Chubykin et al., 2007). Such synaptic refinement activities are known to underlie critical periods for the rearrangement of primary sensory neural circuits and the development of specific aspects of sensory perception. If synaptic pruning is not appropriately carried out during these discrete windows of time, there are lasting deficits in neural circuit organization and sensory perception throughout life (Hubel and Wiesel, 1970). It is therefore interesting to speculate that NL1 may regulate similar developmental processes specifically within mnemonic systems when they are most susceptible to experience dependent modification.

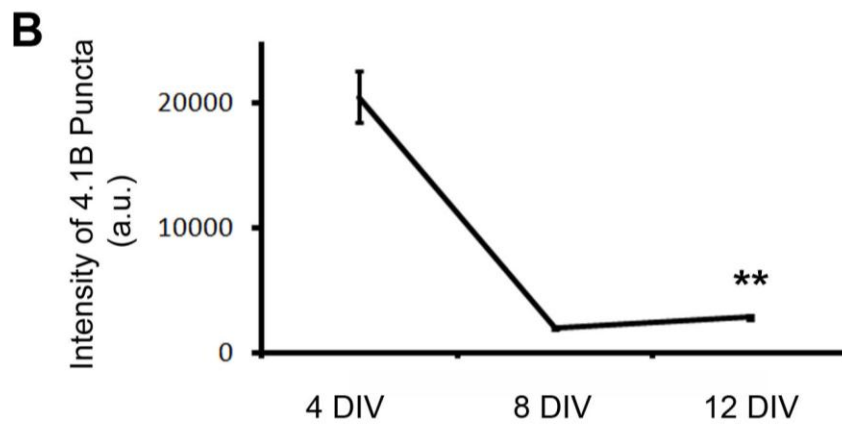
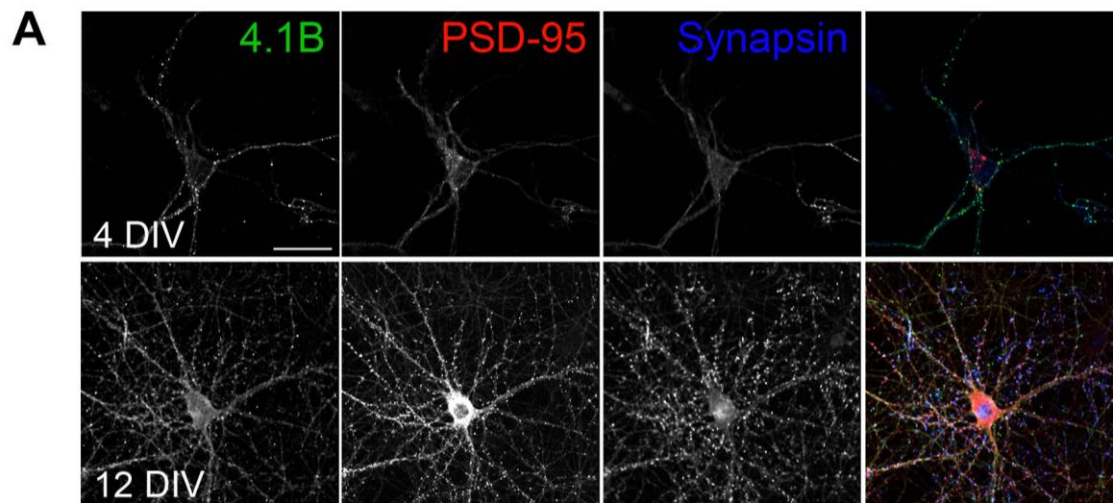
Indeed, it is interesting to speculate that the development of the cortical and hippocampal circuits required to form explicit types of memory in the adult possess such a sensitive period earlier in development. There are some studies to suggest that such a developmental period exists (Langston et al., 2010; Scott et al., 2011). Previous studies of the development of mnemonic systems suggest that prenatal and early postnatal periods of development are particularly vulnerable to pharmacological insults. That is, introduction of particular substances that interfere with global aspects of brain function during discrete stages of development can lead to lasting consequences on learning and memory behaviors in mice (Meng et al., 2011). It is unclear which developmental processes may account for these observations as entire endocrine systems and synapse types were ubiquitously impacted by these perturbations. Therefore, interesting future

experiments will be to specifically assess whether NL1 may critically regulate such a sensitive period for the development of mnemonic and social systems in juvenile mice. Such a study interpreted in light of the data described in this dissertation would point more directly to the specific synaptic activity that has a bearing on the development of learning and memory behavior. This would constitute a thorough understanding of the how, when and where NL1 acts in order to impact behavior, and studies such as these are the necessary first steps towards understanding the biological basis of behavior.

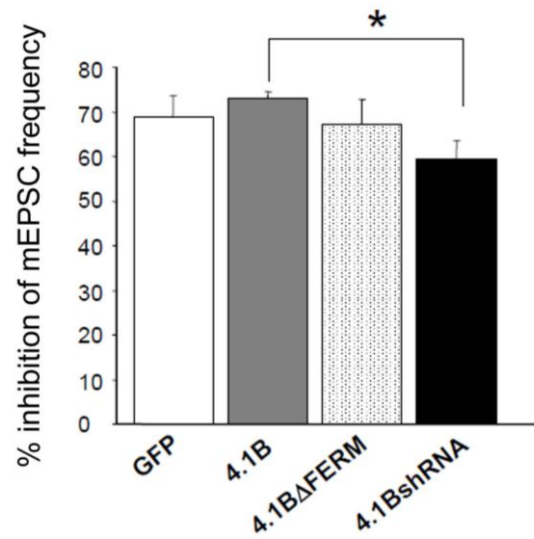
APENDIX A
SUPPLEMENTAL
MATERIAL FOR CHAPTER II



Supplemental Figure 1. Recruitment of effector molecules to sites of HA-SynCAM1 mediated adhesion with microspheres. HA-SynCAM1 clustering via microspheres recruits protein 4.1B, CASK and Syntenin1, but not GRIP1 and PSD-95 (arrowheads).

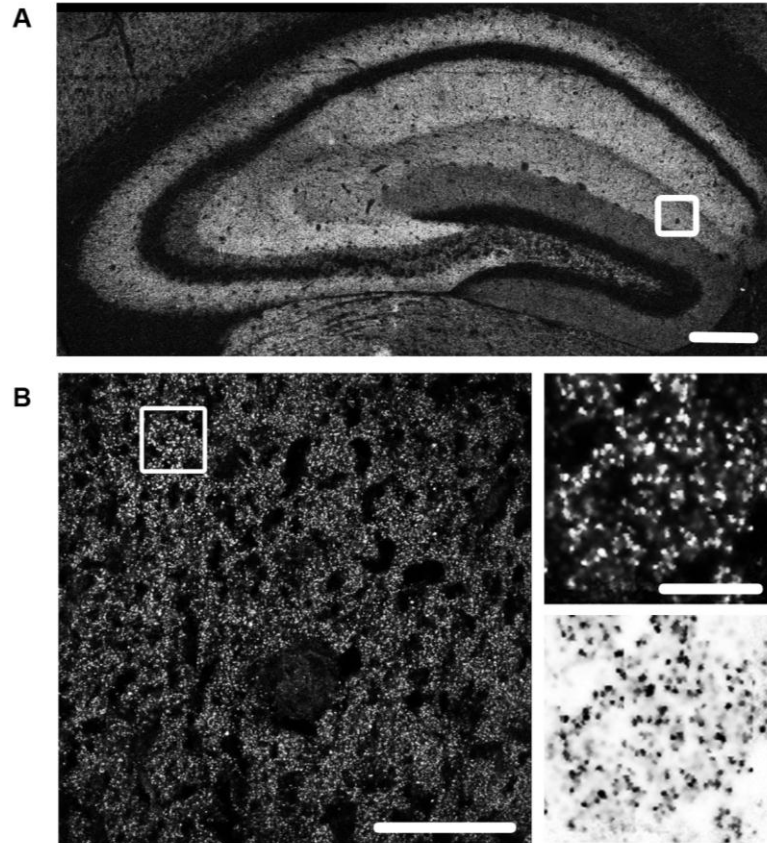


Supplemental Figure 2. Protein 4.1 puncta decrease in intensity during development. (A) Immunolabeling for protein 4.1B, synapsin I and PSD-95 at 4 and 12DIV demonstrates an increase in the number of overall 4.1B puncta and decrease in their intensity. (B) Quantification of the mean puncta intensity for protein 4.1B immunolabeling over time in culture. Errors bars are s.e.m. (n = 11, **p < 0.01).

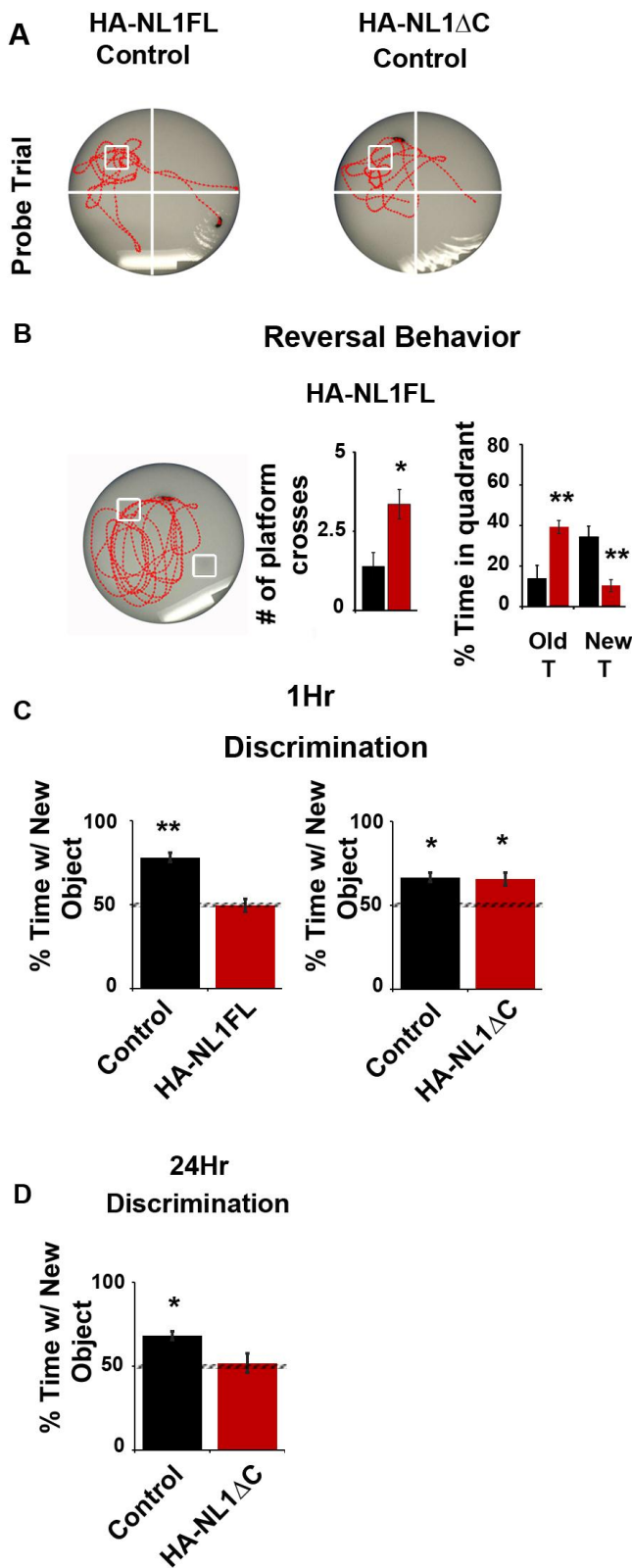


Supplemental Figure 3. Analysis of mEPSCs after ifenprodil application. We measured mEPSC frequency in transfected hippocampal neurons before and during application of the NR1/NR2B containing NMDAR specific antagonist ifenprodil. The only significant difference seen was between 4.1B overexpression and 4.1B knock-down with shRNA ($p = 0.02$, $n = 12$).

APPENDIX B
SUPPLEMENTAL MATERIAL FOR CHAPTER III

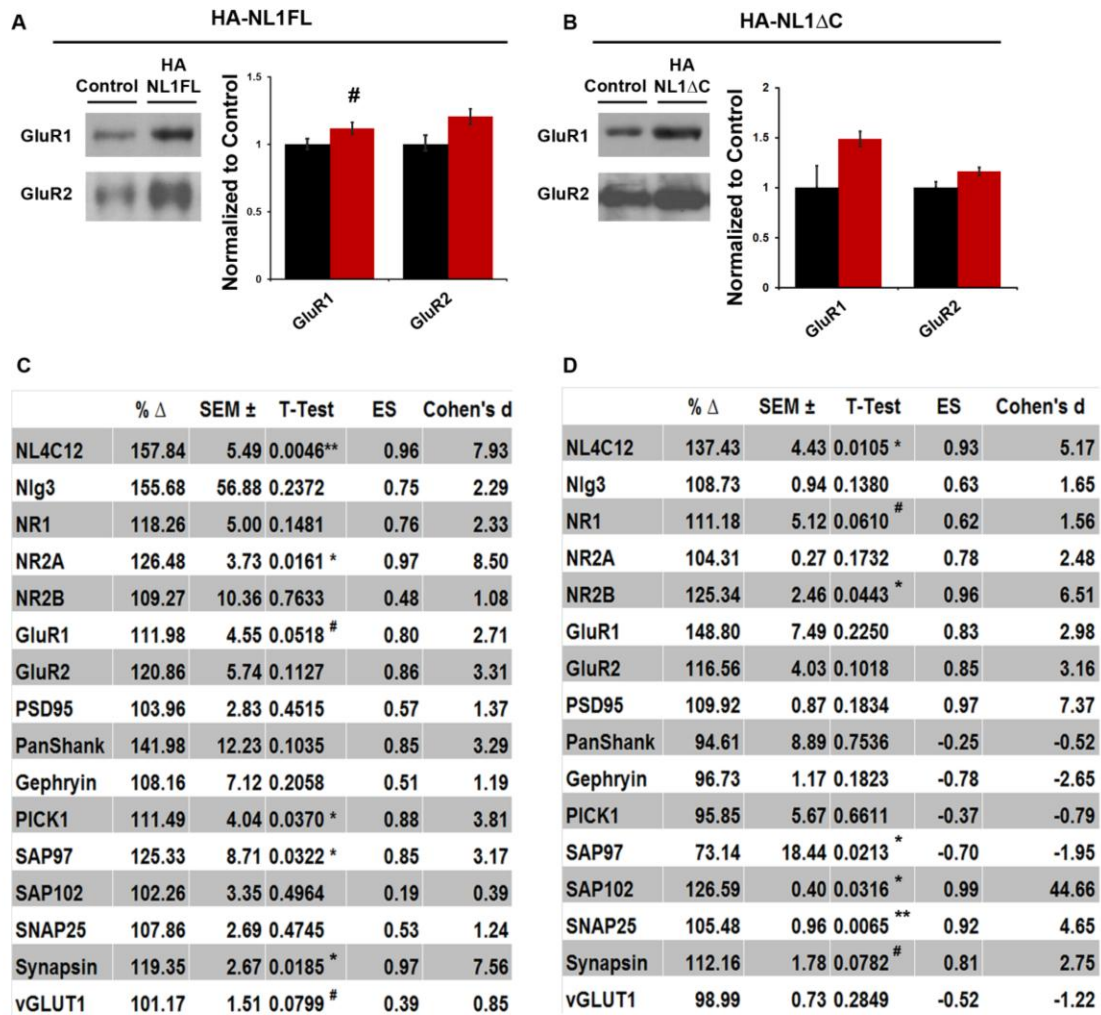


Supplemental Figure 1. (A) Hippocampal section stained for panShank imaged at 10x, scale bar equals 200 μm , white box indicates area depicted in (B) which is magnified at 60x. Scale bar equals 20 μm , white box is area enlarged, de-convolved and analyzed in smaller panels to right. Scale bar in small panel is 5 μm , and lower right panel is the above after black and white inversion to ease perception of puncta characteristics.



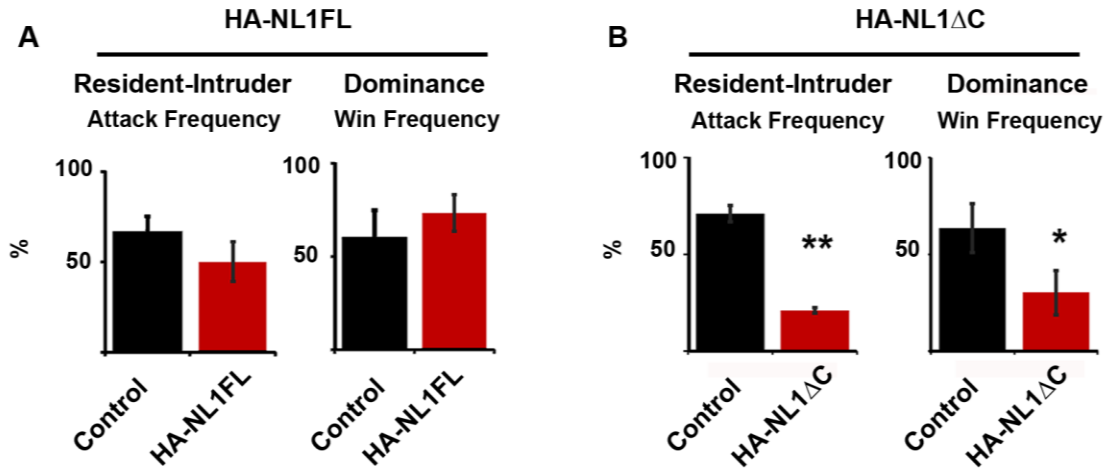
Supplemental Figure 2. Additional measures of learning and memory behaviors in transgenic mice. **(A)** Exemplary tracks from controls from the same cohort of animals tested in Figure 2 in the Morris water maze. The tracks of the controls demonstrate that they performed as expected in the task, persisting in searching a discrete area over the former location of the platform. **(B)** Detailed behavioral analysis of the reversal behavior for the HA-NL1FL line of mice on day two (R2) of reversal training. The number of crosses over the former location was higher in the HA-NL1FL mice as shown by the middle graph (1.4 ± 0.432 vs. 3.4 ± 0.5 , controls vs. HA-NL1FL mice respectively, $p < 0.05$, Student's t-test $n = 10$ pairs). The percent time spent in the quadrant that formerly contained the platform vs. the time spent in the new platform location by the HA-NL1FL mice and controls was different (Old location: 13.7 ± 0.7 vs. $39.2 \pm 3.2\%$ respectively, controls vs. HA-NL1FL mice respectively, $p < 0.01$ New location: $34.2 \pm 5.5\%$ vs. $10.2 \pm 2.9\%$, $p < 0.01$, Student's t-test, $n = 10$ pairs). **(C)** Object recognition results presented as percent time spent with the new object after a 1 hour delay. HA-NL1FL mice failed to prefer the novel object after a 1 hour delay ($76.1 \pm 4.5\%$ vs. $49.9 \pm 5.4\%$ novelty preference, controls vs. HA-NL1FL mice respectively, $p < 0.01$ for controls), while HA-NL Δ C mice performed no differently than controls; both groups preferred the novel object ($62.2 \pm 3.7\%$ vs. $60.2 \pm 1.5\%$ novelty preference, controls vs. HA-

NL1ΔC respectively, $p < 0.05$ in both cases). **(D)** Novel object recognition after a 24 hour delay between exposures revealed a deficit in recognition memory in the HA-NL1ΔC mice ($65.8 \pm 3.4\%$ vs. $49.8 \pm 8.8\%$, controls vs. HA-NL1ΔC mice respectively, $p < 0.05$ for controls and n.s. for HA-NL1ΔC). Error bars are SEM, significance was determined by Wilcoxon-signed rank test, $n = 20$, unless otherwise noted and $* = p < 0.05$, $** = p < 0.01$ and $*** = p < 0.001$.



Supplemental Figure 3. Western blot data from synaptosome preparations and complete statistical analysis of intensity level differences. **(A)** Blots depict representative AMPA subunit levels from a member of the control group (left lane) and the HA-NL1FL mice (right lane). Levels trended towards an increase for both GluR1 and GluR2, but never reached significance. **(B)** Similar results were seen for the HA-NL1ΔC mice. Error bars are SEM, and significance was determined with Student's t-test, # = $p < 0.1$, * = $p < 0.05$, ** = $p < 0.01$

and *** = $p < 0.001$. (C & D) Summary statistics for levels of all synaptic proteins analyzed from hippocampal synaptosome fractions from (C) controls vs. HA-NL1FL mice and (D) controls vs. HA-NL1ΔC mice.



Supplemental Figure 4. Aggressive social interactions are only affected in the HA-NL1ΔC mice. (A) Attack frequency during the resident-intruder task is depicted in the left graph for controls (black) and HA-NL1FL mice (red). Win frequency during the dominance tube test is graphed to the right. No difference between the two groups was observed during either test. (B) HA-NL1ΔC mice (red) were less aggressive as they attacked less frequently than controls during the resident intruder-test (Left graph, $16.7 \pm 1.1\%$ attacked vs. $56.7 \pm 3.3\%$, $p < 0.025$, RMANOVA, $n = 9$ pairs, Tukey's *post hoc*) and lost more bouts in the dominant tube test (right graph, only won $30 \pm 11\%$ of bouts vs. $63 \pm 13\%$, $p < 0.05$, RMANOVA, $n = 9$ pairs, Tukey's *post hoc*). Error bars are SEM, * = $p < 0.05$ and ** = $p < 0.025$.

Supplemental Experimental Procedures

Immunocytochemistry, Microscopy and Image Processing

Slides were blocked in a 1% Roche Block (Roche) and 10% normal goat sera solution in PBS for 1 hr at room temperature. Sections were incubated with the following primary antibodies in the block solution overnight at 4°C: HA (mouse IgG1 Bethyl, TX) 1:300, PSD95 (mouse IgG2a 28/43 NeuroMab, CA) 1:400, Synapsin1 (rabbit polyclonal Millipore, CA) 1:400, panSHANK (mouse IgG1 N23B/49 NeuroMab, CA) 1:400 and NR2B (mouse IgG2a N59/36 NeuroMab, CA) 1:300. Slides were washed 3x 5 minutes in PBS at room temperature with gentle agitation. Alexa Fluor dye labeled secondary antibodies (Invitrogen), 1:500 were incubated for 2 hours at room temperature. Slides were washed 3x 5 minutes with PBS and mounted in Fluoromount G+DAPI (SouthernBiotech).

Synaptosomal Preparations and Western Blotting

Primary antibodies used in western blotting: PSD95 (mouse IgG2a 28/43 NeuroMab, CA), Synapsin1 (rabbit polyclonal Millipore, CA), NR1 (mouse IgG1 BD Pharmingen), NR2B (mouse IgG2a N59/36 NeuroMab, CA), NR2A (rabbit abcam, MA), Neuroligin1 (mouse IgG1 N97A/31 NeuroMab, CA), Neuroligin1 (mouse IgG1 4C12 Synaptic Systems, Germany), HA (rabbit Bethyl, TX), Actin (mouse IgG2 Millipore, CA), Gephyrin (mouse IgG1 Synaptic systems, Germany), GluR1 (rabbit abcam, MA), GluR2 (mouse IgG2a Millipore, CA), panSHANK (mouse IgG1 N23B/49 NeuroMab, CA), Pick1 (mouse IgG1 L20/8 NeuroMab, CA), SAP97 (mouse IgG1 K64/15 NeuroMab, CA), SAP102 (mouse IgG1 N19/2 NeuroMab, CA). Western blots were quantified using Image Pro Plus® and intensity was expressed as percentage of control. Statistical analysis was performed using Students t-test with α level set at 0.05.

Behavior and Morris Water Maze Details

In the visible platform test, each animal was given 4 trials per day, across 2 days, to swim to an escape platform cued by a textured cylinder extending above the surface of the water. For each trial, the mouse was placed in the pool at one of four possible locations (randomly ordered), and then given 60s to find the cued platform. Once on the

platform, even if placed there, they remained for at least 10 seconds. Measures were taken of latency to find the platform, swimming distance, and swimming velocity, via the Image Pro Plus® automated tracking system and custom Matlab programs. Following visual training, mice were trained on the hidden platform test. Using the same procedure as described above, each animal was given four trials per day, for up to 9 days, to learn the location of the submerged platform. At the end of the day that the group met the 15s criterion for learning, or else on day 9 of testing, mice were given a 1-min probe trial in the pool with the platform removed. Quadrant search was evaluated by measuring percent of time spent in each quadrant of the pool, path length to first cross and number of crosses of former location. Following the acquisition phase, mice were tested for reversal learning, using the same procedure but with the target moved to the opposite quadrant.

Elevated Plus-maze Test for Anxiety-like Behaviors

Mice were given one 5-min trial on the plus-maze, which had two closed arms, with walls 40 cm in height, and two open arms. The maze was elevated 50 cm from the floor, and the arms were 21 cm long. Animals were placed on the center section (9.5 cm × 9.5 cm), and allowed to freely explore the maze. Measures were taken of time on, and number of entries into, the open and closed arms. Percent open arm time was calculated as $100 \times (\text{time spent on the open arms} / (\text{time in the open arms} + \text{time in the closed arms}))$. Percent open arm entries were calculated using the same formula, but using the measure for entries.

Social Dominance Tube Test

The dominance tube apparatus (Messeri et al., 1975) was constructed out of plexiglass and consisted of a 36 cm long tube with a diameter of 3.5 cm that is attached on either end to a start cylinder (measuring 10 cm in diameter). At the center of the tube was a removable perforated partition that allowed for olfactory investigation, but not physical contact. A singly housed experimental mouse and an unfamiliar group-housed mouse of similar age, weight and sex were placed in opposite start boxes and allowed to habituate to the apparatus for 3 min. When the animals met in the middle of the tube after the habituation period the center partition was lifted. The test was video recorded and

concluded once one mouse had forced the other back. In the event of a tie, where the mice managed to squeeze past each other, the trial was noted but not included in the comparison statistics. Each mouse was subjected to 3-4 bouts depending on the rare event of a tie. Dominance behavior was measured over 3 separate trials for each mouse as compared to three different strangers. Start sides were randomized. Significance was determined by repeated measures ANOVA with α level set at 0.05 and Tukey's *post hoc* test to report significant differences in mean performances.

Resident-Intruder Test

Mice were housed individually for 7–8 days before an unfamiliar group-housed control mouse of the same sex and comparable weight was introduced to the resident's home cage. Food was removed 1 hour prior to testing and all mice were habituated to the testing room for 1 hour prior to introduction of the intruder mouse. Behavior was monitored and video recorded for the first 10 min after introduction of the intruder, or until an attack occurred, whichever came first. Measures of attack frequency, attack latency, dominant mounting, investigatory sniffing (sniffing directed toward the partner), chasing and grooming were recorded as described (Duncan et al., 2009). All measures were scored by two blinded observers and the total scores between the two observers were averaged. Animals were subject to three rounds of intruder presentation. Significance was determined by repeated measures ANOVA and the α level set at 0.05.

Spine Density and Morphology Quantification

Neurites were selected for analysis on the basis of: 1) location within the hippocampal stratum, 2) isolation from neighboring neurites, 3) clarity of spine labeling, 4) close proximity to tissue surface to minimize light scattering, 5) low frequency of regularly spaced varicosities around $2\mu\text{m}$ in diameter and 6) validation that the neurite came from a CA1 pyramidal neuron. Spine head area in control animals within CA1 SLM ranged from approximately $0.1\mu\text{m}^2$ to $0.78\mu\text{m}^2$, closely resembling measures reported in other studies of spine head size in SLM.

Auditory Cortex Electrophysiology

Mice were anesthetized with a Ketamine (100 mg/kg body mass), Medetomidine and Acepromazine cocktail, and given supplemental doses to maintain anesthesia. Atropine and Dextromethasone were also administered to reduce tracheal secretions and cerebral edema. The mouse's temperature was maintained at 37 +/-1 C.

REFERENCES CITED

- Allison, D.W., Gelfand, V.I., Spector, I., and Craig, A.M. (1998). Role of actin in anchoring postsynaptic receptors in cultured hippocampal neurons: differential attachment of NMDA versus AMPA receptors. *J. Neurosci.* *18*, 2423-2436.
- An, X.L., Takakuwa, Y., Nunomura, W., Manno, S., and Mohandas, N. (1996). Modulation of band 3-ankyrin interaction by protein 4.1. Functional implications in regulation of erythrocyte membrane mechanical properties. *J Biol Chem* *271*, 33187-33191.
- Bangash, M.A., Park, J.M., Melnikova, T., Wang, D., Jeon, S.K., Lee, D., Syeda, S., Kim, J., Kouser, M., Schwartz, J., *et al.* (2011). Enhanced Polyubiquitination of Shank3 and NMDA Receptor in a Mouse Model of Autism. *Cell* *145*, 758-772.
- Barrow, S.L., Constable, J.R., Clark, E., El-Sabeawy, F., McAllister, A.K., and Washbourne, P. (2009). Neuroligin1: a cell adhesion molecule that recruits PSD-95 and NMDA receptors by distinct mechanisms during synaptogenesis. *Neural Dev* *4*, 17.
- Bevins, R.A., and Besheer, J. (2006). Object recognition in rats and mice: a one-trial non-matching-to-sample learning task to study 'recognition memory'. *Nat Protoc* *1*, 1306-1311.
- Biederer, T. (2005). Progress from the postsynaptic side: signaling in synaptic differentiation. *Sci STKE* *2005*, pe9.
- Biederer, T., Sara, Y., Mozhayeva, M., Atasoy, D., Liu, X., Kavalali, E.T., and Sudhof, T.C. (2002). SynCAM, a synaptic adhesion molecule that drives synapse assembly. *Science* *297*, 1525-1531.
- Biederer, T., and Scheiffele, P. (2007). Mixed-culture assays for analyzing neuronal synapse formation. *Nat Protoc* *2*, 670-676.
- Bloch, R.J. (1989). Cell-to-cell interactions during synaptogenesis. *Curr Opin Cell Biol* *1*, 940-946.
- Blundell, J., Blaiss, C.A., Etherton, M.R., Espinosa, F., Tabuchi, K., Walz, C., Bolliger, M.F., Sudhof, T.C., and Powell, C.M. (2010). Neuroligin-1 deletion results in impaired spatial memory and increased repetitive behavior. *J Neurosci* *30*, 2115-2129.
- Blundell, J., Tabuchi, K., Bolliger, M.F., Blaiss, C.A., Brose, N., Liu, X., Sudhof, T.C., and Powell, C.M. (2009). Increased anxiety-like behavior in mice lacking the inhibitory synapse cell adhesion molecule neuroligin 2. *Genes Brain Behav* *8*, 114-126.
- Bourgeron, T. (2009). A synaptic trek to autism. *Curr Opin Neurobiol* *19*, 231-234.

- Bozdagi, O., Sakurai, T., Papapetrou, D., Wang, X., Dickstein, D.L., Takahashi, N., Kajiwara, Y., Yang, M., Katz, A.M., Scattoni, M.L., *et al.* (2010). Haploinsufficiency of the autism-associated Shank3 gene leads to deficits in synaptic function, social interaction, and social communication. *Mol Autism* 1, 15.
- Brewer, G.J., Torricelli, J.R., Evege, E.K., and Price, P.J. (1993). Optimized survival of hippocampal neurons in B27-supplemented Neurobasal, a new serum-free medium combination. *J Neurosci Res* 35, 567-576.
- Brown, R.W., and Kraemer, P.J. (1997). Ontogenetic differences in retention of spatial learning tested with the Morris water maze. *Dev Psychobiol* 30, 329-341.
- Brummelkamp, T.R., Bernards, R., and Agami, R. (2002). A system for stable expression of short interfering RNAs in mammalian cells. *Science* 296, 550-553.
- Cantrill, R., Creedy, D., and Cooke, M. (2004). Midwives' knowledge of newborn feeding ability and reported practice managing the first breastfeed. *Breastfeed Rev* 12, 25-33.
- Carmignoto, G., and Vicini, S. (1992). Activity-dependent decrease in NMDA receptor responses during development of the visual cortex. *Science* 258, 1007-1011.
- Chen, L., Chetkovich, D.M., Petralia, R.S., Sweeney, N.T., Kawasaki, Y., Wenthold, R.J., Brecht, D.S., and Nicoll, R.A. (2000). Stargazin regulates synaptic targeting of AMPA receptors by two distinct mechanisms. *Nature* 408, 936-943.
- Chih, B., Engelman, H., and Scheiffele, P. (2005). Control of excitatory and inhibitory synapse formation by neuroligins. *Science* 307, 1324-1328.
- Cho, K.O., Hunt, C.A., and Kennedy, M.B. (1992). The rat brain postsynaptic density fraction contains a homolog of the Drosophila discs-large tumor suppressor protein. *Neuron* 9, 929-942.
- Chow, I., and Poo, M.M. (1985). Release of acetylcholine from embryonic neurons upon contact with muscle cell. *J Neurosci* 5, 1076-1082.
- Chubykin, A., Atasoy, D., Etherton, M.R., Brose, N., Kavalali, E.T., Gibson, J.R., and Sudhof, T.C. (2007). Activity-dependent validation of excitatory versus inhibitory synapses by Neuroligin-1 versus Neuroligin-2. *Neuron* 54, 919-931.
- Correas, I., Leto, T.L., Speicher, D.W., and Marchesi, V.T. (1986). Identification of the functional site of erythrocyte protein 4.1 involved in spectrin-actin associations. *J Biol Chem* 261, 3310-3315.
- Crair, M.C. (1999). Neuronal activity during development: permissive or instructive? *Curr Opin Neurobiol* 9, 88-93.

Crair, M.C., and Malenka, R.C. (1995). A critical period for long-term potentiation at thalamocortical synapses. *Nature* 375, 325-328.

Creedy, D.K., Cantrill, R.M., and Cooke, M. (2008). Assessing midwives' breastfeeding knowledge: properties of the Newborn Feeding Ability questionnaire and Breastfeeding Initiation Practices scale. *Int Breastfeed J* 3, 7.

Dahlhaus, R., and El-Husseini, A. (2010). Altered neuroligin expression is involved in social deficits in a mouse model of the fragile X syndrome. *Behav Brain Res* 208, 96-105.

Dahlhaus, R., Hines, R.M., Eadie, B.D., Kannangara, T.S., Hines, D.J., Brown, C.E., Christie, B.R., and El-Husseini, A. (2010). Overexpression of the cell adhesion protein neuroligin-1 induces learning deficits and impairs synaptic plasticity by altering the ratio of excitation to inhibition in the hippocampus. *Hippocampus* 20, 305-322.

de Villers-Sidani, E., Chang, E.F., Bao, S., and Merzenich, M.M. (2007). Critical period window for spectral tuning defined in the primary auditory cortex (A1) in the rat. *J Neurosci* 27, 180-189.

Dean, C., Scholl, F.G., Choih, J., DeMaria, S., Berger, J., Isacoff, E., and Scheiffele, P. (2003). Neurexin mediates the assembly of presynaptic terminals. *Nat Neurosci* 6, 708-716.

Dillon, C., and Goda, Y. (2005). The actin cytoskeleton: integrating form and function at the synapse. *Annu Rev Neurosci* 28, 25-55.

Dresbach, T., Neeb, A., Meyer, G., Gundelfinger, E.D., and Brose, N. (2004). Synaptic targeting of neuroligin is independent of neurexin and SAP90/PSD95 binding. *Mol Cell Neurosci* 27, 227-235.

Duncan, G.E., Inada, K., Farrington, J.S., Koller, B.H., and Moy, S.S. (2009). Neural activation deficits in a mouse genetic model of NMDA receptor hypofunction in tests of social aggression and swim stress. *Brain Res* 1265, 186-195.

Duncan, G.E., Moy, S.S., Perez, A., Eddy, D.M., Zinzow, W.M., Lieberman, J.A., Snouwaert, J.N., and Koller, B.H. (2004). Deficits in sensorimotor gating and tests of social behavior in a genetic model of reduced NMDA receptor function. *Behav Brain Res* 153, 507-519.

Durand, C.M., Betancur, C., Boeckers, T.M., Bockmann, J., Chaste, P., Fauchereau, F., Nygren, G., Rastam, M., Gillberg, I.C., Anckarsater, H., *et al.* (2007). Mutations in the gene encoding the synaptic scaffolding protein SHANK3 are associated with autism spectrum disorders. *Nat Genet* 39, 25-27.

Durand, G.M., and Konnerth, A. (1996). Long-term potentiation as a mechanism of functional synapse induction in the developing hippocampus. *J Physiol Paris* 90, 313-315.

Ehlers, M.D., Zhang, S., Bernhardt, J.P., and Huganir, R.L. (1996). Inactivation of NMDA receptors by direct interaction of calmodulin with the NR1 subunit. *Cell* 84, 745-755.

Feng, W., and Zhang, M. (2009). Organization and dynamics of PDZ-domain-related supramodules in the postsynaptic density. *Nat Rev Neurosci* 10, 87-99.

Fletcher, T.L., Cameron, P., De Camilli, P., and Banker, G. (1991). The distribution of synapsin I and synaptophysin in hippocampal neurons developing in culture. *J Neurosci* 11, 1617-1626.

Fu, Z., Logan, S.M., and Vicini, S. (2005). Deletion of the NR2A subunit prevents developmental changes of NMDA-mEPSCs in cultured mouse cerebellar granule neurones. *J Physiol* 563, 867-881.

Fu, Z., Washbourne, P., Ortinski, P., and Vicini, S. (2003). Functional excitatory synapses in HEK293 cells expressing neuroligin and glutamate receptors. *J Neurophysiol* 90, 3950-3957.

Funke, L., Dakoju, S., and Brecht, D.S. (2005). Membrane-associated guanylate kinases regulate adhesion and plasticity at cell junctions. *Annu Rev Biochem* 74, 219-245.

Gallo, V., Kingsbury, A., Balazs, R., and Jorgensen, O.S. (1987). The role of depolarization in the survival and differentiation of cerebellar granule cells in culture. *J Neurosci* 7, 2203-2213.

Gardoni, F., Mauceri, D., Fiorentini, C., Bellone, C., Missale, C., Cattabeni, F., and Di Luca, M. (2003). CaMKII-dependent phosphorylation regulates SAP97/NR2A interaction. *J Biol Chem* 278, 44745-44752.

Gerrow, K., Romorini, S., Nabi, S.M., Colicos, M.A., Sala, C., and El-Husseini, A. (2006). A preformed complex of postsynaptic proteins is involved in excitatory synapse development. *Neuron* 49, 547-562.

Glessner, J.T., Wang, K., Cai, G., Korvatska, O., Kim, C.E., Wood, S., Zhang, H., Estes, A., Brune, C.W., Bradfield, J.P., *et al.* (2009). Autism genome-wide copy number variation reveals ubiquitin and neuronal genes. *Nature* 459, 569-573.

Gordon, J.A. (2011). Oscillations and hippocampal-prefrontal synchrony. *Curr Opin Neurobiol.*

Hasselmo, M.E., and Schnell, E. (1994). Laminar selectivity of the cholinergic suppression of synaptic transmission in rat hippocampal region CA1: computational modeling and brain slice physiology. *J Neurosci* 14, 3898-3914.

Hasselmo, M.E., Schnell, E., and Barkai, E. (1995). Dynamics of learning and recall at excitatory recurrent synapses and cholinergic modulation in rat hippocampal region CA3. *J Neurosci* 15, 5249-5262.

Hensch, T.K. (2004). Critical period regulation. *Annu Rev Neurosci* 27, 549-579.

Hensch, T.K., and Fagiolini, M. (2005). Excitatory-inhibitory balance and critical period plasticity in developing visual cortex. *Prog Brain Res* 147, 115-124.

Hines, R.M., Wu, L., Hines, D.J., Steenland, H., Mansour, S., Dahlhaus, R., Singaraja, R.R., Cao, X., Sammler, E., Hormuzdi, S.G., *et al.* (2008). Synaptic imbalance, stereotypies, and impaired social interactions in mice with altered neuroligin 2 expression. *J Neurosci* 28, 6055-6067.

Hollmann, M., and Heinemann, S. (1994). Cloned glutamate receptors. *Annu Rev Neurosci* 17, 31-108.

Hoover, K.B., and Bryant, P.J. (2000). The genetics of the protein 4.1 family: organizers of the membrane and cytoskeleton. *Curr Opin Cell Biol* 12, 229-234.

Hubel, D.H., and Wiesel, T.N. (1970). The period of susceptibility to the physiological effects of unilateral eye closure in kittens. *J Physiol* 206, 419-436.

Hung, A.Y., Futai, K., Sala, C., Valtschanoff, J.G., Ryu, J., Woodworth, M.A., Kidd, F.L., Sung, C.C., Miyakawa, T., Bear, M.F., *et al.* (2008). Smaller dendritic spines, weaker synaptic transmission, but enhanced spatial learning in mice lacking Shank1. *J Neurosci* 28, 1697-1708.

Hunt, C.A., Schenker, L.J., and Kennedy, M.B. (1996). PSD-95 is associated with the postsynaptic density and not with the presynaptic membrane at forebrain synapses. *J Neurosci* 16, 1380-1388.

Iida, J., Hirabayashi, S., Sato, Y., and Hata, Y. (2004). Synaptic scaffolding molecule is involved in the synaptic clustering of neuroligin. *Mol Cell Neurosci* 27, 497-508.

Insel, T.R., and Fernald, R.D. (2004). How the brain processes social information: searching for the social brain. *Annu Rev Neurosci* 27, 697-722.

Irie, M., Hata, Y., Takeuchi, M., Ichtchenko, K., Toyoda, A., Hirao, K., Takai, Y., Rosahl, T.W., and Sudhof, T.C. (1997). Binding of neuroligins to PSD-95. *Science* 277, 1511-1515.

Isaac, J.T., Crair, M.C., Nicoll, R.A., and Malenka, R.C. (1997). Silent synapses during development of thalamocortical inputs. *Neuron* 18, 269-280.

- Jamain, S., Quach, H., Betancur, C., Rastam, M., Colineaux, C., Gillberg, I.C., Soderstrom, H., Giros, B., Leboyer, M., Gillberg, C., and Bourgeron, T. (2003). Mutations of the X-linked genes encoding neuroligins NLGN3 and NLGN4 are associated with autism. *Nat Genet* 34, 27-29.
- Jamain, S., Radyushkin, K., Hammerschmidt, K., Granon, S., Boretius, S., Varoqueaux, F., Ramanantsoa, N., Gallego, J., Ronnenberg, A., Winter, D., *et al.* (2008). Reduced social interaction and ultrasonic communication in a mouse model of monogenic heritable autism. *Proc Natl Acad Sci U S A* 105, 1710-1715.
- Jeyifous, O., Waites, C.L., Specht, C.G., Fujisawa, S., Schubert, M., Lin, E.I., Marshall, J., Aoki, C., de Silva, T., Montgomery, J.M., *et al.* (2009). SAP97 and CASK mediate sorting of NMDA receptors through a previously unknown secretory pathway. *Nat Neurosci* 12, 1011-1019.
- Jung, S.Y., Kim, J., Kwon, O.B., Jung, J.H., An, K., Jeong, A.Y., Lee, C.J., Choi, Y.B., Bailey, C.H., Kandel, E.R., and Kim, J.H. (2010). Input-specific synaptic plasticity in the amygdala is regulated by neuroligin-1 via postsynaptic NMDA receptors. *Proc Natl Acad Sci U S A* 107, 4710-4715.
- Kasai, H., Fukuda, M., Watanabe, S., Hayashi-Takagi, A., and Noguchi, J. (2010a). Structural dynamics of dendritic spines in memory and cognition. *Trends Neurosci* 33, 121-129.
- Kasai, H., Hayama, T., Ishikawa, M., Watanabe, S., Yagishita, S., and Noguchi, J. (2010b). Learning rules and persistence of dendritic spines. *Eur J Neurosci* 32, 241-249.
- Kentros, C., Hargreaves, E., Hawkins, R.D., Kandel, E.R., Shapiro, M., and Muller, R.V. (1998). Abolition of long-term stability of new hippocampal place cell maps by NMDA receptor blockade. *Science* 280, 2121-2126.
- Kim, J., Jung, S.Y., Lee, Y.K., Park, S., Choi, J.S., Lee, C.J., Kim, H.S., Choi, Y.B., Scheiffele, P., Bailey, C.H., *et al.* (2008). Neuroligin-1 is required for normal expression of LTP and associative fear memory in the amygdala of adult animals. *Proc Natl Acad Sci U S A* 105, 9087-9092.
- Kim, S., Burette, A., Chung, H.S., Kwon, S.K., Woo, J., Lee, H.W., Kim, K., Kim, H., Weinberg, R.J., and Kim, E. (2006). NGL family PSD-95-interacting adhesion molecules regulate excitatory synapse formation. *Nat Neurosci* 9, 1294-1301.
- Ko, J., Kim, S., Chung, H.S., Kim, K., Han, K., Kim, H., Jun, H., Kaang, B.K., and Kim, E. (2006). SALM synaptic cell adhesion-like molecules regulate the differentiation of excitatory synapses. *Neuron* 50, 233-245.

- Kohr, G., and Mody, I. (1994). Kindling increases N-methyl-D-aspartate potency at single N-methyl-D-aspartate channels in dentate gyrus granule cells. *Neuroscience* 62, 975-981.
- Kohr, G., and Seeburg, P.H. (1996). Subtype-specific regulation of recombinant NMDA receptor-channels by protein tyrosine kinases of the src family. *J Physiol* 492 (Pt 2), 445-452.
- Konur, S., and Ghosh, A. (2005). Calcium signaling and the control of dendritic development. *Neuron* 46, 401-405.
- Langston, R.F., Ainge, J.A., Couey, J.J., Canto, C.B., Bjerknes, T.L., Witter, M.P., Moser, E.I., and Moser, M.B. (2010). Development of the spatial representation system in the rat. *Science* 328, 1576-1580.
- Lister, J.P., and Barnes, C.A. (2009). Neurobiological changes in the hippocampus during normative aging. *Arch Neurol* 66, 829-833.
- Malinow, R., and Malenka, R.C. (2002). AMPA receptor trafficking and synaptic plasticity. *Annu Rev Neurosci* 25, 103-126.
- Mauceri, D., Gardoni, F., Marcello, E., and Di Luca, M. (2007). Dual role of CaMKII-dependent SAP97 phosphorylation in mediating trafficking and insertion of NMDA receptor subunit NR2A. *J Neurochem* 100, 1032-1046.
- McAllister, A.K. (2007). Dynamic Aspects of CNS Synapse Formation. *Annu Rev Neurosci*.
- Meng, X.H., Liu, P., Wang, H., Zhao, X.F., Xu, Z.M., Chen, G.H., and Xu, D.X. (2011). Gender-specific impairments on cognitive and behavioral development in mice exposed to fenvalerate during puberty. *Toxicol Lett* 203, 245-251.
- Messeri, P., Eleftheriou, B.E., and Oliverio, A. (1975). Dominance behavior: a phylogenetic analysis in the mouse. *Physiol Behav* 14, 53-58.
- Meyer, G., Varoqueaux, F., Neeb, A., Oeschli, M., and Brose, N. (2004). The complexity of PDZ domain-mediated interactions at glutamatergic synapses: a case study on neuroligin. *Neuropharmacology* 47, 724-733.
- Monyer, H., Burnashev, N., Laurie, D.J., Sakmann, B., and Seeburg, P.H. (1994). Developmental and regional expression in the rat brain and functional properties of four NMDA receptors. *Neuron* 12, 529-540.
- Moore, D.R., and Irvine, D.R. (1979). A developmental study of the sound pressure transformation by the head of the cat. *Acta Otolaryngol* 87, 434-440.

Mott, D.D., Doherty, J.J., Zhang, S., Washburn, M.S., Fendley, M.J., Lyuboslavsky, P., Traynelis, S.F., and Dingledine, R. (1998). Phenylethanolamines inhibit NMDA receptors by enhancing proton inhibition. *Nat Neurosci* 1, 659-667.

Moy, S.S., Nadler, J.J., Magnuson, T.R., and Crawley, J.N. (2006). Mouse models of autism spectrum disorders: the challenge for behavioral genetics. *Am J Med Genet C Semin Med Genet* 142, 40-51.

Moy, S.S., Nadler, J.J., Perez, A., Barbaro, R.P., Johns, J.M., Magnuson, T.R., Piven, J., and Crawley, J.N. (2004). Sociability and preference for social novelty in five inbred strains: an approach to assess autistic-like behavior in mice. *Genes Brain Behav* 3, 287-302.

Murase, K., Ryu, P.D., and Randic, M. (1989). Excitatory and inhibitory amino acids and peptide-induced responses in acutely isolated rat spinal dorsal horn neurons. *Neurosci Lett* 103, 56-63.

Nakagawa, T., Futai, K., Lashuel, H.A., Lo, I., Okamoto, K., Walz, T., Hayashi, Y., and Sheng, M. (2004). Quaternary structure, protein dynamics, and synaptic function of SAP97 controlled by L27 domain interactions. *Neuron* 44, 453-467.

Nam, C.I., and Chen, L. (2005). Postsynaptic assembly induced by neurexin-neurologin interaction and neurotransmitter. *Proc Natl Acad Sci U S A* 102, 6137-6142.

Nunomura, W., Takakuwa, Y., Parra, M., Conboy, J.G., and Mohandas, N. (2000). Ca(2+)-dependent and Ca(2+)-independent calmodulin binding sites in erythrocyte protein 4.1. Implications for regulation of protein 4.1 interactions with transmembrane proteins. *J Biol Chem* 275, 6360-6367.

Oertner, T.G., and Matus, A. (2005). Calcium regulation of actin dynamics in dendritic spines. *Cell Calcium* 37, 477-482.

Pampanos, A., Volaki, K., Kanavakis, E., Papandreou, O., Youroukos, S., Thomaidis, L., Karkelis, S., Tzetis, M., and Kitsiou-Tzeli, S. (2009). A substitution involving the NLGN4 gene associated with autistic behavior in the Greek population. *Genet Test Mol Biomarkers* 13, 611-615.

Parra, M., Gascard, P., Walensky, L.D., Gimm, J.A., Blackshaw, S., Chan, N., Takakuwa, Y., Berger, T., Lee, G., Chasis, J.A., *et al.* (2000). Molecular and functional characterization of protein 4.1B, a novel member of the protein 4.1 family with high level, focal expression in brain. *J Biol Chem* 275, 3247-3255.

Peca, J., Feliciano, C., Ting, J.T., Wang, W., Wells, M.F., Venkatraman, T.N., Lascola, C.D., Fu, Z., and Feng, G. (2011). Shank3 mutant mice display autistic-like behaviours and striatal dysfunction. *Nature* 472, 437-442.

- Penzes, P., Cahill, M.E., Jones, K.A., VanLeeuwen, J.E., and Woolfrey, K.M. (2011). Dendritic spine pathology in neuropsychiatric disorders. *Nat Neurosci* 14, 285-293.
- Perez-Otano, I., and Ehlers, M.D. (2004). Learning from NMDA receptor trafficking: clues to the development and maturation of glutamatergic synapses. *Neurosignals* 13, 175-189.
- Peters, L.L., Weier, H.U., Walensky, L.D., Snyder, S.H., Parra, M., Mohandas, N., and Conboy, J.G. (1998). Four paralogous protein 4.1 genes map to distinct chromosomes in mouse and human. *Genomics* 54, 348-350.
- Petralia, R.S., Esteban, J.A., Wang, Y.X., Partridge, J.G., Zhao, H.M., Wenthold, R.J., and Malinow, R. (1999). Selective acquisition of AMPA receptors over postnatal development suggests a molecular basis for silent synapses. *Nat Neurosci* 2, 31-36.
- Petralia, R.S., Sans, N., Wang, Y.X., and Wenthold, R.J. (2005). Ontogeny of postsynaptic density proteins at glutamatergic synapses. *Mol Cell Neurosci*.
- Prange, O., Wong, T.P., Gerrow, K., Wang, Y.T., and El-Husseini, A. (2004). A balance between excitatory and inhibitory synapses is controlled by PSD-95 and neuroligin. *Proc Natl Acad Sci U S A* 101, 13915-13920.
- Prybylowski, K., Fu, Z., Losi, G., Hawkins, L.M., Luo, J., Chang, K., Wenthold, R.J., and Vicini, S. (2002). Relationship between availability of NMDA receptor subunits and their expression at the synapse. *J Neurosci* 22, 8902-8910.
- Roberts, A.C., Diez-Garcia, J., Rodriguez, R.M., Lopez, I.P., Lujan, R., Martinez-Turrillas, R., Pico, E., Henson, M.A., Bernardo, D.R., Jarrett, T.M., *et al.* (2009). Downregulation of NR3A-containing NMDARs is required for synapse maturation and memory consolidation. *Neuron* 63, 342-356.
- Rossier, J., and Schenk, F. (2003). Olfactory and/or visual cues for spatial navigation through ontogeny: olfactory cues enable the use of visual cues. *Behav Neurosci* 117, 412-425.
- Rudy, J.W. (1994). Ontogeny of context-specific latent inhibition of conditioned fear: implications for configural associations theory and hippocampal formation development. *Dev Psychobiol* 27, 367-379.
- Sala, C., Piech, V., Wilson, N.R., Passafaro, M., Liu, G., and Sheng, M. (2001). Regulation of dendritic spine morphology and synaptic function by Shank and Homer. *Neuron* 31, 115-130.
- Saneyoshi, T., Wayman, G., Fortin, D., Davare, M., Hoshi, N., Nozaki, N., Natsume, T., and Soderling, T.R. (2008). Activity-dependent synaptogenesis: regulation by a CaM-kinase kinase/CaM-kinase I/betaPIX signaling complex. *Neuron* 57, 94-107.

- Sans, N., Racca, C., Petralia, R.S., Wang, Y.X., McCallum, J., and Wenthold, R.J. (2001). Synapse-associated protein 97 selectively associates with a subset of AMPA receptors early in their biosynthetic pathway. *J Neurosci* *21*, 7506-7516.
- Sara, Y., Biederer, T., Atasoy, D., Chubykin, A., Mozhayeva, M.G., Sudhof, T.C., and Kavalali, E.T. (2005). Selective capability of SynCAM and neuroligin for functional synapse assembly. *J Neurosci* *25*, 260-270.
- Scheiffele, P., Fan, J., Choih, J., Fetter, R., and Serafini, T. (2000). Neuroligin expressed in nonneuronal cells triggers presynaptic development in contacting axons. *Cell* *101*, 657-669.
- Schluter, O.M., Xu, W., and Malenka, R.C. (2006). Alternative N-terminal domains of PSD-95 and SAP97 govern activity-dependent regulation of synaptic AMPA receptor function. *Neuron* *51*, 99-111.
- Scott, C., Keating, L., Bellamy, M., and Baines, A.J. (2001). Protein 4.1 in forebrain postsynaptic density preparations: enrichment of 4.1 gene products and detection of 4.1R binding proteins. *Eur J Biochem* *268*, 1084-1094.
- Scott, R.C., Richard, G.R., Holmes, G.L., and Lenck-Santini, P.P. (2011). Maturation dynamics of hippocampal place cells in immature rats. *Hippocampus* *21*, 347-353.
- Sharma, K., Fong, D.K., and Craig, A.M. (2006). Postsynaptic protein mobility in dendritic spines: long-term regulation by synaptic NMDA receptor activation. *Mol Cell Neurosci* *31*, 702-712.
- Shen, L., Liang, F., Walensky, L.D., and Huganir, R.L. (2000). Regulation of AMPA receptor GluR1 subunit surface expression by a 4.1N-linked actin cytoskeletal association. *J Neurosci* *20*, 7932-7940.
- Sheng, M., Cummings, J., Roldan, L.A., Jan, Y.N., and Jan, L.Y. (1994). Changing subunit composition of heteromeric NMDA receptors during development of rat cortex. *Nature* *368*, 144-147.
- Sheng, M., and Kim, E. (2000). The Shank family of scaffold proteins. *J Cell Sci* *113* (Pt 11), 1851-1856.
- Shipman, S.L., Schnell, E., Hirai, T., Chen, B.S., Roche, K.W., and Nicoll, R.A. (2011). Functional dependence of neuroligin on a new non-PDZ intracellular domain. *Nat Neurosci* *14*, 718-726.
- Southwell, D.G., Froemke, R.C., Alvarez-Buylla, A., Stryker, M.P., and Gandhi, S.P. (2010). Cortical plasticity induced by inhibitory neuron transplantation. *Science* *327*, 1145-1148.

- Sun, C.X., Robb, V.A., and Gutmann, D.H. (2002). Protein 4.1 tumor suppressors: getting a FERM grip on growth regulation. *J Cell Sci* *115*, 3991-4000.
- Sytnyk, V., Leshchyn'ska, I., Delling, M., Dityateva, G., Dityatev, A., and Schachner, M. (2002). Neural cell adhesion molecule promotes accumulation of TGN organelles at sites of neuron-to-neuron contacts. *J Cell Biol* *159*, 649-661.
- Takayanagi, Y., Fujita, E., Yu, Z., Yamagata, T., Momoi, M.Y., Momoi, T., and Onaka, T. (2010). Impairment of social and emotional behaviors in *Cadm1*-knockout mice. *Biochem Biophys Res Commun* *396*, 703-708.
- Tallafuss, A., Constable, J.R., and Washbourne, P. (2010). Organization of central synapses by adhesion molecules. *Eur J Neurosci*.
- Tang, Y.P., Shimizu, E., Dube, G.R., Rampon, C., Kerchner, G.A., Zhuo, M., Liu, G., and Tsien, J.Z. (1999). Genetic enhancement of learning and memory in mice. *Nature* *401*, 63-69.
- Tovar, K.R., and Westbrook, G.L. (1999). The incorporation of NMDA receptors with a distinct subunit composition at nascent hippocampal synapses in vitro. *J Neurosci* *19*, 4180-4188.
- van Zundert, B., Yoshii, A., and Constantine-Paton, M. (2004). Receptor compartmentalization and trafficking at glutamate synapses: a developmental proposal. *Trends Neurosci* *27*, 428-437.
- Vicini, S., Wang, J.F., Li, J.H., Zhu, W.J., Wang, Y.H., Luo, J.H., Wolfe, B.B., and Grayson, D.R. (1998). Functional and pharmacological differences between recombinant N-methyl-D-aspartate receptors. *J Neurophysiol* *79*, 555-566.
- Vorhees, C.V., and Williams, M.T. (2006). Morris water maze: procedures for assessing spatial and related forms of learning and memory. *Nat Protoc* *1*, 848-858.
- Wang, C.Y., Chang, K., Petralia, R.S., Wang, Y.X., Seabold, G.K., and Wenthold, R.J. (2006). A novel family of adhesion-like molecules that interacts with the NMDA receptor. *J Neurosci* *26*, 2174-2183.
- Wang, K., Zhang, H., Ma, D., Bucan, M., Glessner, J.T., Abrahams, B.S., Salyakina, D., Imielinski, M., Bradfield, J.P., Sleiman, P.M., *et al.* (2009). Common genetic variants on 5p14.1 associate with autism spectrum disorders. *Nature* *459*, 528-533.
- Washbourne, P., Bennett, J.E., and McAllister, A.K. (2002). Rapid recruitment of NMDA receptor transport packets to nascent synapses. *Nat Neurosci* *5*, 751-759.

Washbourne, P., Dityatev, A., Scheiffele, P., Biederer, T., Weiner, J.A., Christopherson, K.S., and El-Husseini, A. (2004a). Cell adhesion molecules in synapse formation. *J Neurosci* *24*, 9244-9249.

Washbourne, P., Liu, X.B., Jones, E.G., and McAllister, A.K. (2004b). Cycling of NMDA receptors during trafficking in neurons before synapse formation. *J Neurosci* *24*, 8253-8264.

Wechsler, A., and Teichberg, V.I. (1998). Brain spectrin binding to the NMDA receptor is regulated by phosphorylation, calcium and calmodulin. *Embo J* *17*, 3931-3939.

Wilbrecht, L., Holtmaat, A., Wright, N., Fox, K., and Svoboda, K. (2010). Structural plasticity underlies experience-dependent functional plasticity of cortical circuits. *J Neurosci* *30*, 4927-4932.

Wittenmayer, N., Korber, C., Liu, H., Kremer, T., Varoqueaux, F., Chapman, E.R., Brose, N., Kuner, T., and Dresbach, T. (2009). Postsynaptic Neuroligin1 regulates presynaptic maturation. *Proc Natl Acad Sci U S A* *106*, 13564-13569.

Wu, G., Malinow, R., and Cline, H.T. (1996). Maturation of a central glutamatergic synapse. *Science* *274*, 972-976.

Wyszynski, M., Lin, J., Rao, A., Nigh, E., Beggs, A.H., Craig, A.M., and Sheng, M. (1997). Competitive binding of alpha-actinin and calmodulin to the NMDA receptor. *Nature* *385*, 439-442.

Yageta, M., Kuramochi, M., Masuda, M., Fukami, T., Fukuhara, H., Maruyama, T., Shibuya, M., and Murakami, Y. (2002). Direct association of TSLC1 and DAL-1, two distinct tumor suppressor proteins in lung cancer. *Cancer Res* *62*, 5129-5133.

Zheng, C.Y., Petralia, R.S., Wang, Y.X., Kachar, B., and Wenthold, R.J. (2010). SAP102 is a highly mobile MAGUK in spines. *J Neurosci* *30*, 4757-4766.

Zheng, C.Y., Seabold, G.K., Horak, M., and Petralia, R.S. (2011). MAGUKs, Synaptic Development, and Synaptic Plasticity. *Neuroscientist*.

Zhiling, Y., Fujita, E., Tanabe, Y., Yamagata, T., Momoi, T., and Momoi, M.Y. (2008). Mutations in the gene encoding CADM1 are associated with autism spectrum disorder. *Biochem Biophys Res Commun* *377*, 926-929.

Zoghbi, H.Y. (2003). Postnatal neurodevelopmental disorders: meeting at the synapse? *Science* *302*, 826-830.